THE HYDROLOGIC CONTROL ON SHALLOW LANDSLIDE TRIGGERING: EMPIRICAL AND MONTE CARLO PYSICALLY-BASED APPROACHES

Ph.D. Dissertation

David Johnny PERES

DOTTORATO DI RICERCA IN INGEGNERIA DELLE INFRASTRUTTURE IDRAULICHE, SANITARIO-AMBIENTALI E DEI TRASPORTI
XXV Ciclo

COMMISSIONE EUROPEA
FONDO SOCIALE EUROPEO

UNIVERSITÀ DI CATANIA
Dipartimento di Ingegneria
Civile e Ambientale

Sedi consorziate:

UNIVERSITÀ DI MESSINA
Dipartimento di Ingegneria Civile

Tesi per il conseguimento del titolo

THE HYDROLOGIC CONTROL ON SHALLOW LANDSLIDE TRIGGERING: EMPIRICAL AND MONTE CARLO PYSICALLY-BASED APPROACHES

David Johnny PERES

Tutor:
Prof. Ing. Antonino CANCELLIERE

Coordinatore del Dottorato:
Prof. Ing. Salvatore Damiano CAFISO

Catania, Dicembre 2012

Is this the real life?
Is this just fantasy?
Caught in a landslide
No escape from reality

[Freddie Mercury, *Bohemian Rhaposdy*]

Contents

Abstract **1**

1 Introduction **5**
1.1 Overview 5
1.2 Aim of the research 6
1.3 Research methodology 7
1.4 Outline of the dissertation 8

2 Landslide triggering by rainfall **11**
2.1 Landslide phenomena and risk mitigation 11
2.2 Empirical approaches 14
2.3 Physically-based models 16

3 Empirical rainfall thresholds for the Peloritani Mountains area, Italy **25**
3.1 Prelimary remarks 25
3.2 The Peloritani Mountains case study area 25
3.3 Application of FLaIR model 28
3.3.1 Method 28
3.3.2 Data 32
3.3.3 Results and discussion 32
3.4 Method based on annual maxima rainfall data 34
3.4.1 Method 34
3.4.2 Data 35
3.4.3 Results and discussion 37
3.5 Conclusive remarks 39

4 Monte Carlo physically-based simulation methodology **41**
4.1 Preliminary remarks 41
4.2 Simulation scheme 42
4.3 Identification of rainfall events 42
4.4 Methodology of analysis of simulation 44
4.4.1 Return period 45
4.4.2 Rainfall-Landslide occurrence relationship 45

4.5 Software 46

5 Neyman-Scott Rectangular Pulses rainfall model 49
5.1 Preliminary remarks 49
5.2 Process 50
5.3 Properties of the NSRP process 53
5.4 Calibration 54

6 Landslide triggering physically-based modeling 57
6.1 The TRIGRS model 57
6.1.1 Overview 57
6.1.2 Governing equations 59
6.1.3 Unsaturated zone 59
6.1.4 Saturated zone 61
6.1.5 Infiltration, Runoff, and Flow Routing 63
6.1.6 Slope stability 63
6.2 Integration of TRIGRS with a water table recession model 64
6.3 Model performance assessment 64

7 Application to Loco catchment in the Peloritani Mountains, Italy 67
7.1 Preliminary remarks 67
7.2 Calibration and validation of the NSRP rainfall model 68
7.2.1 Analysis of Fiumedinisi rainfall data 68
7.2.2 Model Calibration 70
7.2.3 Model validation 75
7.3 Application of the physically-based model 79
7.3.1 Data and preliminary analyses 79
7.3.2 Results 83
7.4 Applications of the Monte Carlo physically-based approach 90
7.4.1 Return period estimation 90
7.4.2 Intensity-Duration model evaluation 92

8 Conclusions 101

List of Figures 119

List of Tables 119

References 119

Abstract

Shallow rapidly moving landslides, triggered by rainfall infiltration, cause many fatalities and much destruction worldwide.

Understanding the hydrological control on shallow landslide triggering, is fundamental in landslide risk mitigation, at least for two reasons.

The first reason is that landslide early warning systems require information on the link between rainfall and landslide occurrence. The second reason is that knowledge of the hydrologic conditions that trigger landslides in a spatially-distributed fashion allows to map return period of landslide triggering within a landslide-prone region. This is one of the fundamental steps for production of hazard and risk maps that may be effectively used as an aid for urban and landslide mitigation planning.

In the dissertation, a Monte Carlo approach, that combines stochastic and deterministic modeling approaches, is used to analyze the hydrological control on shallow landslide triggering.

In particular an integrated stochastic rainfall and deterministic landslide simulator has been developed for the purpose.

The simulator is composed by the following components: (i) a seasonal Neyman-Scott Rectangular Pulses (NRSP) model to generate synthetic hourly point rainfall data; (ii) a module for rainfall event identification and separation from dry intervals; (iii) the Transient Rainfall Infiltration and Grid-Based Regional Slope-Stability (TRIGRS) model, version 2 (Baum et al., 2008, 2010) to simulate landslide triggering by rainfall infiltration, combined with a water table recession (WTR) model that computes the initial water table height to consider in simulating rainfall events with TRIGRS.

The Monte Carlo simulator has been applied to the Loco catchment in the Peloritani Mountains in northeastern Sicily of Italy, an area with high landslide risk, as recently demonstrated by the regional debris-flow event that occurred on 1st October 2009, which caused 37 casualties and millions of euros of damage.

The NRSP model resulted capable of capturing the most important and many other stochastic features of rainfall observed nearby the study case area; model validation, carried out by testing the reproduction of rainfall event characteristics important with respect to landslide triggering such as event intensity and duration, has given satisfactory results.

Suitability for modeling the triggering of landslides in the investigated area of the TRIGRS - WTR model has been tested by applying it to the three-event

sequence that provoked landslides on 1stOctober 2009. Model performance has been assessed by comparing mapped slides for the 1stOctober 2009 event with model output, also in terms of ROC-based (Receiver Operating Characteristic) indices. Model performs at least as well as other known applications of the TRIGRS model to other study cases areas (ROC-accuracy and precision are respectively greater than 0.80 and 0.30).

The Monte Carlo approach has been applied for estimation of return periods of shallow landslide triggering and for the evaluation of the most commonly-used types of empirical rainfall threshold.

Use of the Monte Carlo approach for estimation of the return period of landsling, represents an advance to approaches based on rainfall Intensity-Duration-Frequency (IDF) curves, applied by several different researchers, for two reasons. Firstly because the response of an hillslope to hyetographs of rectangular (or any other predifined) shape may be significantly different from that to a real-like stochastically variable hyetograph. Secondly, and more importantly, the use of the Monte Carlo approach, in which water table depths at the beginning of each rainfall event are determined in response to antecedent rainfall time history, allows to avoid the drawback of assuming an arbitrary initial water table depth (for instance equal to zero), which has a probability to occur that should be taken into account in estimating the return period. In fact, IDF-based return period estimation is in principle flawed by the fact that in estimating return period the conditional probability of the rainfall event, given the assumed initial water table height, should be considered.

Monte Carlo simulations have allowed to map return period of landslide triggering (i.e. a factor of safety $FS \leqslant 1$) on the case-study catchment.

Simulation results have been analyzed to evaluate from a theoretical perspective the Intensity-Duration empirical model paradigm, i.e. to understand if the stochastic nature of rainfall combined with the physical processes of soil-water movement provide a theoretical justification to this most widely used empirical model. In fact, in spite of its consolidated use, no particular theoretical justification for the use of the Intensity-Duration empirical model exists. The paradigm is that a rainfall threshold for landslide triggering assumes a straight line in a bi-logarithmic rainfall (mean) Intensity - Duration plane.

The obtained results allow to state that, actually, stochastic structure of real rainfall events combined with the infiltration response reveal in a certain sense a theoretical justification to the I - D relationship. Iso-pore-pressure points, in the bi-logarithmic rainfall (mean) Intensity - Duration plane, lay, with relatively low scattering, around a straight line, in the cases that initial water table height is negligible.

This means that the I-D model represents a valid model to interpret data in the case that memory of pore pressures is negligible. This holds true basically when the hydraulic conductivity of the soil is relatively high, in relation to rainfall characteristics (relatively isolated rainfall events) and hillslope position in the catchment (low values of upslope contributing area).

In other, most likely, cases, the I-D model should be coupled with an antecedent

rainfall model.

The iso-pore-pressure scatter plots derived from the Monte Carlo simulations have been also compared with iso-pore-pressure curves that result in response to a rectangular hyetograph of same (mean) intensity and duration (assuming in this case an initial water table depth of zero), in order to study the influence of rainfall intensity stochastic variability on landslide triggering . This analysis has been conducted considering separately the simulation points relative to a negligible initial water table height from the ones relative to a not negligible initial water table height.

Comparison in the former case reveal that for regular rainfall event durations, say $D < 12$ h, a real variable-intensity hyetograph may produce a pore-pressure response less than the one induced by a rectangular hyetograph of the same (mean) intensity and duration, while the opposite occurs for high durations. From the comparison relative to the latter case, it can be stated that in dependence of the initial water table depth (i.e. rainfall time history preceding the event) even rainfall events of low intensity and duration may trigger landslides.

Chapter 1

Introduction

1.1 Overview

Debris flows and other shallow rapidly moving landslides triggered by rainfall infiltration cause many fatalities and heavy economical damages worldwide (cf., e.g, Highland and Bobrowsky, 2008). Like most natural hazards, it is largely recognized that the most devastating impacts can be significantly reduced, provided appropriate mitigation measures are implemented.

Landslide risk mitigation measures are distinguished in structural and non structural. The former may consist in debris flow basins, retaining walls, check dams, techniques of slope stabilization, etc.; the latter consist in landslide early warning, insurance against landslide damage and urban planning restrictions. Non structural measures do not prevent or attenuate landslide occurrence, but in principle cost drastically less than structural measures for the same extent of protected area.

Knowledge of the hydrological control on shallow landslide triggering, i.e. the rainfall conditions that trigger landslides, is important in landslide risk mitigation, for at least two reasons. First of all it represents a prerequisite to develop early warning models able to promptly warn about the potential triggering of a landslide in an area. Furthermore, knowledge of the hydrological control in a spatially-distributed fashion, enables the mapping of landslide hazard at the catchment scale (cf., e.g. Montgomery and Dietrich, 1994; Rosso et al., 2006; Salciarini et al., 2008). Such a mapping can find useful application both for urban planning, as well as to rank priorities for the construction of landslide mitigation structures.

Models for determining the rainfall conditions that trigger landslides can be broadly divided into two catagories, namely *empirical* and *physically-based*.

In the first case, rainfall triggering threshold is determined by the analysis of observed data of rainfall that (or did not) resulted in landslides. Generally this is carried out by empirically analyzing the link between rainfall events characteristics (for instance duration and mean intensity) and landslide occurrence. A rainfall threshold is then identified with some method, usually consisting in tracing a lower-

bound curve. The most widely-used curve (Guzzetti et al., 2007) assumes the form $I = \alpha D^{\beta}$, where D is rainfall duration (measured from the beginning of the event to the instant of incipient slope failure) and $I = H/D$ is mean rainfall intensity (H is cumulative rainfall observed on time interval D).

In the second case, landslide occurrence is investigated by means of equations attempting to physically describe the processes governing slope failure (Iverson, 2000). Hence they are composed by an hydrological model of unsaturated and saturated groundwater flow, coupled with a geomechanical slope-failure model. To this end, frequently infinite slope stability analysis is applied. These models are usually applied in a spatially-distributed fashion at an area that may have the extension of one or more drainage basins.

Empirical models may be advantageous for the little information on hillslope hydraulic and geotechnical properties that they in principle require, and for their simplicity of application. The performance of the early warning system based on such models, obviously will depend on the reliability and completeness of the data used, and on the plausibility of the form of equation chosen to draw the threshold. However, at best they can warn about the presence of conditions that in the past have led to landslides over a large area, and therefore their predictive ability requires the assumption of stationarity of the landslide triggering mechanisms. Moreover, empirical methods do not generally provide information on the magnitude, the location of the landslide event triggered, and in fact do not allow to produce detailed maps of landslide hazard.

Physically-based models on the other hand are in principle capable to assessing both long and short term landslide risk not just with reference to a large area but also to a specific basin. Although they are more data and computational demanding since they require more knowledge of physical properties for their application, yet they are potentially able to take into account the influence of changes in land use and in climate forcing, as well as to provide a probabilistic assessment of landslide risk.

1.2 Aim of the research

The aim of the dissertation is to contribute to an improved understanding of the hydrologic control on shallow landslides.

In particular, the general objective is to develop a Monte Carlo simulation framework in order to take into account the stochastic nature of the rainfall forcing on landslide triggering. The proposed methodology is based on coupling a stochastic point rainfall model and a physically-based infiltration and slope stability model in order to take into account the stochastic nature of rainfall forcing on landslide triggering mechanisms. The Monte Carlo procedure has been developed in order to pursue the following specific objectives:

- to investigate the link between rainfall event characteristics and landslide occurrence in order to provide insights for the development of rainfall thresholds for landslide triggering;

- to compare the effect of time variability of precipitation on landslide triggering potential with that induced by rectangular hyetographs (constant intensity);
- to estimate return period of landslide occurrences thus providing a tool for landslide risk mapping.

The direct link between rainfall event characteristics and landslide occurrence has been investigated by several researchers using the Intensity-Duration model $I = \alpha D^{\beta}$ equation to interpret simultaneous observations of rainfall and landslides and determine empirical rainfall thresholds of landslide triggering.

In spite of its consolidated use, no particular theoretical justification for the use of that equation exists (Guzzetti et al., 2007). Thus, the aim of the dissertation on this issue is to evaluate from a theoretical perspective empirical models, i.e. to understand if the stochastic nature of rainfall combined with the physical processes of soil-water moviment provide, in a certain measure, a theoretical justification to the most widely used empirical models, such as the I-D model.

Estimation of the return period of landslide occurrence has been carried out by several researchers based on Rainfall Intensity-Duration-Frequency (IDF) curves and rectangular or predifined-shape hyetographs (cf., e.g., D'Odorico et al., 1995; Rosso et al., 2006; Salciarini et al., 2008). In fact, when the IDF curves are utilized, an hypothesis on initial water table depth has to be made. The pitfall in assuming an arbitrary value for the initial water table height (such as zero), is that this has a certain probability to occur, which should be accounted for in return period estimation. The Monte Carlo approach, in which water table depths at the beginning of each rainfall event are determined in response to antecedent rainfall time history, such as the one utilized in this dissertation, allow to avoid the above-mentioned pitfall.

1.3 Research methodology

The Monte Carlo simulation technique developed in this dissertation is based on the combination of a stochastic rainfall model with a spatially-distributed physically-based hydrological model.

In particular, the Neyman-Scott Rectangular Pulses (NSRP) model is utilized to generate hourly rainfall at a point. NSRP model is chosen because it represents a compromise between flexibility and complexity (only five parameters per season) and numerous applications corroborate its validity (cf., e.g. Rodriguez-Iturbe et al., 1987b; Cowpertwait et al., 1996; Calenda and Napolitano, 1999).

The Transient Rainfall Infiltration and Grid-Based Regional Slope-Stability model (TRIGRS), version 2 (Baum et al., 2008, 2010), developed by a research group of the United States Gelogical Survey, is utilized for the spatially-distributed physically-based hydrological model. The unsaturated version of the model is considered, which solves the 1-D (vertical) Richards' equation particularized for the exponential Soil Water Retention Curve proposed by Gardner (1958). This formulation is chosen for its computational efficiency, being analytical solutions available for this case, after Srivastava and Yeh (1991).

As TRIGRS assumes vertical infiltration, it is an *event − based* model, because lateral pore pressure diffusion becomes important in the dry time intervals from one storm to another (storm interarrivals).

Hence, initial conditions for each event, represented by the initial water table depth at each cell of the analyzed domain, have to be specified, and are very important to correctly simulate response to rainfall events (Baum et al., 2008).

In order to overcome this problem, in this study the TRIGRS model is integrated with a simple drainage model, that is applied with reference to dry periods to compute, from the final output of each event, the initial conditions to the following event. This drainage, or Water Table Recession (WTR) model, is based on model by Rosso et al. (2006) applied to the storm interarrivals, and may be interpreted as a linear-reservoir drainage model where the constant is expressed as a function of the hydraulic properties of the soil.

In the Monte Carlo simulation framework the above-described modeling modules are combined together. A specific rainfall event separation algorithm is developed in order to univocally identify rainfall events (and dry periods) to simulate soil water content either by TRIGRS or by the WTR model. Furthermore this enable to more correctly interpret the simulation outputs.

The methodology is applied to a real case study. In particular the Loco catchment in the Peloritani Mountains in Sicily, Italy, located upslope of the urban area of Giampilieri (ME), is considered. This catchment is prone to shallow landslides that evolve in debris flows, and it is among the ones involved by the 1 October 2009 regional debris-flow event that has caused 37 casualties and tens of millions of euros of damage (Foti et al., 2012).

The simulator is applied with reference to a single cell with properties valid for the case study. Due to the fact that TRIGRS is a vertical model, single cell results can be applied to each cell to map results in a spatially-distributed fashion with a reasonable simulation time. Drainage model introduces interaction among cells, that however may be easily accounted for simulating for a range of cell upslope contributing areas A.

The results of simulations are utilized to derive return period of cell geomechanical failure, corresponding to a factor of safety less than 1.

Instants at which $FS = 1$ provide landslide triggering instants, that are used to compute rainfall quantities, such as mean intensity I and duration D, and to investigate on the direct relation of those quantities with landslide triggering. This allows to evaluate, from a stochastic physically-based perspective, the widely-used $I - D$ empirical model.

1.4 Outline of the dissertation

This dissertation is divided in eight chapters including the present introduction.

In chapter 2 literature on landslide triggering by rainfall is reviewed.

Chapter 3 presents the application of empirical models for determination of rainfall thresholds for landslide early warning, with reference to the Peloritani Mountains area, in northeastern Sicily. In particular, the FLaIR model (Sirangelo

and Versace, 1992), an empirical model that has found several applications to other case studies in Italy, has been applied to that area. A separate empirical methodology is then developed and applied to the same areas. This methodology represents an advance over numerous empirical approaches as it addresses the problem of determining the rainfall thresholds also considering the non-triggering events, and accounts for false, missed, correct alarms and correct non alarms in its calibration procedure. Another advantage of the procedure is that it uses the most comprehensive databases of Italy and hence it has in principle the possibility of being applied as a general procedure for identifying landslide early warning thresholds for prone regions of Italy. Although this chapter fits fully in the subject under study, it can be considered as independent from the rest of the work. This chapter is a summary of three publications (Peres and Cancelliere, 2011, 2012) to which readers are referred for further details.

In chapter 4 the Monte Carlo simulation methodology is illustrated in detail.

Chapter 5 illustrates the adopted stochastic Neyman-Scott Rectangular Pulses point rainfall model.

Chapter 6 describes the physically based model. In this chapter the TRIGRS v.2 model is summarized at a certain level of detail, but this description cannot certainly substitute reading of the manual of the program (Baum et al., 2008) and the related journal article (Baum et al., 2010).

In chapter 7 applications carried out with reference to the Loco case-study catchment are illustrated.

Conclusions of the research are delineated in chapter 8.

Chapter 2

Landslide triggering by rainfall

2.1 Landslide phenomena and risk mitigation

Landslides cause a lot of damage and deaths in many countries. Worldwide, landslides occur and cause thousands of casualties and billions in monetary losses annually (Highland and Bobrowsky, 2008). Being both related to intense or prolonged precipitation, landsliding and flooding are closely allied, and it is consequently difficult to carry out separate quantifications of damage.

Guzzetti et al. (2005) compiled databases on landslide and flood occurrence and damage in Italy. In particular, analysis of the database indicates that more than 50593 people died, went missing, or were injured in 2580 flood and landslide events, in the 724-year period from AD 1279 to 2002. At least 733000 people were evacuated in that same period. An analysis by Kahn (2005) on the the role of income, geography, and institutions on the death toll from natural disasters, revealed that though richer nations do not experience fewer natural disasters than poorer nations, richer nations do suffer less death from disaster, and consequently that economic development provides implicit insurance against nature's shocks.

Landslide risk mitigation starts from understanding the types of landslide that threaten the area under study, because this knowledge determines many fundamental aspects that are important to plan and adopt appropriate mitigative action, such as the potential speed of movement, likely volume of displacement, distance of run-out, as well as the possible effects of the landslide.

A landslide may be defined as a downslope movement of rock or soil, or both, occurring on the surface of rupture in which much of the material often moves as a coherent or semi-coherent mass with little internal deformation (Highland and Bobrowsky, 2008).

The most widely used classification of landslides is the one by Cruden and Varnes (1996) (modified from Varnes (1978)). According to that classification, landslides may be classified on the basis of the type of movement and the type of material involved. The former may be: *fall*, *topple*, *slide* or *flow*, while the latter may be either rock or soil (or both). Soil can then be classified as *earth* if

mainly composed of sand-sized or fine particles and *debris* if composed by coarser fragments. Figure 2.1 illustrates the most common types of landslides that may be observed in nature. It is not uncommon that a landslide may change from one type to another while it occurs. Many debris flows are generated as a subsequent phase of slides. Pore pressure increase as a consequence of slope saturation by water, is a primary cause of landslides. Slope saturation may be induced by intense rainfall, snowmelt, changes in groundwater levels, and water level changes along coastlines, earth dams, and the banks of lakes, reservoirs, canals, and rivers.

Landslide risk mitigation measures can be categorized into two classes: structural and non-structural. The former consist in structures aimed to slope stabilization and debris retaining, and thus they prevent landslide from occurring or travel into urbanized areas, while the latter may consist in actions that may involve little structure construction.

Structural measures are generally more effective, but have an high cost per unit of protected area, so actually only areas that have been threatened by devastating landslides are interested by these measures.

The most important non-structural measure is landslide early warning.

Landslide early warning may lessen damage and victims, but usually do not prevent landslide occurrence. Yet it has a low cost per unit of protected area, when compared to structural measures.

Landslide early warning systems are based on the identification of rainfall thresholds of landslide triggering (Yano and Senoo, 1985; Keefer et al., 1987; Capparelli and Tiranti, 2010; Fathani et al., 2009; Takara and Apip Bagiawan, 2009; Baum and Godt, 2010). Thus understanding the timing and the location of landslide triggering is important from a scientific and practical perspective.

Based on the time scales of triggering and speed of the sliding mass, triggering to be coupled (in relation to the characteristic time scale of the phenomena) with meteorological forecasts (cf. Capparelli and Versace, 2011), that may include also stochastic quantitative now-casting of rainfall (Sirangelo et al., 2007; Versace et al., 2009), since the forecasts usually do not provide rainfall at a fine temporal resolution, as required for the early warning.

Models for determining the rainfall conditions that trigger landslides are categorized in two classes:

- *Empirical*: a triggering threshold is determined by the analysis of observed data of rainfall and knowledge of landslide events. The statistical dependence is analyzed between characteristic quantities of rainfall events and landslide occurrence (or not occurrence). A threshold is then identified with some method, that commonly consists in drawing a lower bound line/curve, i.e. all points that triggered landslides have observed precipitation with characteristics that exceed the line/curve. Sometimes more than one thresholds is drawn, to correspond to various levels/states of warning (such as attention, alert, alarm) or the range of observed rainfall within landslides have been observed are given (i.e. both the lower and the upper bound are drawn).

- *Physically-based*: landslide occurrence is investigated by mean of equations

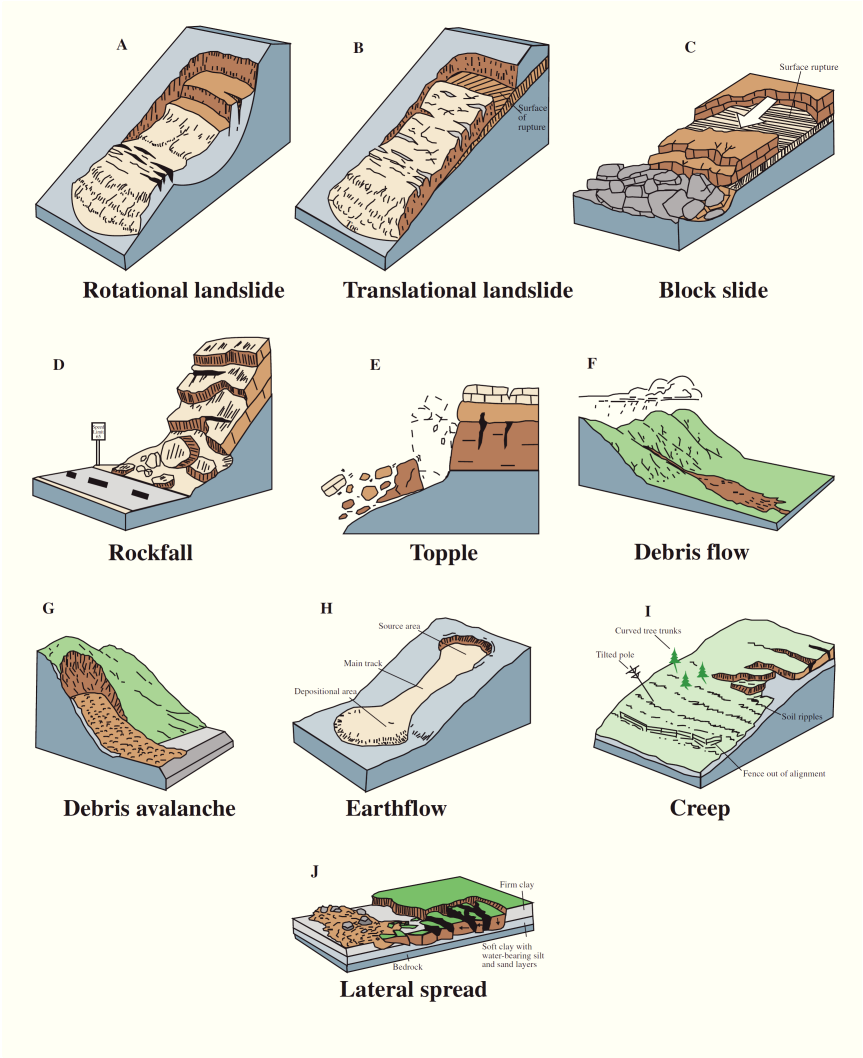

Figure 2.1: Landslide types (after Highland and Bobrowsky, 2008)

that describe the processes governing slope failure. Typically, this models treat the case of rain infiltration-induced landslides. They are then composed by subsurface-oriented hydrological model and a slope failure model. Most of the models are GRID-based, and investigate an area that may have the extension of one or more watersheds. In some cases behavior of individual slopes is investigated, making use of more accurate description and numerical modeling than the GRID based ones, for which the same modeling may be prohibitively time consuming (cf. e.g. Capparelli and Versace, 2011).

2.2 Empirical approaches

Studies from Campbell (1975) and Caine (1980) are among the first ones related to determination of rainfall thresholds of landslide triggering.

Campbell (1975) found an empirical association between soil slips and rainfall, based on the analysis of detailed data on landslides and simultaneous rainfall events for the Santa Monica Mountains in Southern California. He observed that in all cases in which soil slip failure has been observed, the rainfall intensity exceeded 0.20 inch/h (5 mm/h) per hour, and nearly all exceeded 0.25 inch/h (6.4 mm/h) per hour. This latter value has been interpreted to be the minimum rate at which surface infiltration exceeds subsoil drainage for most of the colluvial soils of the area. Moreover, cumulative rainfall at the triggering of the observed landslides have exceeded 10 inches (250 mm), value that Campbell indicated as a threshold and as the value of antecedent rainfall required to bring most of the colluvial soil of the area to field capacity.

Based on the analysis of 73 landslide events that resulted into shallow landslides or debris flows Caine (1980) obtained a lower bound line given by the formula:

$$I = 14.82D^{-0.39} \tag{2.1}$$

best defined for rainfall durations between 10 minutes and 10 days. The so-called $Intensity - Duration\ model$ (ID) introduced by Caine has become the most common type of threshold used in the literature, whose general form is (Guzzetti et al., 2007):

$$I = c + aD^{-\beta} \tag{2.2}$$

Since Caine (1980) formula has been published, plenty of studies have focused on the determination of landslide thresholds, most of them site-specific, i.e. relative to a small landslide-prone region, sometimes resulting in just a slight modification of the coefficient and exponent of equation 2.1, (cf., e.g. Guzzetti et al., 2007).

A bibliographic review by the Italian National Council of Research, Institute of Research for Hydro-geological Protection (CNR-IRPI) (Guzzetti et al., 2007) yielded a list of 125 rainfall thresholds, which is also available at the website `http://rainfallthresholds.irpi.cnr.it/`. Among the 125 thresholds, 54 are relative to areas within Italy.

According to the study of Guzzetti et al. (2007), empirical thresholds in the collection can be distinguished in four sub-categories:

- intensity-duration thresholds;
- thresholds based on the total event rainfall;
- rainfall event-duration thresholds;
- rainfall event-intensity thresholds.

Also, investigators normalize the rainfall intensity values using empirical measures of the local climate, in order to obtain comparable rainfall thresholds prepared for different areas or regions (normalized ID thresholds). Typically, normalization is obtained dividing the event rainfall intensity by the mean annual precipitation (MAP) (e.g. Cannon, 1988; Aleotti, 2004). A few authors have attempted to establish thresholds for the initiation of landslides based on the total amount of precipitation during the landslide triggering event (thresholds based on measurements of the event precipitation), and some of these thresholds are defined as percentages of the MAP. Other methods consider other characteristic quantities of rainfall events, such as antecedent precipitation indexes (Glade et al., 2000).

Perhaps the main justification for the empirical approach lies on the fact that practical difficulties in understanding the rainfall triggering mechanism from a deterministic standpoint generally arise due to the lack of estimates of spatially distributed hydraulic and mechanical parameters, and to complexities of ground conditions on susceptible slopes. Moreover, its simplicity and easy understanding by the operators of early warning systems, which may not always be highly specialized to run sophisticated physically-based models, has perhaps determined the spreading of this approach. Yet drawbacks of the approach include:

- high dependence of the threshold on the characteristic quantities chosen for the formulation of the model and on the the form of the empirical relationship used;
- high uncertainty in the definition of the triggering time instant, and hence of rainfall duration (used in most of the empirical models);
- reliable data often is not available;
- impossibility of have information about the magnitude, the location of the landslide event triggered;
- when only the triggering rainfall events are considered in the statistical analysis, the case of false positives is not accounted for (false alarms);
- role of antecedent precipitation is not fully understood.

An attempt to generalize empirical models has been conducted by Sirangelo and Versace (1992), that have proposed the FLaIR (*F*orecasting of *La*ndslides

*I*nduced by *R*ainfall) model. FLaIR model has found several applications in Italy, in particular: to the Calabria region (Sirangelo et al., 1996; Sirangelo and Versace, 1996; FLA), to Sarno in the Campania region (Sirangelo and Braca, 2004) and to the Lanzo area in Piedmont, where an experimental early warning system based on FLaIR is active (Capparelli and Tiranti, 2010).

In FLaIR model the definition of the warning threshold is based on the computation of a *mobility function*, that is the convolution between a rainfall time series at a representative location and a parametric impulse response distribution, which characterizes the area with respect to its behavior to landslides. Calibration of the parametric function is carried out through the use of historical rainfall series and landslide events.

More in detail, given a rainfall time series $I(t)$, the mobility function $Y(t)$ is given by the convolution integral of $I(t)$ with a *filter function* $\psi(t)$:

$$Y(t) = \int_0^t \psi(t-\tau) I(\tau) d\tau \tag{2.3}$$

FLaIR model is based on the concept that the whole time history of the rainfall input affects the probability of slope failure in a given area of interest, for which the model itself is calibrated. As shown in Capparelli and Versace (2011), through the use of an appropriate filter function form equation 3.1 reproduces the Intensity-Duration model (v. eqn 2.2)

In fact, the *mobility function* is not known on a physical basis; hence it is assumed to be parametric and of a chosen form. The parametric distribution that has been mostly used in applications is the gamma distribution, which contains two parameters.

Once the set of parameters, and hence the mobility function, is univocally determined, early warning of landslides may be based on comparison of the mobility function with a critical value, usually assumed as the minimum value of the calibrated mobility function for which landslide triggering has been observed.

Performances of early warning systems based on the FLaIR model, implemented in the Calabria region (Italy), have been investigated recently in terms of indicators based on the number of correct alarms CA, missed alarms MA and false alarms FA. Hit rate $HR = FA/(CA + FA)$ and False Positive Rate $FPR = FA/(CA + FA)$ varied in the range 0.14 - 0.66 and 0.34 - 0.86, respectively (Versace et al., 2012).

2.3 Physically-based models

These approaches are based on the computation of a factor of safety FS with respect to slope stability. The region of analysis usually consists in a catchment, which is subdivided in elements or cells, on a spatially-distributed GRID or contour basis.

The factor of safety explicitly depends on the soil water pressure. Thus an hydrological model, focused mainly on subsurface water dynamics, that allows computation of pore pressures from rainfall input, is a fundamental part of these type

of models. The slope stability model is usually expressed as one formula for the safety factor, and unstable cells are identified as the ones for which $FS < 1$.

In the following sections, the principal slope stability and hillslope hydrology models used by researchers are reviewed. The determination of return period of landslides is then focused.

Slope stability analysis

In many of the modeling approaches, it is assumed that the potential failure surface lies at a depth d_{LZ} below the surface that is small if compared with the length of the slope, so that the edging effects are negligible. This allows one to use the *infinite-slope* stability analysis (Haefeli, 1948; Taylor, 1948). In this case, the factor of safety is determined from the analysis of a slice of material of unit width and thickness (see figure 2.2).

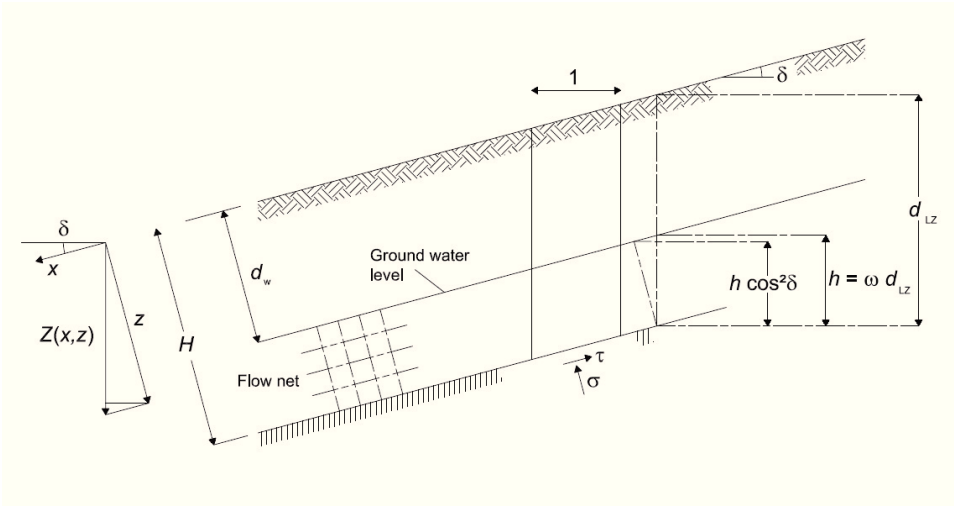

Figure 2.2: Scheme for infinite slope equilibrium analysis (adapted from Rosso et al., 2006). On the left, the coordinate system used by Iverson (2000)

Factory of safety is in general defined as the ratio between shear strength τ_f and shear stress τ:

$$FS = \frac{\tau_f}{\tau}. \tag{2.4}$$

According to the principle of effective stress, the shear strength may be expressed as:

$$\tau_f = c' + (\sigma - \psi) \tan \delta \tag{2.5}$$

with c' denoting soil cohesion, σ the normal total stress, ψ the pore water pressure, δ the slope angle and ϕ' the angle of shearing resistance of the soil mantle.

If γ represents the average bulk unit weight of soil above the groundwater level and γ_{sat} the saturated unit weight of soil under the groundwater level, the expressions or σ, τ and ψ are:

$$\begin{aligned} \sigma &= [(1-\omega)\gamma + \omega\gamma_{sat}]d_{LZ}\cos^2\delta \\ \tau &= [(1-\omega)\gamma + \omega\gamma_{sat}]d_{LZ}\sin\delta\cos\delta \\ \psi &= \omega d_{LZ}\gamma_w\cos^2\delta \end{aligned} \tag{2.6}$$

where $\omega = h/d_{LZ}$ as shown in 2.2, and represents the *wetness* factor.

Substitution of the above formulas in 2.5 and 2.4 yields the following expression for the safety factor, used in the model by Rosso et al. (2006):

$$FS = \frac{c' + [(1-\omega)\gamma + \omega\gamma']d_{LZ}\cos^2\delta\tan\phi'}{[(1-\omega)\gamma + \omega\gamma_{sat}]d_{LZ}\sin\delta\cos\delta}. \tag{2.7}$$

Montgomery and Dietrich (1994) used the a simplified version of this formula, which considers a cohesionless soil mantle ($c' = 0$) and $\gamma = \gamma_{sat}$:

$$FS = \frac{\gamma_{sat} - \omega\gamma_w}{\gamma_{sat}}\frac{\tan\phi'}{\tan\delta}. \tag{2.8}$$

A more general expression than equation 2.7, that has been used within models that provide the pore pressure distribution also in the unsaturated zone (e.g. Baum et al., 2010; Capparelli and Versace, 2011) accounts for the degree of saturation in the unsaturated zone by multiplying pore pressure for the approximation given by Vanapalli and Fredlund (2000) of the Bishop's Bishop effective stress parameter $\chi = (\theta - \theta_s)/(\theta_s - \theta_r)$, being $\theta = V_w/V_t$ the actual soil water content (volume of water V_w per unit volume of soil V_t).

The infinite slope scheme tendentiously leads to underestimation of the actual factor of safety, being the edging effects neglected. Actually, heterogeneities in the soil characteristics may add a degree of uncertainty that may lead also to overestimations of FS, due for example to overestimation of the soil mechanical properties c' and ϕ'.

Baum et al. (2012) used also a factor of safety based on a finite 3-D slope scheme, obtaining better results than with the 1-D slope, with the same pore pressure distribution calculated with the vertical infiltration model TRIGRS v. 2.0 (Baum et al., 2008), described after.

Hillslope hydrology

Early models are based on mass conservation of groundwater in the scheme like the one of figure 2.3, where a impermeable bed is at depth d_{LZ}. Mass-conservation equation may be expressed as the following (Rosso et al., 2006):

$$Ap - q = \frac{dS}{dt}, \quad \text{for} \quad h \leqslant d_{LZ} \tag{2.9}$$

and

$$Ap - q - r = 0, \quad \text{for} \quad h > d_{LZ} \tag{2.10}$$

where t is measured from the beginning of the storm, S the water storage in the element, and r the overland flow discharge occurring when soil is saturated (i.e. $S_r = 1$).

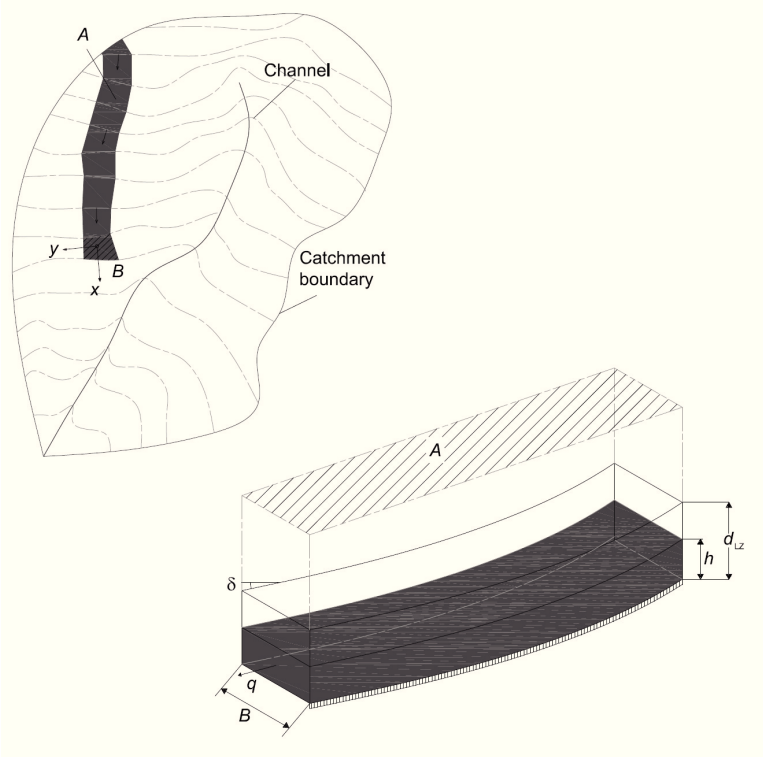

Figure 2.3: Scheme of contour-based models (adapted from Rosso et al., 2006)

Rosso et al. (2006) expressed water storage as $S = V_w(t) - V_w(0) = \frac{V_w(t)-V_w(0)}{V_t} V_t = \frac{e}{1+e}(1 - S_r)Ah$, hence considering a non-null initial degree of saturation S_r.

The Darcy law then provides the seepage flow in the groundwater table as:

$$q = (Bh\cos\delta)K_s \tan\delta = BhK_s \sin\delta, \tag{2.11}$$

being K_s the saturated hydraulic conductivity of the soil and $\tan\delta$ head gradient, assumed to be parallel to the local ground slope.

Integration of the differential equation 2.9 yields to:

$$h = \frac{p}{p^*} d_{LZ} \left[1 - \exp\left(-\frac{1}{A_1} p^* \frac{t}{d_{LZ}}\right)\right] + h_i \exp\left(-\frac{1}{A_1} p^* \frac{t}{d_{LZ}}\right), \quad \text{for} \quad \frac{p}{p^*} \leqslant 1 \tag{2.12}$$

where $h_i = h(0)$ is the initial water table height, $A_1 = \frac{e}{1+e}(1-S_r)$ and $p^* = \frac{T_s B \sin\delta}{A}$

is the saturation precipitation rate ($T_s = K_s z$ denotes hydraulic transmissivity of the soil mantle).

If net rainfall exceeds the saturation precipitation rate p^*, one obtains saturation of the soil mantle after a certain time t^*:

$$h = \begin{cases} \text{eqn. } 2.12 & \text{if} \quad t \leqslant t^* \\ d_{LZ} & \text{if} \quad t > t^* \end{cases} \tag{2.13}$$

and

$$t^* = -A_1 \frac{z}{p^*} \log \left(\frac{z(1 - \frac{p^*}{p})}{h_i - \frac{pz}{p^*}} \right) \tag{2.14}$$

A previous, and simpler, model by Montgomery and Dietrich (1994), considered the steady state case, i.e. the previous equation with the time-dependent term $\frac{dS}{dt} = 0$, and factory of safety FS given by equation 2.8, which yields the following failure criterion, in terms of "critical" wetness:

$$\omega_{CR} = \frac{\gamma_{sat}}{\gamma_w} \left[1 - \frac{\tan \delta}{\tan \phi'} \right], \tag{2.15}$$

which implies that topographic elements where

$$A/B \geqslant (T_s/p) \sin \delta (\gamma_{sat}/\gamma_w)[1 - \tan \delta / \tan \phi'] \tag{2.16}$$

are predicted to be unstable.

As observed by the same authors, the elements within a catchment may be distinguished in four stability classes: *unconditionally unstable, unstable, stable*, and *unconditionally stable*. Unconditionally unstable elements are those predicted to be unstable even when dry (this may be equivalent of saying that bedrock outcropping corresponds to these elements). Potentially unstable elements are then classified by a model as stable or unstable if the failure criterion is satisfied or not, respectively (e.g. equation 2.16). Unconditionally stable elements are those that are stable even at the maximum possible pore pressures, that generally correspond to saturation of the entire soil mantle.

If soil properties are constant in space, Montgomery and Dietrich (1994) model simulates the *topographic* control on the location of shallow landsliding. The successive enhancement to this model by Rosso et al. (2006) is capable to account for the combined effect of storm duration and intensity, i.e. to simulate *hydrologic* control on shallow landsliding.

Iverson (2000) provided an insight of physical mechanism underlying landslide triggering by rainfall, based on the solution of particular cases of the Richards' equation.

Iverson (2000) argued that self-contradictory results are yielded by utilizing approaches based on slope parallel flow and mass conservation of groundwater in a scheme of flow domain bounded by an impermeable bed at depth d_{LZ}, such as the models just illustrated. Thus Iverson (2000) points out that vertical infiltration, modeled by Richards' equation may be appropriate for understanding short-term

response of the hillslope to transient rainfall, in order to assess hydrological conditions that trigger landslides.

According to Iverson2000's Iverson2000 analysis the following three time scales, on which physical process governing landslides operates, may be distinguished:

- A/D_0 as the minimum time scale necessary for establishment of steady background water pressures that develop at (x, y, H) in response to rainfall averaged over periods that commonly range from days to decades (long-term response). These steady groundwater pressures influence the propensity for landsliding at (x, y, H) but they do not trigger slope failure.
- H^2/D_0 as a characteristic time associated with transient pore pressure transmission during and following storms (short-term response). Failure results form rainfall over this time scale, that commonly ranges from minutes to months.
- $\sqrt{H/g}$ as the timescale on which post-failure landslide motion occurs, an another important aspect of landslide related research (cf., e.g. Iverson, 1997; O'Brien et al., 1993; Armanini et al., 2009).

With reference to the coordinate system (x, y, z) illustrated in figures 2.2 and 2.3, Richards (1931) equation may be written as (cf., e.g. Bras, 1990) :

$$\begin{aligned} \frac{\partial \psi}{\partial t}\frac{d\theta}{d\psi} &= \frac{\partial}{\partial x}\left[K_L(\psi)\left(\frac{\partial \psi}{\partial x} - \sin\delta\right)\right] + \frac{\partial}{\partial y}\left[K_L(\psi)\left(\frac{\partial \psi}{\partial y}\right)\right] + \\ &+ \frac{\partial}{\partial z}\left[K_z(\psi)\left(\frac{\partial \psi}{\partial z} - \cos\delta\right)\right], \end{aligned} \tag{2.17}$$

in which ψ is groundwater pressure head, θ is soil volumetric water content, t is time and δ is the slope angle, $0 \leqslant \delta < 90$. Iverson (2000) then defines the ratio ε between pressure diffusion timescales H^2/D_0 and A/D_0:

$$\varepsilon = \sqrt{\frac{H^2 D_0}{A D_0}} = \frac{H}{\sqrt{A}}. \tag{2.18}$$

This ratio plays a key role in analyzing pressure head responses to rainfall on slopes, and Iverson (2000) made simplifications of the Richards' equation based on the hypothesis that $\varepsilon \ll 1$.

To analyze long-term behavior equation of Richards' may be written in terms of the dimensionless time $t^* = \frac{D_0}{A}t$. In the case of $\varepsilon \ll 1$, Richards' equation simplifies to:

$$\frac{\partial}{\partial z^*}\left[{K_z}^*\left(\frac{\partial \psi^*}{\partial z^*} - \cos\alpha\right)\right] = 0 \tag{2.19}$$

where $\psi^* = \psi/H$, $z^* = z/H$, $x^* = x/\sqrt{A}$ and $y^* = y/\sqrt{A}$ are normalized variables.

Frequently in applications, the long-term average infiltration rate in the z direction at ground surface $(I_z)_{LT}$ is specified by a constant flux boundary condition

$(I_z)_{LT} = -K_z(\partial h/\partial z)$ and the soil is assumed homogeneous (Iverson, 2000). In the case that infiltration is sufficiently slow that $(I_z/K_z)_{LT} \ll \cos\delta$ the previous equation describes slope-parallel groundwater flow:

$$\psi = (z - d_w)\cos\delta, \tag{2.20}$$

where d_w is the water table depth measured normal to the ground surface.

The short-term approximation, may be derived expressing Richards' equation 2.17 in terms of the short-term dimensionless time $t^* = \frac{D_0}{H^2}t$. For $\varepsilon \ll 1$, in this case equation reduces to the standard Richards' equation for vertical infiltration in a hillslope of slope δ:

$$\frac{C(\psi)}{C_0}\frac{\partial \psi^*}{\partial t^*} = \frac{1}{\cos^2\delta}\frac{\partial}{\partial Z^*}\left[K_z^*\left(\frac{\partial \psi^*}{\partial Z^*} - 1\right)\right], \tag{2.21}$$

where $C(\psi) = d\theta/d\psi$ and C_0 the minimum value of $C(\psi)$, typically observed when the soil is saturated, and $K_z^* = K_z(\psi)/K_s$.

Equation 2.21 is still a non-linear, and, in general, requires numerical methods for its integration, and the superimposition of solutions is not possibile, which makes of difficult calculation responses to real rainfall sequences. In the case of wet initial conditions, one may assume $K_z \approx K_s$ and $(\psi) = d\theta/d\psi \approx C_0$, and derive the following linear equation:

$$\frac{\partial \psi}{\partial t} = \frac{D_0}{\cos^2\delta}\frac{\partial^2 \psi}{\partial Z^2} \tag{2.22}$$

In the case of a infinite basal boundary depth and a constant hyetograph of intensiy I_Z and duration T, 2.22 has the following solution:

$$\frac{\psi}{Z}(Z, t \leqslant T) = \beta(1 - d/Z) + \frac{I_Z}{K_Z}[R(t^*)] \tag{2.23}$$

$$\frac{\psi}{Z}(Z, t > T) = \beta(1 - d/Z) + \frac{I_Z}{K_Z}[R(t^*) - R(t^* - T*)] \tag{2.24}$$

in which

$$R(t^*) = \sqrt{(t^*/\pi)}\exp(-1/t^*) - \mathrm{erfc}(1/\sqrt{t^*}) \tag{2.25}$$

is a pressure head response function, which depends only on normalized time $t^* = t/(Z^2/\hat{D})$, $T^* = T/(Z^2/\hat{D})$ is a normalized duration, $\hat{D} = 4D_0/\cos^2\delta$ is an effective hydraulic diffusivity, erfc is the complementary error function and $(\beta = \cos^2\delta)$ in the case of slope-parallel groundwater flow.

Baum et al. (2002) extended Iverson (2000) solution (equations 2.23−2.25) for the case of a finite basal boundary, producing and distributing related software to apply this model on a regional scale and GRID-basis, named TRIGRS (*T*ransient *R*ainfall *I*nfiltration and *G*rid-based *R*egional *S*lope-Stability Model), version 1.0. This model also considers instantaneous runoff routing, that occurs when rainfall intensity exceeds infiltration capacity of soil. This routing is accounted in the model

only on the fact that the runoff from one cell may totally or partially infiltrate in downslope cells.

A later model by the same authors (Baum et al., 2008, 2010, 2011), has been based on the analytical solution of Richards' equation 2.21 with the exponential soil-water retention curve of Gardner (1958), for which a closed form solution to the resulting linearized equation is available, provided by Srivastava and Yeh (1991).

The TRIGRS, version 2.0 model is described in its details in chapter 6, being this model used in the research developed in this thesis.

One advantage of the physically-based approach is that it allows, at least in principle, to account for anthropogenic action, land use and climate change.

Wu and Sidle (1995) is one of the first works that analyzed the role of root strength and harvesting on shallow landslides triggering. Other works investigate on the role of anthropogenic action, such as roads and wildfire (Istanbulluoglu et al., 2004; Rulli and Rosso, 2005; Rulli et al., 2006; Parise and Cannon, 2012)

It has to be noticed that, in principle, every hydrological model that allows effective estimation of groundwater pore pressures is in principle suitable for landslide analysis if the triggering mechanism is due to rain infiltration (cf., e.g. Simoni et al., 2008).

Deterministic rainfall thresholds and return period of landsliding

Physically-based models described in the previous section, enable to determine deterministic triggering thresholds in terms of topographic, hydraulic and geomechanical parameters. For the Montgomery and Dietrich (1994) model, the threshold results in terms of a steady state rainfall rate:

$$p_{CR} = [T \sin\delta(\gamma_s/\gamma_w)(A/B)][1 - \tan\delta/\tan\phi)] \tag{2.26}$$

Yet this result does not allow to assess the return period of landslide triggering, because the return period of precipitation depends both on storm intensity and duration (D'Odorico et al., 1995). The probabilistic models that allow estimation of return period of precipitation, i.e. the well-known and commonly used Intensity-Duration-Frequency (IDF) curves, require both rain intensity and duration. (cf. Stedinger et al., 1993; Burlando and Rosso, 1996)

The result of Rosso et al. (2006), accounts for transient precipitation, and hence for rainfall rate p_{CR} and duration t, and the following deterministic threshold is yielded:

$$p_{CR}(t) = \frac{T_s \frac{B}{A} \sin\delta \left[\frac{(G_s + eS_r)\left(1 - \frac{\tan\delta}{\tan\phi'}\right)}{1 + e - e(1 - S_r)\left(1 - \frac{\tan\delta}{\tan\psi'}\right)} - \frac{h_i}{z} \exp\left(- \frac{1+e}{e - eS_r} \frac{T_s B \sin\delta}{Az} t \right) \right]}{1 - \exp\left(- \frac{1+e}{e - eS_r} \frac{T_s B \sin\delta}{Az} t \right)}, \tag{2.27}$$

For short durations, this relationship is practically linear in a $\log(D) - \log(I)$ plot , then it starts departing from it reaching quite rapidly the horizontal asymptote $\omega_{CR} p^*$, being ω_{CR} critical wetness for the Rosso et al. (2006) model. Salciarini

et al. (2008) has made an analogous investigation of Rosso et al. (2006), using the TRIGRS v.1 model (Baum et al., 2002).

D'Odorico et al. (1995) used Montgomery and Dietrich (1994) model to express the long-term solution of Iverson (2000) and analyzed the effects of hyetograph characteristics on potential for landsliding, using hyetographs shaped as beta-functions, instead of rectangular (i.e. of constant intensity) hyetographs. They concluded that for a given rainfall depth, hyetographs with a peak near the end of the storm produce peak pressure heads higher than uniform hyetographs, thus decreasing the return period of rainfall events causing landsliding.

In fact return period depends, in general, on the whole time history of rainfall, which determine also the initial conditions, that should not be neglected or be arbitrarly assumed, as occurs in the above cited studies.

Chapter 3

Empirical rainfall thresholds for the Peloritani Mountains area, Italy

3.1 Prelimary remarks

This chapter focuses on empirical model of rainfall thresholds that may be used for landslide early warning. Analyses are focused on the case study area of Peloritani Mountains, described in following section 3.2.

In particular, firstly the FLaIR model (Sirangelo and Versace, 1992) is applied.

Then a new method is proposed and applied. It enables computation of a threshold in terms of cumulative rain on a moving time window of duration d. The method is particularly suitable for Italy, since it is based on the use of the data that cover the longest historical period, and that are of most easy availability: the sub-daily rainfall annual maxima series and the landslide information from AVI database (Archivio Aree Vulnerate Italiane) of CNR - IRPI (Consiglio Nazionale delle Ricerche, Istituto per la Ricerca sulla Protezione Idrogeologica) (Guzzetti et al., 1994; Guzzetti and Tonelli, 2004). Thesholds are determined via the maximization of an objective function that approximates the benefits of early warning, as it accounts for the both rainfall events that resulted and did not resulted in landslides.

3.2 The Peloritani Mountains case study area

The Peloritani are a mountain range of north-eastern Sicily, in southern Italy, extending for about 65 km along the Ionian coastline. The range is made up by a long series of peaks, with an average height of 800-1000 m.The topography

determines small catchments, with impulsive flash-flood response. The complex orography of the area affects induces high spatial variability of rainfall. The regolith strata, composed by loamy sands often with an high gravel percentage, is likely to slide and evolve as fast and devastating debris flows.

Many landslide events of significant magnitude have interested this area during the last decade. In particular landslides have been observed on the following dates: 15 September 2006, 25 October 2007, 23 September 2009, 1 October 2009, 1 March 2011 and 23 November 2011.

Among these events, the most damaging has been the one that occurred on 1 October 2009. In that date, about 250 mm of rainfall fell in 9 hours, and triggered more than 600 landslides, in an area of 50 km^2, mostly evolving into devastating debris flows (see figures 3.1 and 3.2). This event caused the death of at least 37 persons, about 100 casualties, and about 1700 evacuated people (Foti et al., 2012).

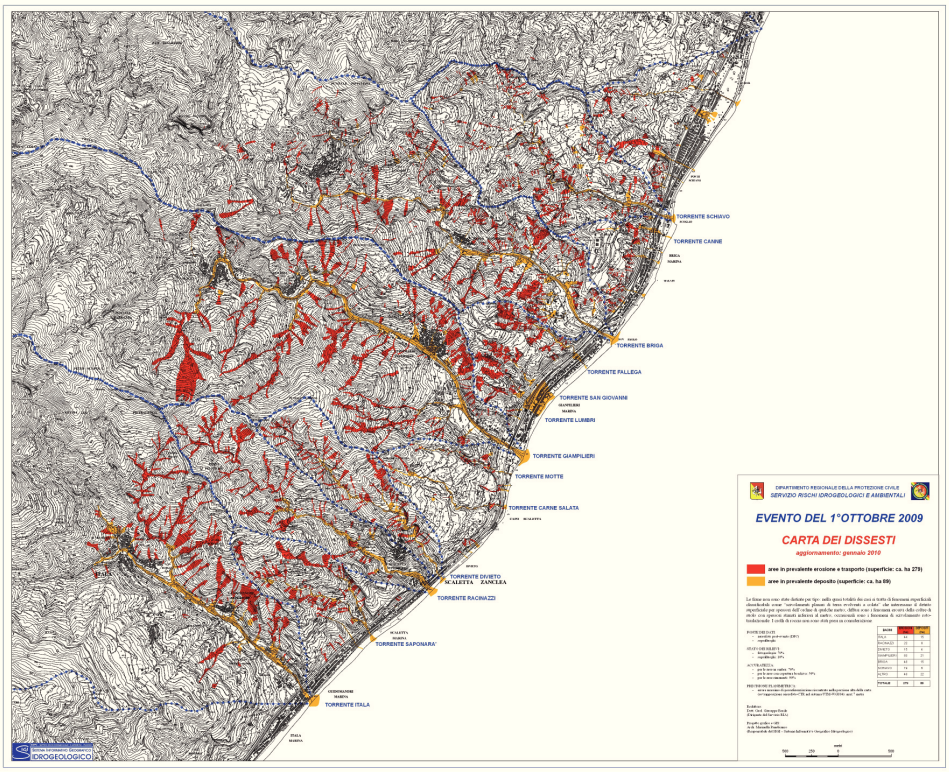

Figure 3.1: Map of landslides triggered on 1 October 2009 in the Peloritani area

Improper land use and urbanization exacerbated the magnitude of damage caused by the debris flows.

Return period of the single rainfall event, measured by the rain gauges in the

Figure 3.2: Some photographs showing destruction caused by debris flows occurred on 1 October 2009 in the Peloritani Mountains area, southern-eastern Sicily, Italy

area (see figure 3.3) of 1 October 2009, has been estimated to be of the order of hundreds of years (Foti et al., 2012). However, the exceptional magnitude of the landslide event may be related also to an high 15 days antecedent cumulative precipitation, which is greater than 100 mm in the nearest rain gauge of S. Stefano di Briga (see figure 3.4). In fact, just seven days before, a significant rainfall event has hit the nearby southern part of the Peloritani area. As shown in figure 3.4 rain gauges in that southern part have measured cumulative rainfall amounts greater than the 1 October event. Landslide have been triggered in the southern area, but had a smaller magnitude, perhaps for less proneness of the area in addition to different antecedent precipitation conditions.

Following the event, the area has been interested by a campaign of structural mitigative measures. Although these structural measures have demonstrated their effectiveness in mitigating debris flow risk in recent occasions (Foti et al., 2012), there is interest in the implementation of a landslide early warning system, and hence on the identification of landslide triggering thresholds.

3.3 Application of FLaIR model

3.3.1 Method

In FLaIR model the definition of the warning threshold is based on the computation of a *mobility function*, that is the convolution between a rainfall time series at a representative location and a impulse response distribution, which characterizes the area with respect to its behavior to landslides. The model is calibrated through the use of historical rainfall series and landslide events observed simultaneously.

More in detail, given a rainfall time series $I(t)$, the mobility function $Y(t)$ is given by the convolution integral of $I(t)$ with a *filter function* $\psi(t)$:

$$Y(t) = \int_0^t \psi(t-\tau) I(\tau) d\tau \tag{3.1}$$

Authors give the possibility to use instead of precipitation an pre-processed variable that may resemble infiltration such as $I(u) = cp(u)$ if $p(u) \leqslant p_0$; and $I(u) = cp_0$, if $p(u) > p_0$, where p_0 may represent infiltration capacity and c a soil-dependent capacity (Sirangelo and Versace, 1996); however, in applications the rainfall time series is used directly.

The mobility function resembles the formula for calculation of discharge in a river basin by means of the *Instantaneous Unit Hydrograph*. Being the latter founded on the hypothesis of linear and time-invariant behavior of the watershed, the FLaIR model implicitly makes this assumption. FLaIR model is based on the concept that the whole time history of the rainfall input affects the probability of slope failure in a given area of interest, for which the model itself is calibrated. Moreover, as shown in Capparelli and Versace (2011), through the use of an appropriate filter function, FLaIR model is able to reproduce the Intensity-Duration model (cf. equation 2.2).

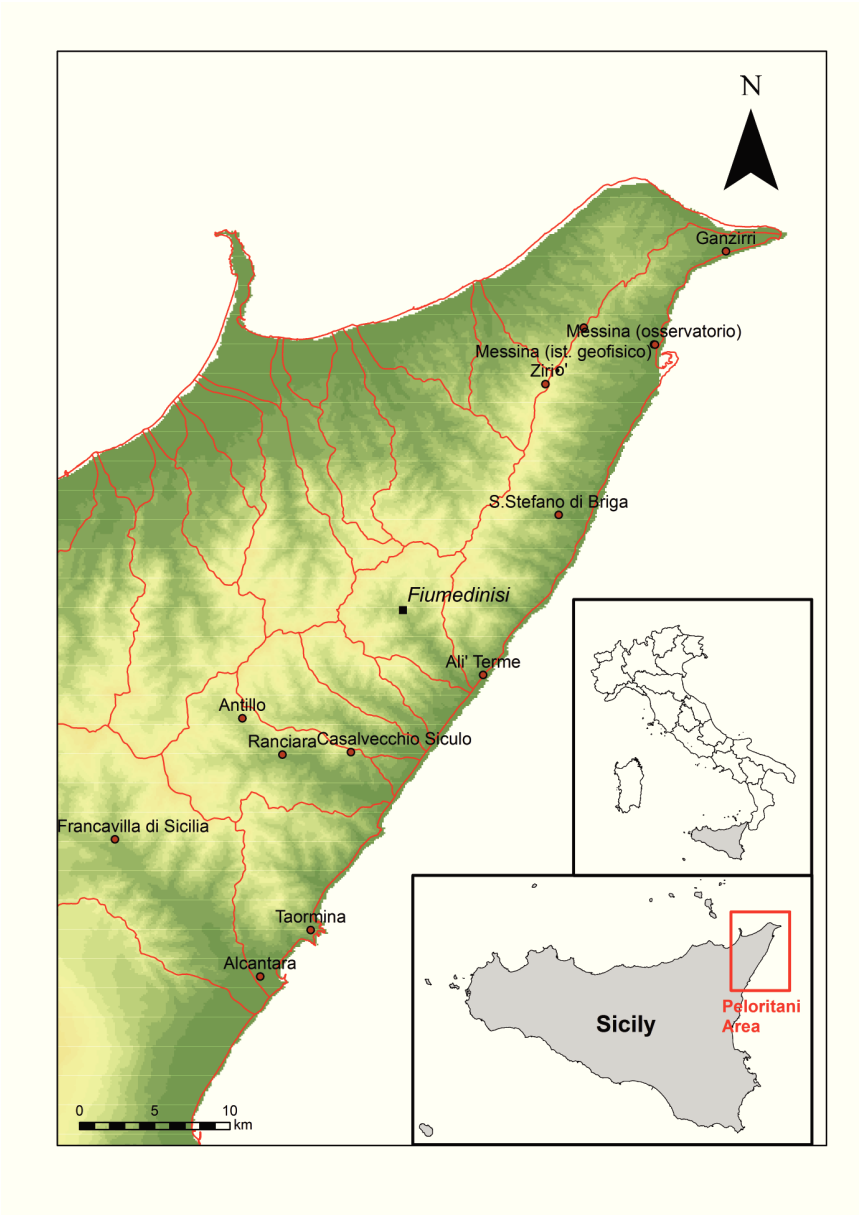

Figure 3.3: Map showing location of the Peloritani area and location of rain gauges of interest

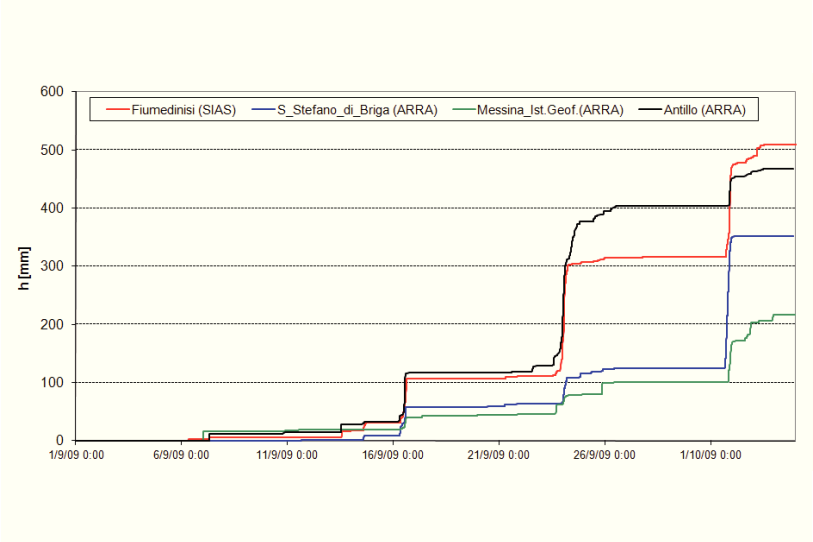

Figure 3.4: Cumulative rainfall path that yielded debris flows in the Peloritani Mountains on 1 October 2009, in rain gauges located nearby the area

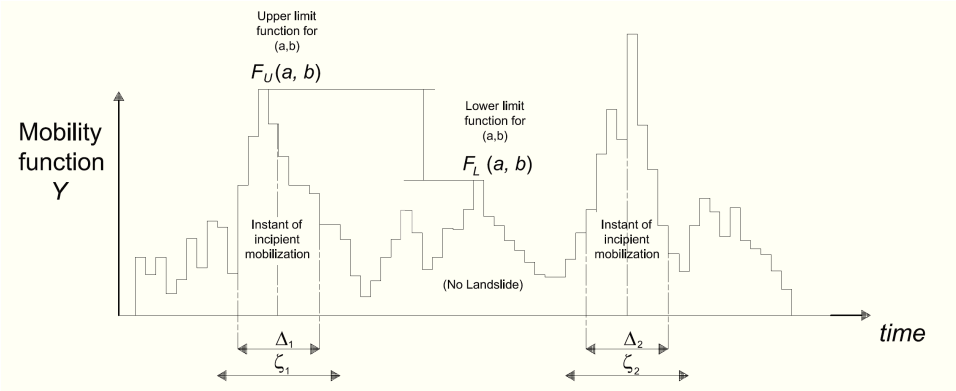

Figure 3.5: Sketch relative to calibration of FLaIR model (cf. Sirangelo and Versace, 1996)

The *mobility function* is assumed to be of a chosen parametric form. The parametric distribution that has been mostly used in applications is the gamma distribution, which is governed by two parameters a and b:

$$\psi(t;a,b) = \frac{1}{b^a\Gamma(a)} t^{a-1} \exp\left(-\frac{x}{b}\right) \tag{3.2}$$

where $\Gamma(a) = \int_0^{+\infty} \mathrm{e}^{-z} z^{a-1} dz$ is the well-known gamma function.

Other families of distributions suggested (cf., e.g., Sirangelo et al., 1996; Capparelli and Tiranti, 2010) include the single-parameter exponential distribution (in fact, a particular case of the gamma, obtained letting $a = 1$), a mixture of two exponentials (2 parameters) and the beta one (4 parameters).

Two methods of calibration of the FLaIR model have been proposed: the *ranking method* and the *crossing* method (Sirangelo et al., 1996). The *ranking method* seems to be the most used in the applications (cf. Sirangelo et al., 1996; Sirangelo and Versace, 1996; Capparelli and Tiranti, 2010). According to this criterion, see scheme of figure 3.5, a given set of parameters is admissible when the K highest values of the mobility function occur within all the K time intervals Δ_k that each include the instant of incipient of a slope failure. In fact, more precisely, for of those K time intervals, only the maximum value within each of the intervals Δ_k is considered for the ranking. Typically, for a given form for the ψ distribution, more than one set of parameters is compatible with the above described criterion. Hence, a *region of admissible parameters* may result. Within this region, an upper limit function F_U and a lower limit function F_L are defined. The upper limit function represents the minimum of the K maxima of Y within the intervals Δ_k, while the lower limit function represents the maximum of the mobility function not associated with landslides, i.e. outside the maximum of Y outside the $_k$ time intervals. The $_k$ should delimit values of the mobility function that have significant statistical dependence (clusters).

Although in a probabilistic approach to overcome the not-univocal identification of parameters was proposed by the model Authors (cf., e.g. Sirangelo et al., 1996; Sirangelo and Versace, 1996), perhaps the most practical way to univocally determine the best parameters within the admissibility region, is to choose the one that maximizes the difference between the upper limit and the lower limit function.

Once the parameters, and hence the mobility function, are determined, early warning of landslides may be based on comparison of the mobility function with a critical value Y_{cr} determined as the upper limit function value corresponding to the parameters (alternatively, and more conservatively, the lower limit function value may be chosen; even though this may yield to an increase of the false alarm rate).

In particular, according to the structure of early warning of the Italian Civil Protection Agency, various levels of protection may be activated as proportions ξ of the critical value, Y_{cr}. For instance, Versace and Capparelli (2008) used a value of $\xi = 0.4$, $\xi = 0.6$ and $\xi = 0.8$ for the watch, the alert and the alarm levels, respectively.

Performances of early warning systems based on the FLaIR model, implemented in the Calabria region (Italy), have been investigated recently in terms of indicators

based on the number of correct alarms CA, missed alarms MA and false alarms FA. Hit rate $HR = FA/(CA + FA)$ and False Positive Rate $FPR = FA/(CA + FA)$ varied in the range $0.14-0.66$ and $0.34-0.86$, respectively (Versace et al., 2012).

3.3.2 Data

For the implementation of the FLaIR model, the hourly series of rain gauge of Fiumedinisi (440 m a.s.l.) managed by SIAS (Servizio Informativo Agrometeorologico Siciliano, `http://www.sias.regione.sicilia.it/` has been used (figure 3.3.

Within the period covered by such series (21 February 2002 - 9 February 2011), four landslide events occurred in several locations in the investigated area: (I) 15 September 2006 (11:00), (II) 25 October 2007 (14:00), (III) 23 September 2009 (23:00) and (IV) 1 October 2009 (19:00). The time of occurrence in brackets has been determined analyzing various documents available. The uncertainty of this time occurrence has lead to the choice of intervals δ_k equal to 7 hours, i.e. 3 h after + 3 h before + the hour indicated above.

Calibration is carried out on the landslides events (I), (II) and (IV), while the event of 23 September 2009 was discarded and used for validation.

3.3.3 Results and discussion

Among the possible choices, the gamma distribution was chosen.

In figure 3.5 the admissible region for the parameters of the gamma impulse response function is shown, together with the values of the difference $F_L - F_U$ in a colorscale. The best pair of parameters is $a = 17.615$ and $b = 0.115$, as those values correspond to the maximum difference $F_L - F_U$. The filter function corresponding to the calibrated parameters is shown in 3.7.

The critical value of the mobility function, i.e. the lowest value for which a landslide was triggered, resulted $Y_{cr} = 46.93$. Monitoring and eventually forecasting of rainfall and thus of the mobility function for the calibrated parameters, and comparison of this function with its critical value Y_{cr} can be the basis of the implementation of an early warning system in the case-study area.

Comparison of the mobility function with the watch, alert and alarm levels (fixed respectively at $\xi = Y/Y_{cr} = 0.4, 0.6, 0.8$) is shown in 3.8.

From such a comparison it can be noticed that the watch level has been reached in 5 dates (4 September 2003, 22 October 2005, 28 October 2008, 2 November 2010 and 16 September 2009) while the alert in two cases (22November and 13 October) and the alarm in all the four dates corresponding to four landslide dates, including 23 September 2009, which was not accounted for in calibration.

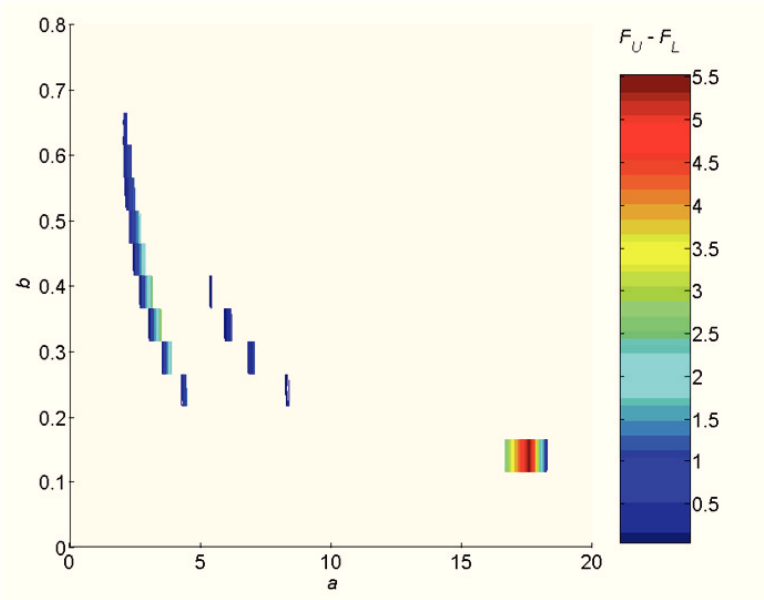

Figure 3.6: Admissibility region for the parameters of the gamma impulse response function and difference between upper limit and lower limit functions. Best pair of parameters is $a = 17.615$, $b = 0.115$

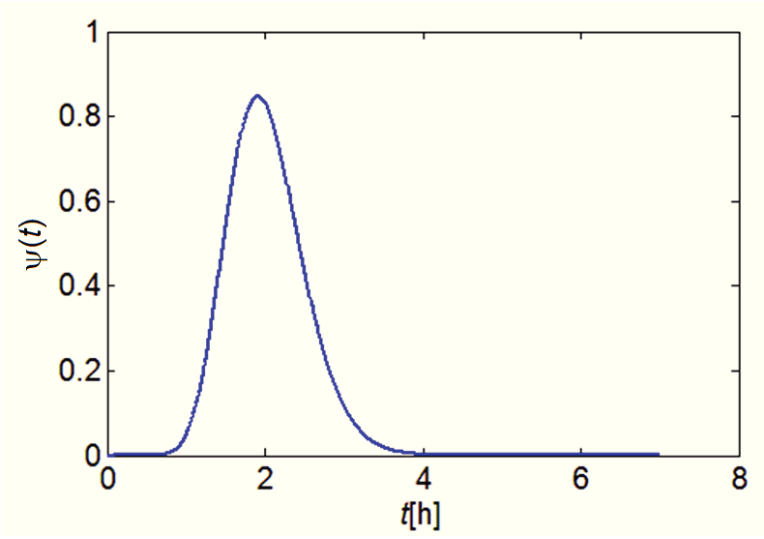

Figure 3.7: Filter function for the FLaIR model, resulting from calibration

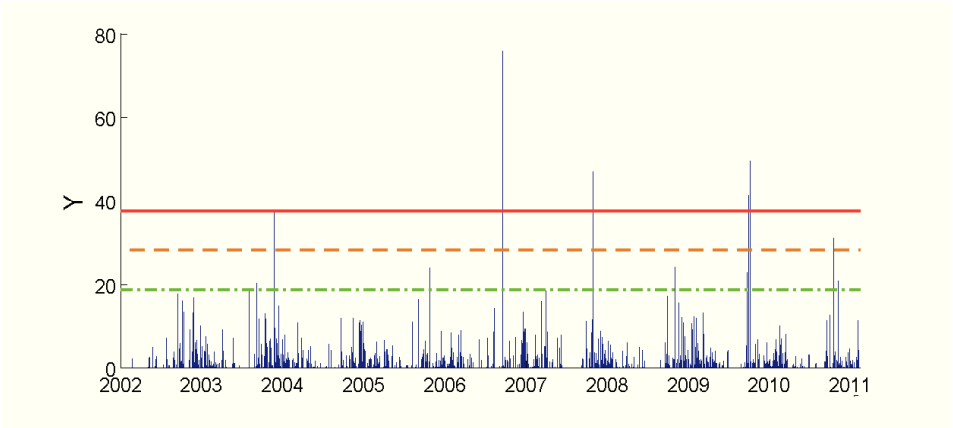

Figure 3.8: Plot of the mobility ratio and comparison with warning levels and rainfall hourly series

3.4 Method based on annual maxima rainfall data

3.4.1 Method

The annual maximum of rainfall $h_i^{(d)}$ for a given duration d is the maximum of cumulative rainfall of duration d that was observed within the $i-th$ year, $i = 1, 2, ..., n$.

These data are typically used for calculation of IDF curves that allow estimation of design hyetograph of fixed return period.

If the starting dates $t_i^{(d)}$ corresponding to the maxima $h_i^{(d)}$, are known, these data may be used, in combination with landslide occurrence information (i.e. date of landslide occurrence), to derive thresholds in terms of rainfall cumulated over duration d.

If more durations are available, one can try with different durations d_j, with $j = 1, 2, ...n_d$ and get the most performing threshold.

The method does not consider the incipient instant of triggering, and just determines thresholds that may be used for landslide early warning because of the correlation with the occurrence of landslides.

With reference to a given duration d, the proposed method consists in the following steps:

1. Identification of the rain gauges of pertinence for the investigated area.
2. Retrieval of the data of annual maxima (date of start and cumulative rain value) of precipitation at the given duration d, for the all the rain gauges of step 1.
3. Retrieval of the historical landslides events occurred in the area (date of occurrence, and if available type of landslide)

4. Classification of the rainfall events in (1) raw positives, i.e. rainfall events having the same start date of a landslide and raw negatives, i.e. rainfall events whose starting date is not the same of a landslide date. This "raw" classification is then refined by keeping only one rainfall event per date, if more than one gauges has the corresponding annual maxima in the same date. In the case that accurate information on the location of landslide is not available, the maximum among the gauges may be a reasonable choice. For raw negatives, this same choice may be reasonable too. At the end a set of Positives P (indipendent rainfall amounts associated with landslide occurrence) and Negatives N (indipendent rainfall amounts not associated with landslide occurrence) results, of size N_P and N_N respectively.

5. Determination of the threshold, by maximization of an objective function B that measures the performances of an hypothetical early warning system based on threshold $x^{(h)}$. This objective function may be based on the *confusion matrix* (in certain contexts denominated *contingency matrix*), shown in tab:confusionmatrix. According to that table, a general objective function may be:

$$B(x^{(h)}) = w_{TP}N_{TP} - w_{FN}N_{FN} + w_{TN}N_{TN} - w_{FP}N_{FP} \tag{3.3}$$

where $w_{XY}, X = F\text{alse}, T\text{rue}, Y = F\text{alse}, T\text{rue}$ are weights given to the corresponding cases of table, for example to account for the different disadvantages associated with a false positive rather than to a false negative (usually the last are greater than the first ones) . A particularly reasonable choice may be $w_{TP} = w_{FN} = w_P$ and $w_{TN} = w_{FP} = w_N$ and $w = w_N/w_P \leqslant 1$. That choice is such that the advantage of a true positive is that it avoids a false negative to occur, and that the same holds when comparing a false positive with a true negative. In this way one may resolve the quantification of the costs of life, because advantage is not quantified in terms of money but in terms of avoided disadvantage, that may include injury and death. The $w \leqslant 1$ condition expresses the fact that the damage induced by a false negative (i.e. missed alarm) usually does not exceed the damage induced by a false positive (i.e. false alarm). These choice yield to the following form of the objective function:

$$B(x^{(h)}) = (N_{TP} - N_{FN}) + w(N_{TN} - N_{FP}) \tag{3.4}$$

3.4.2 Data

Annuall maxima rainfall data of durations 1, 3, 6, 12 and 24 hours of all the rain gauge stations in figure 3.3 , excluded Fiumedinisi are utilized. The period of observation for these stations varies from few years to about 70 for the ones that were installed first, around the 1920s. Averaged, 50 rainfall event dates are available per station (annual maxima in a same station for a same years in general

Table 3.I: Confusion matrix

		Actual	
		Landslide (P)	No landslide (N)
Predicted	Landslide: $h_i^{(d)} > x^{(d)}$	True Positive, TP	False positive, FP
	No Landslide: $h_i^{(d)} \leqslant x^{(d)}$	False Negative, FN	True Negative, TN

do have different starting date, even though it is quite common that the 5 annual maxima of different durations have the same starting date).

Information on landslides are retrieved from the AVI database, which has been consulted from the SICI (Sistema Informativo sulle Catastrofi Idrogeologiche, Informative System on Hydro-geological Disasters) website `http://sici.irpi.cnr.it/` (**?**). This database is updated to 2001. It was firstly queried for the Messina province, then a selection of landslides occurred in the Peloritani Mountains was made, yielding 59 landslide events for the period 1924 (?)- 2001.

It was made an attempt to distinguish among the various types of landslides that occurred, in order to understand if more than one type of threshold were necessary, but information of this type was seldom available, at least for this investigated area. Hence I relied on the fact that in the area is mostly homogeneous with respect to landslide types observed (shallow landslides, debris-flows).

Slightly anticipating the results of applications, 3.9 shows the plot in time of the number of landslides in the AVI database and the number of dates for which also an annual maxima was observed, in at least one of the selected stations, and for at least one duration among $1 - 24$ hours.

In total the proportion of these rainfall data to the landslide data is of $25/59 = 42\%$. This percentage this occurs mainly because landslides may had occurred for dates for which rainfall amount did not result to be an annual maximum at any duration. Yet, the database of landslides is far from being complete, and this is more true the more one goes back in time, as demonstrated by the drastic decrease of landslide information (very strong in the period 1997-2001, i.e. the last 5 years). However, this may be the effect of excessive land use and/or of climate change, of difficult quantification.

With the aim of updating the available data, information was searched from various sources, such as newspapers and Civil protection Bulletins. For calibration of the model the following events were added to the AVI database information, the Messina 01/10/2009 (rainfall data available from S. Stefano di Briga station);

Moreover, in order to somehow validate the results of the methodology, we use the 10 minutes rainfall time series of the automatic rain gauge of Fiumedinisi, managed by SIAS, Servizio Informativo Agrometeorologico Siciliano (Sicilian AgroMeteorological Information Service). Data from this station used here cover the period from 21/02/2002 to 2009. Validation has been carried out applying the derived threshold to the d-hours rainfall time series, computed form the 10 minutes series, and the landslide events of the dates: 15 September 2006, 25 October 2007, 24-September-2009 and 1 October 2009. The inclusion in the validation of dates

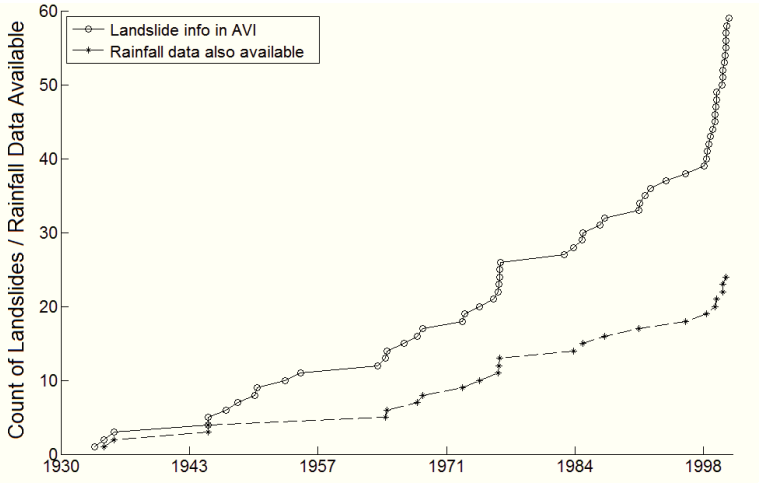

Figure 3.9: Time plot of number of landslides from the AVI database and simultaneous rainfall data availability

already considered in model calibration has been considered possible, because the rain gauges considered in the calibration do not include Fiumedinisi.

3.4.3 Results and discussion

Plot of figure 3.10 shows the results of the match of landslide and rainfall information. The plot shows results for all the durations 1, 2, 3, 6, 12, and 24 hours considered. Cumultative rainfall amounts of the same stations and same date are joined with a line. This is not the plot of event's cumulative rainfall time history, because annual maxima are computed starting from a different time instant in general, but may give an idea of that time history. However this is not important for application of the methodology, since it is aimed to determine a threshold to apply to a given d hours duration cumulative rainfall series, updated instant per instant.

Red lines in figure 3.10 denote that the rainfall amounts are associated with landslides (as mentioned before, these sum to 25 events), while in green are represented the rain data that did are associated with landslides. Being seldom available accurate information on the location of landslides, the greatest value of rainfall was chosen for each duration. In fact a slightly modified criterion was applied, i.e. the rainfall event that produced the maximum rainfall at the maximum duration available (in most of the cases 24 hours) was considered.

From the plot one notices a wide scattering of the data, both in the cases of association and not association of landslides. There is also a noticeable superimposition of these two cases, yet a significant difference between the corresponding minimum values of rainfall can be observed.

Surely this behavior is a consequence of the significant degree of and to the simplicity of the model, but it puts into evidence that presumably threshold based

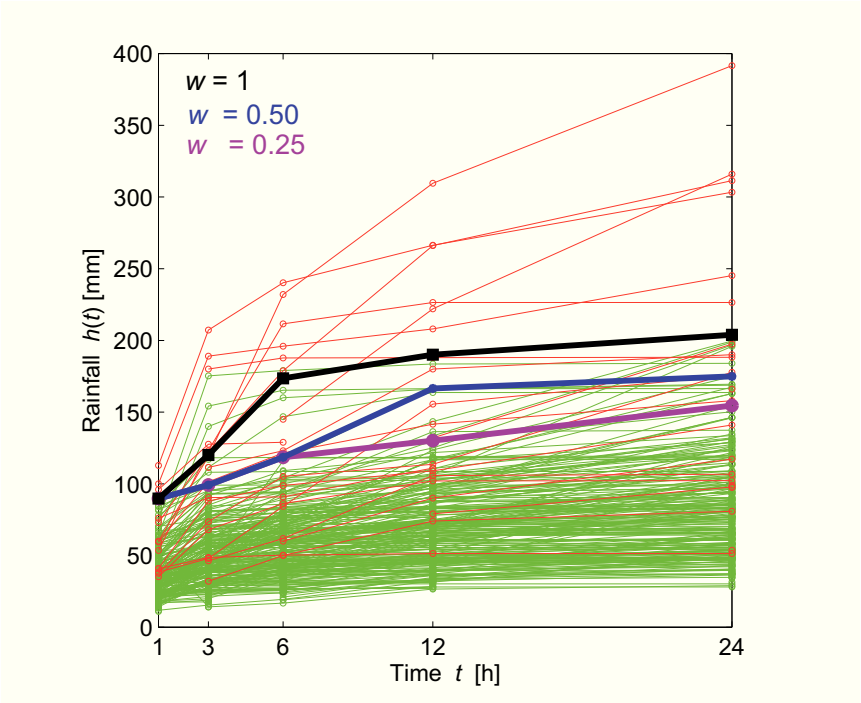

Figure 3.10: Plot showing empirical thresholds and data from which they are derived

on the triggering events only are of questionable reliability, and may lead to a great number of False Alarms. This is in concordance with the findings of other researches (**?**, cf., e.g.), relatively to the I-D thresholds.

Maximization of the objective function 3.4, for different values of w $(1, \frac{1}{2} and \frac{1}{4})$ yield the thresholds shown in the same figure 3.10. Results are also shown, for sake of clarity, in 3.II , together with the results of the validation.

Validation, carried out only for the $w = 0.5$ case, show that the performances of the threshold vary with duration. Best results were obtained for the duration of 3 hours, for which threshold was exceeded only for all the 4 observed landslide events. Thus, a good threshold for the Peloritani Mountains area may be: $x^{(3)} = 100$ mm.

Table 3.II: Thesholds maximizing the objective function, at various cumulative rain durations a w values. Results of validation of the thresholds

Duration d	Threshold [mm]			Model validation
[h]	$w = 1$	$w = 0.5$	$w = 0.25$	landslide dates
1	90	90	90	ii
3	120	99	99	i,ii,iii,iv
6	174	119	119	i, ii
12	190	167	130	i, ii
24	204	175	155	i, ii

3.5 Conclusive remarks

This chapter has focused on empirical methodologies for the determination of rainfall thresholds for landslide early warning.

Results related to the application of two approaches for determining rainfall thresholds have been illustrated, with reference to the case-study area of the Peloritani Mountains.

Firstly, FLaIR model application has been carried out. Results seem to indicate the suitability of this model for early warning in the area, even though a longer series than the one available (9 years long) may be desiderable, in order to better calibrate and validate the model. A point related to this issue is that FLaIR model may be sensitive to completeness of knowledge of historical landslide dates. In fact, the more long the series is, the more likely is to have incomplete landslide information. As a consequence, the model may erroneously result "incongruent" (FLA) and hence not suitable.

Secondly, and approach that derives rainfall thresholds by combining annual maximum precipitation for fixed duration data with landslide occurrences observed in the past has been proposed and applied. The main advantage of this approach is the use of a large dataset of rainfall data (about 80 years long) available for the entire Italian territory, also in order to better exploit the AVI collection of landslide events, that covers all the past century. The method accounts for both triggering

and not triggering rainfall events. This method may not account sufficiently for antecedent precipitation, which however seems to be more important for deeper slides than the ones observed in the investigated area.

The final conclusion is that empirical model may give an easy and practical solution to the problem of determining rainfall thresholds for regional landslide early warning, yet the quality of data controls quality and reliability of the threshold. Accounting for the rainfall events that have not triggered landslides, and not only the ones that did, may be an easy way to assess model's reliability and soundness.

Chapter 4

Monte Carlo physically-based simulation methodology

4.1 Preliminary remarks

This chapter illustrates the Monte Carlo simulation method used in this work to study the hydrologic control on shallow landslide triggering.

The methodology consists in the coupling a stochastic rainfall generator and a physically-based model for infiltration and slope stability analysis.

Monte Carlo method allows the generation of a statistically ideal dataset, in which rainfall, pore pressure and factor of safety are known continuously for an unlimited period. Simultaneous observations of rainfall and landslides, are in most of the cases available only for few years and are not of comparable detail.

Potentiality of the the Monte Carlo method has been put in light by Metropolis and Ulam (1949). Uncountable are the technical and research applications of this method in hydrology.

Some applications in the research field of landslides do exist.

In particular, some studies focus on sensitivity analysis of slope-stability hydrologic physically-based models to geotechnical properties (e.g. Zhou et al., 2003; Frattini et al., 2009). Other researches investigated issues related to debris-flow run-out (cf., e.g. Luna et al., 2012). Calvo and Savi (2009) utilized the Neyman-Scott Rectangular Pulses model in combination with empirical models of landslide triggering and the FLO-2D debris-flow run-out model (O′Brien et al., 1993) to assess debris-flow risk.

A similar methodology to the one utilized here, has been applied to flood-flood risk assessment by Rulli and Rosso (2002), in which a Generalized Neyman-Scott Rectangular Pulses rainfall model (Cowpertwait, 1994; Cowpertwait and O'Connell, 1997) is coupled with a spatially distributed physically-based rainfall-runoff model.

4.2 Simulation scheme

Figure 4.1 illustrates schematically the Monte Carlo simulation methodology applied in this work.

A rainfall time series is used to calibrate and validate a stochastic rainfall model. In particular, the Neyman-Scott Rectangular Pulses (NSRP) model is utilized to generate hourly rainfall at a point. NSRP model is chosen because it represents a compromise between flexibility and complexity (only five parameters per season). Numerous applications corroborate its validity, so that NSRP represent a classical choice that its worthwhile to investigate.

The synthetic rainfall time series is then preprocessed to separate rainfall events from dry time intervals (event interarrivals). This event separation is important for two reasons: firstly, to properly use the physically-based hydrological model, as described below, and, secondly, to univocally define input and output quantities to be analyzed.

The result of rainfall preprocessing is then used as input to the physically-based hydrological and slope stability model.

In particular, the TRIGRS v.2 model (Baum et al., 2008) is used to simulate transient infiltration and slope stability within rainfall events. Then the final input of TRIGRS, represented in figure 4.1 as $\psi_i(t_f)$ is used in input to a water-table recession (WTR) model to estimate the initial water table depth $d_i(0)$ at the beginning of event $i+1$, that is simulated with TRIGRS. The binary signal at the bottom of figure, represent the running times of TRIGRS and WTR models. Procedure may be started with an arbitrary value of the initial water table depth $d_1(0)$ for the first simulation (in that case first years of simulation are discarded), or with a known/plausible value.

The simulations are applied to a single cell of the analyzed domain. Cell properties are varied to meet all values in the domain, at a sufficient discetization. Results are then applied to the whole domain, in a spatially-distributed fashion, by interpolation (cf. section 7.4.1).

The NSRP model and the TRIGRS-WTR model are described in detail in chapters 5 and 6, respectively. The methods for rainfall event identification and of simulation output analysis are described in the following two sections.

4.3 Identification of rainfall events

Rainfall events within a continuous (observed or synthetic) time series, aggregated at a fixed time scale, are in this work defined by means of the following parameters, applied in sequence:

1. A threshold of minimum rainfall Δh_{min}. Rainfall at the fixed aggregation time is neglected if it is less than Δh_{min}. This threshold may be useful to remove very low values of precipitation in the synthetic time series. In particular, application of the Δh_{min} threshold is particularly useful to validate

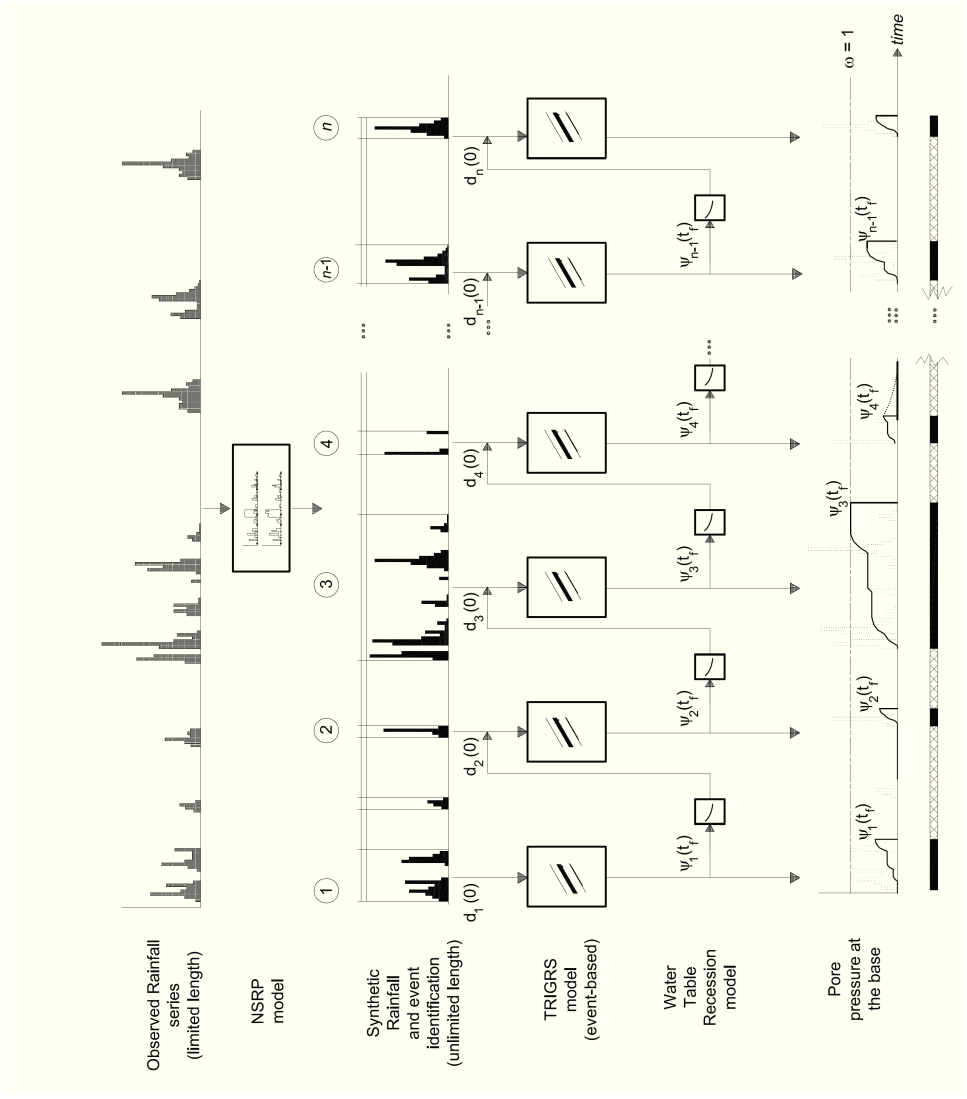

Figure 4.1: Scheme of the Monte Carlo Simulation used to investigate hydrologic control on landslide triggering

the stochastic rainfall model, because observed series do have this threshold, related to the sensitivity of the rain gauge. For instance, in an observed hourly rainfall time series, sensitivity may be of 0.2 mm.

2. A minimum interarrival time Δt_{min}, for event separation. If the time interval covered by a run of zeros in the series $\Delta t_{i,i+1}$ is not greater than Δt_{min} then the successive sequence of non-zero precipitation is joined to the previous one. Otherwise two separate rainfall events are considered. For example, in figure 7.2.3 the first rainfall event is the result of two wet spells; its total volume (cumulative rainfall) and duration are $W_1 = w_1 + w_2$ and $D_1 = \Delta t_1 + \Delta t_{1,2} + \Delta t_2$. Δt_{min} may be assumed to be of a couple of hours, in relation to climate and hydraulic properties of the simulated area (cf. section 6.2).

3. A minimum volume W_{min} threshold. This is applied only for computational convenience, i.e. It is assumed that if $W < W_{min}$, the response (in terms of pore pressure or factor of safety) is negligible.The use of this threshold is shown in figure 4.1: simulation is not carried out for the rainfall event in between ① and ②, because its cumulative rain is less than W_{min}. Application of W_{min} drastically reduces the computation time, because no simulation is carried out for seasons of low precipitation (e.g., summer months in the Mediterranean area)

4. An *after-rain* time parameter Δt_a. The TRIGRS event-based continues running for Δt_a hours after the end of the event. This is done because the peak of pore pressure may occur after the rainfall event, especially for short durations (cf., e.g. Iverson, 2000; D'Odorico et al., 1995).

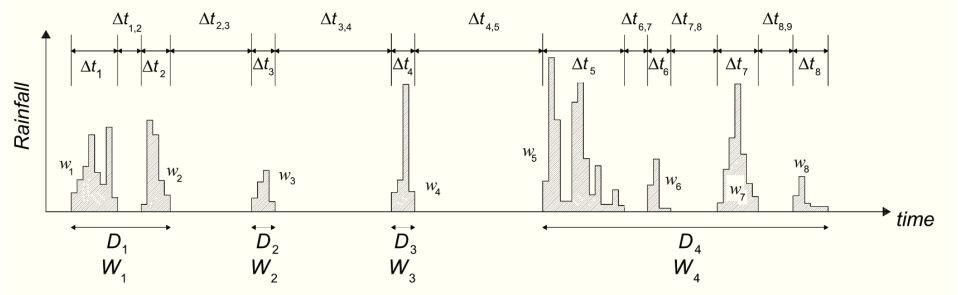

Figure 4.2: Definition of total duration, volume and interarrival time of rainfall events

4.4 Methodology of analysis of simulation

The output of simulations is utilized in this work to analyze:

- The return period of landslide triggering (or, more generally, of a given pore pressure or factor of safety);
- The direct relationship between rainfall events and slope stability (rainfall threshold).

4.4.1 Return period

Return period is defined as the expected value of the inter-arrival time of a given event of interest.

In the case of landslide modeling, main interest is on the determination of the return period of $FS \leqslant 1$. Equivalently, the event $FS \leqslant 1$ may be expressed as $\psi > \psi_{cr}$, where ψ_{cr} is the pore pressure at which corresponds an $FS = 1$.

Pore pressures are generated at the same temporal resolution of the input rainfall series (hourly).

Statistical auto-dependence occurs within such a series, because the generic initial water table depth $d_i(0)$ is the result of antecedent rainfall.

Yet this statistical dependence is in many cases limited to the hydrological year. For instance, in the Mediterranean area, the summer season is usually dry and long enough to bring to zero the surficial water table height at the beginning of the rainy season (September).

This allows to consider annual maxima of pore pressure statistically independent, and to compute the return period of ψ_{cr} pore pressure, with the formula:

$$T_R = \frac{1}{1 - F(\psi_{cr})}. \tag{4.1}$$

where $F(\psi_{cr})$ is the non-exceedance probability of ψ_{cr}. Because simulations are carried out for a large number of years, no parametric distribution is assumed for ψ_{cr} and the empirical cumulative frequency distribuition is are directly used for $F(\psi_{cr})$.

4.4.2 Rainfall-Landslide occurrence relationship

As discussed in section 2.2, several empirical models have been proposed for assessing rainfall thresholds of landslide triggering, that try to relate directly rainfall and landslide occurrence.

The Monte Carlo approach is utilized in this work to investigate on the relationship between rainfall and landslide occurrence, i.e. to evaluate the effect of the stochastic nature of rainfall (randomly variable rainfall intensity) on landslide triggering thresholds.

The relationship between rainfall intensity and duration and landslide occurrence is investigated in this work, because it is perhaps the most interesting case, considering its widespread and consolidated use in determination of empirical thresholds.

Intensity I and duration D to landsliding, are defined according to the usual empirical reference scheme (see, e.g., Aleotti, 2004), as shown in figure 4.3. In

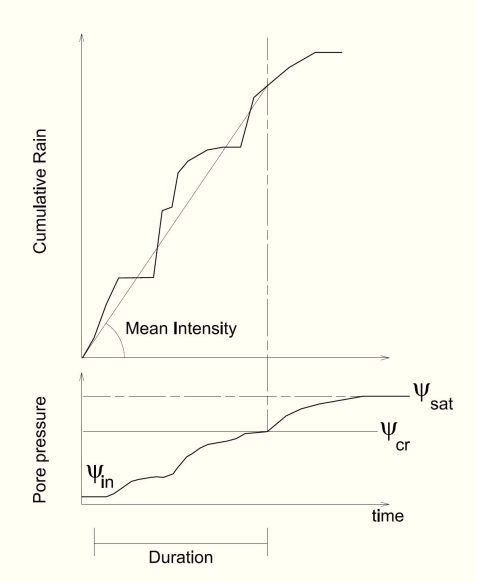

Figure 4.3: Definition of rainfall duration D and (mean) intensity I to landsliding

particular, antecedent rainfall induces the presence of an initial water table height, that is, a initial pore pressure ψ_{in}. Then pore pressure increases in response to rainfall, and the critical pore pressure $= \psi_{cr}$, with subsequent slope failure, may be reached. Figure 4.3 also puts in evidence that pore pressure cannot exceed the one corresponding to a water table at the ground surface ψ_{sat}, i.e. a fully saturated soil.

Simulations yield to a large dataset of intensities and durations corresponding to landsliding. Confrontation of simulation results with an empirical models equation, allows to evaluate from a stochastic physically-based perspective the empirical model itself. In an ideal situation, the pore pressure (equivalently, the factor of safety) may be constant for curves that are represented by the empirical model's equation. For instance, for the I-D empirical model, iso-ψ simulation points should lay on a straight line in the $\log D$ -$\log I$ plane.

4.5 Software

Computer programs where developed and used to apply the Monte Carlo methodology described in this chapter.

In particular, for the NSRP rainfall model, all codes were specifically developed for the application herein, in MATLAB®. The developed programs allowed

to calibrate, validate and then simulate rainfall at the desired aggregation time. Minimization of the objective function for NSRP parameter estimation 5.20, has been carried out by optimization algorithms implemented in MATLAB optimization toolbox® , which is based on Nelder-Mead simplex method (Nelder and Mead, 1965), that was successfully used for the scope by other researchers (cf. e.g. Favre et al., 2004)

The TRIGRS FORTRAN program, version 2.0 model physically-based model for simulating landslide triggering is available to interested users at the website `http://pubs.usgs.gov/of/2008/1159/`. The source code of this program is also available for customization. Manual (Baum et al., 2008) that describes the theoretical basis and operation of the program, is available from the same website. It is worthwhile to say that a previous version of the model (Baum et al., 2002), version 1.0, is available from another website. This model is a spatially-distributed extension of the Iverson (2000) model, coupled with a diffusive model for . The version 2.0 used here is still a vertical-infiltration-based model, but it is based on less restrictive assumptions than the model of Iverson (2000) (see chapter 6).

No internal modification of the FORTRAN program was carried out, and the executable files of TRIGRS were directly used, as distribuited on the website mentioned above. Externally-operating codes have been developed to allow interaction between the NSRP, the TRIGRS and the WTR models, that involves what is described in this chapter (rainfall separation algorithm, and analysis of simulation output). These codes are dedicated to automatically write the input text files for TRIGRS (stochastically generated rainfall events), collect the output of multiple simulations, and finally perform the analysis briefly described in the previous section.

Chapter 5

Neyman-Scott Rectangular Pulses rainfall model

5.1 Preliminary remarks

In many hydrological problems and related hazard and risks analysis, the length of historical records of the hydrological variable of interest may be insufficient to enable reliable statistical analysis of data. Such is often the case of landslides, and also of many other natural hazards.

Synthetic generation of time series of the variable of interest via stochastic models, such as precipitation, has been used by many researchers in order to perform Monte Carlo simulations aimed to characterize probabilistically the output of interest.

Stochastic models of rainfall have been used to generate rainfall data for use in a variety of situations, such as reservoir design (at a time scale from daily to monthly), flood studies (at a time scale from hourly to daily) and design of sewerage systems (at a sub-hourly time scale)

In the present chapter the Neyman-Scott Rectangular Pulses (NSRP) model of rainfall is exploited to generate hourly rainfall at a point, based on the calibration on a station of interest. Cluster models, like the NSRP, are appealing for rainfall time series simulation, as they have built into their structure the capability of representing rain cells (Cowpertwait, 1991), which are known to exist in actual rainfall events (Amo). Also the NSRP is able to preserver rainfall statistics over a range of time scales (Rodriguez-Iturbe et al., 1987b) as it may be able to match the statistical properties of temporal rainfall at different scales of aggregation which go from 1-24 hours (Rodriguez-Iturbe et al., 1987b). Hence, one may be able to infer the statistical properties at a finer time scale than the one at which rainfall was observed, which may be useful in many practical situations. In other words the model would statistically match simultaneously the 1-, 6-, 12-, and 24-hour past history.

Although various improvements of the NSRP model have been suggested by

researchers (see section 5.2), this model is here chosen because it represents a compromise between flexibility and complexity (only five parameters per season) and numerous applications corroborate its validity.

5.2 Process

A brief introduction to point process modelling is given in Salas (1993). A distinction is made between *simple point processes* and *cluster processes*. In the first case only one precipitation burst, i.e. a random a rainfall amount (e.g. *Poisson White Noise* process, PWN) or pulse (e.g. *Poisson Rectangular Pulse* model process, PRP), is associated with a storm. In the second case for each storm more than one precipitation bursts are in general associated with each storm, in terms of random rainfall amounts (e.g. *Neyman-Scott White Noise* process, NSWN) or pulses (e.g. *Neyman-Scott Rectangular Pulses* process, NSRP).

More precisely, the NSRP process may be described with reference to the sketch of figure 5.1, as follows:

- Storm-generating mechanisms (systems), or simply *storms* or *origins*, arrive governed by a Poisson process of parameter λt. It follows that , the interarrival times t_i between storms are exponential distribuited with parameter λ, namely with cdf (Mood et al., 2001):

$$F_T(t) = 1 - \lambda \mathrm{e}^{-\lambda t}. \tag{5.1}$$

- For each origin a random number C of precipitation bursts (or rain cells) are generated, typically according to a geometric or Poisson distribution. In particular, in the first case it is assumed that the variable $C' = C - 1$ follows a geometric distribution of mean $\nu - 1$, i.e. the mass probability function (pmf) of C' is

$$p_{C'}(c') = \frac{1}{\nu}\left(1 - \frac{1}{\nu}\right)^{c'}. \tag{5.2}$$

  with $c' = 0, 1, 2, ...$ (which implies $c = 1, 2, ...$). In the second case C' is assumed Poisson distributed with mean $\nu - 1$, i.e. pmf is

$$p_{C'}(c') = \frac{\nu^{c'}}{c'!}\mathrm{e}^{-\nu} \tag{5.3}$$

  The Poisson assumption may be advantageous for calibration, because the dry spells probabilities and dry-dry and wet-wet transition probabilities are also available as a function of parameters after Cowpertwait (1991), as described below.

- Each cell has origin at time $\tau_{i,j}$ with $j = 1, 2, ..., c_i$ from t_i, according to an exponential random variable of parameter β:

$$F(\tau) = 1 - \beta \mathrm{e}^{-\beta \tau}. \tag{5.4}$$

- With each rain cell, a rectangular pulse of duration $d_{i,j}$ and intensity $x_{i,j}$ is associated. Pulses typically are assumed to have duration D exponential distributed with parameter η: $F_D(d) = 1 - \eta e^{-\eta d}$. Intensities X are typically extracted from a exponential distribution of parameter ξ. Also the Weibull is suitable for the pulse intensities, which has cdf

$$F_X(x) = 1 - e^{-\xi x^b} \tag{5.5}$$

  In this case, typically only ξ participates to the calibration procedure and an $0 < b < 1$ is fixed (typically $b = 0.6 - 0.9$). This may lead to better fits in the extreme value distribution of data (cf., e.g., Cowpertwait et al., 1996).

- Finally, the total intensity at any point in time is the sum of the intensities of all active cells at that point: if $Y(t)$ is the total intensity at time t given by the NSRP model and $X_{t-u}(u)$ is the intensity at time t owing to a cell with origin at $t - u$, then

$$Y(t) = \int_{u=0}^{u=+\infty} X_{t-u}(u) dN(t-u) \tag{5.6}$$

  where:

$$dN(t-u) = \begin{cases} 1 & \text{if there is a cell origin at} \quad t-u \\ 0 & \text{otherwise} \end{cases} \tag{5.7}$$

  and

$$X_{t-u}(u) = \begin{cases} X & \text{with probability} \quad \exp(-\eta u) \\ 0 & \text{with probability} \quad 1 - \exp(-\eta u) \end{cases} \tag{5.8}$$

Various improvements of the NSRP model have been suggested by researchers.

Rectangular pulses may be of low physical meaning; Rodriguez-Iturbe et al. (1987b), suggested by that an improvement may be achieved by assuming a triangular or gamma-like shape for the pulses, because it may describe better the rain intensity of a cell through its life cycle.

Another point is that the NSRP model assumes independence between cell intensity and duration, which may be unrealistic; this issue was addressed by Evin and Favre (2008) by means of a copula approach aimed to model dependence between cell depth and duration.

Furthermore, from a physical perspective, the NSRP model only allows for the existence of one type of rectangular pulse, i.e. one type of rain cell. It is well known that commonly different types of cells are responsible for rainfall observed at a point. Therefore, it may be argued that the parameter estimates for the intensity and duration of the cells in the NSRP model are likely to be average values over the various types of precipitation that can occur in the same precipitation field. To overcome this shortcoming Cowpertwait (1994); Cowpertwait and O'Connell (1997) developed a Generalized version of the NSRP process, that allows existence of more than one type of cell (typically two types: one that mimics stratiform cells and another convective cells). Furthermore Cowpertwait (2004) proposed another model where rainfall is generated by the superimposition of two independent NSRP processes.

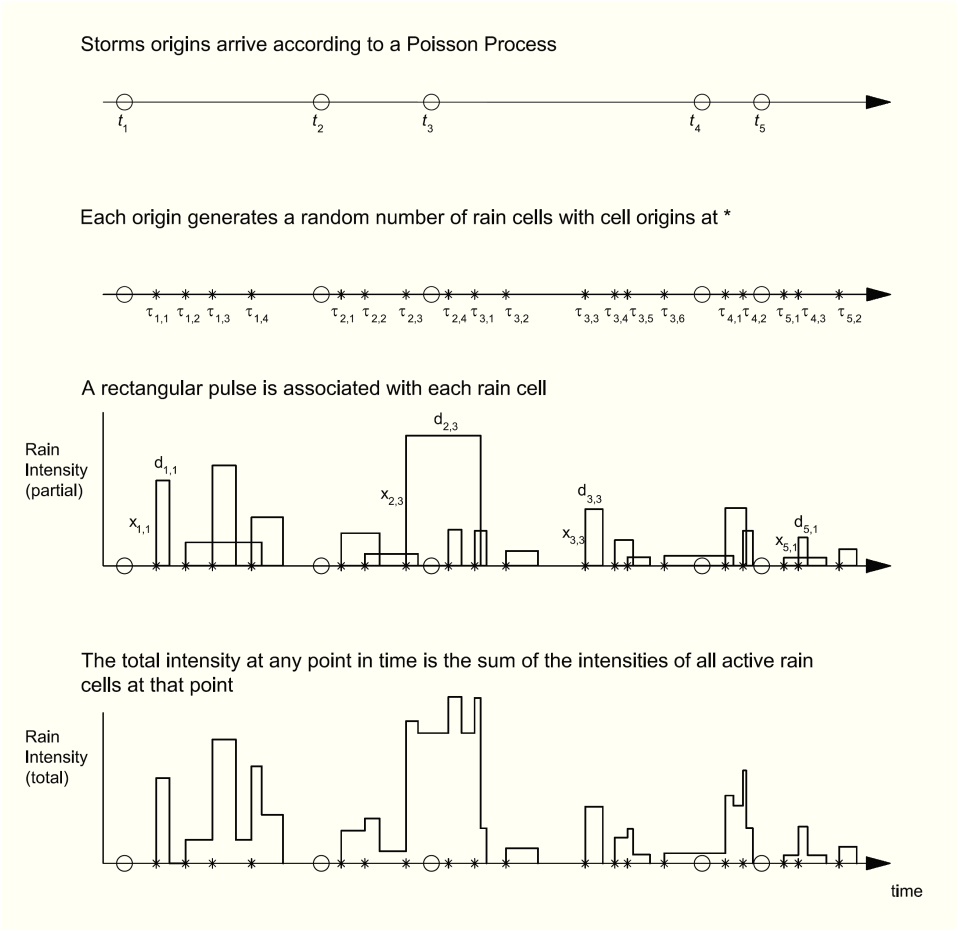

Figure 5.1: Sketch of the Neyman-Scott Rectangular Pulses process (adapted from Cowpertwait et al. (1996) and Salas (1993))

5.3 Properties of the NSRP process

Of main interest are the properties of the NSRP process aggregated at a time scale h, because rainfall data are usually only available in that form, e.g. as historical records of hourly- or daily-aggregated totals.

Let $Y_i^{(h)}$ be the aggregated rainfall depth in the ith time interval of length h so that:

$$Y_i^{(h)} = \int_{(i-1)h}^{ih} Y(t)dt \tag{5.9}$$

Thus, if h is measured in hours, the series $\{Y_i^{(h)} : i = 1, 2, ...\}$ is a rainfall time series at the h-hour level of aggregation, i.e. an h-hourly rainfall time series.

Second-order properties of $Y_i^{(h)}$ were derived by Rodriguez-Iturbe et al. (1987a), as follows:

$$\mu(h) = E[Y_i^{(h)}] = \frac{h\lambda E[C]E[X]}{\eta} \tag{5.10}$$

$$\begin{aligned}\gamma(h) &= Var[Y_i^{(h)}] = \frac{\lambda(\eta h - 1 + \mathrm{e}^{-\eta h})(2E[C]E[X^2] + E[C^2 - C]E^2[X]\beta^2)}{(\beta^2 - \eta^2)\eta^3} + \\ &- \frac{\lambda(\beta h - 1 + \mathrm{e}^{-\beta h})E[C^2 - C]E^2[X]}{\beta(\beta^2 - \eta^2)}\end{aligned} \tag{5.11}$$

$$\begin{aligned}\gamma(h,l) &= Cov[Y_i^{(h)}, Y_{i+l}^{(h)}] = \frac{\lambda(1 - \mathrm{e}^{-\eta h})^2\mathrm{e}^{-\eta(l-1)h}(E[C]E[X^2] + \frac{1}{2}E[C^2 - C]E^2[X]\beta)}{(\beta^2 - \eta^2)\eta^3} + \\ &- \frac{\lambda(1 - \mathrm{e}^{-\beta h})^2\mathrm{e}^{-\beta(l-1)h}E[C^2 - C]E^2[X]}{2\beta(\beta^2 - \eta^2)}\end{aligned} \tag{5.12}$$

where $l \geqslant 1$ denoting the time lag.

Expression for the expectations that appear in equations 5.10 − 5.12, may be derived from well-known properties of the expected value and variance. In the case that a Poisson distribution is chosen to model the number of rain cells $C = C' + 1$:

$$\begin{aligned}E[C] &= E[C' + 1] = E[C'] + 1 = \nu \\ E[C^2 - C] &= E[C^2] - E[C] = \\ &= (\mathrm{Var}[C] + E^2[C]) - \nu = \\ &= \mathrm{Var}[C' + 1] + E^2[C] - \nu = \mathrm{Var}[C'] + E^2[C] = \nu^2 - 1\end{aligned} \tag{5.13}$$

Expression of expectations for the intensity X, in the general case that it is modeled by a Weibull distribution, are (in the case that an exponential distribution is used,

expression are obtained letting $b = 1$):

$$\begin{aligned} E[X] &= \left(\frac{1}{\xi}\right)^{\frac{1}{b}} \Gamma\left(1+\frac{1}{b}\right) \\ E[X^2] &= \mathrm{Var}[X] + E^2[X] = \left(\frac{1}{\xi}\right)^{\frac{2}{b}} \left[\Gamma\left(1+\frac{2}{b}\right) + \Gamma^2\left(1+\frac{1}{b}\right)\right] + \frac{1}{\xi^2}\Gamma^2\left(1+\frac{1}{b}\right) = \\ &= \left(\frac{1}{\xi}\right)^{\frac{2}{b}} \Gamma\left(1+\frac{2}{b}\right) - \left[\frac{1}{\xi^2} - \left(\frac{1}{\xi}\right)^{\frac{2}{b}}\right] \Gamma\left(1+\frac{1}{b}\right) \end{aligned} \tag{5.14}$$

Use of equations 5.10 − 5.12 at two different time scales has been the usual procedure for estimating parameters of the NSRP through the method of moments (Calenda and Napolitano, 1999), as described after. In particular autocorrelation $\rho(h,l) = \gamma(h,l)/\gamma(h)$, typically at lag $l = 1$, is used in place of covariance.

In the case the it is assumed that $C - 1$ follows a Poisson distribution with mean $\nu - 1$, the following expression for the probability that an arbitrary interval of length h is dry was derived by Cowpertwait (1991):

$$\begin{aligned} \phi(h) = \mathbb{P}[Y_i^{(h)} = 0] = \exp\Bigg(-\lambda h + \lambda \frac{1 - \exp[1 - \nu + (\nu-1)\exp(-\beta h)]}{\beta(\nu-1)} + \\ - \lambda \int_0^\infty [1 - p_h(t)]dt \end{aligned} \tag{5.15}$$

where

$$\begin{aligned} p_h(t) &= \left[\mathrm{e}^{-\beta(t+h)} + 1 - \frac{\eta \mathrm{e}^{-\beta t} - \beta \mathrm{e}^{-\eta t}}{\eta - \beta}\right] \times \\ &\times \exp\left\{(1-\nu)\beta \frac{\mathrm{e}^{-\beta t} - \mathrm{e}^{-\eta t}}{\eta - \beta} - (\nu-1)\mathrm{e}^{-\beta t} + (\nu-1)\mathrm{e}^{-\beta(t+h)}\right\} \end{aligned} \tag{5.16}$$

The transition probabilities, $\mathbb{P}[Y_{i+1}^{(h)} > 0 | Y_i^{(h)} > 0]$ and $\mathbb{P}[Y_{i+1}^{(h)} = 0 | Y_i^{(h)} = 0]$, denoted as $\phi_{WW}(h)$ and $\phi_{DD}(h)$, respectively, can be expressed in terms of $\phi(h)$ and follow as (Cowpertwait, 1991):

$$\phi_{DD}(h) = \phi(2h)/\phi(h) \tag{5.17}$$

$$\phi(h) = \phi_{DD}(h)\phi(h) + \{1 - \phi_{WW}(h)\}\{1 - \phi(h)\} \tag{5.18}$$

so that:

$$\phi_{WW}(h) = \{1 - 2\phi(h) + \phi(2h)/\{1 - \phi(h)\} \tag{5.19}$$

5.4 Calibration

Calibration of the NSRP model can be carried out by exploiting the properties of the NSRP process, shown above. In particular, the method of moments is generally employed for its simplicity (Calenda and Napolitano, 1999).

In particular, model parameters ($\lambda, \nu, \beta, \eta$ and ξ) may be estimated using as many moments as the parameters of the model (five), usually considering various properties (moments) at various time scales h_i (typically, $i = 2$: for instance, $h_1 = 1$ h and $h_2 = 24$ h), and solving the related equation system, where the theoretical expressions, containing the parameters, are equated to the sample moments. Early applications considered the following choice: $\mu(h_1)$,$\gamma(h_1)$,$\gamma(h_2)$,$\rho(h_1, 1)$ and $\rho(h_2, 1)$.

Because the equation system that is obtained is non linear, it must be solved by numerical minimization of an objective function S, that measures the global error between theoretical and sample moments. In fact, more than the strictly necessary moments can be exploited to match more properties. Commonly the following objective function is utilized:

$$S(\lambda, \nu, \beta, \eta, \xi) = \sum_{i=1}^{n_p} w_i \left(\frac{\hat{f}_i - f_i}{\hat{f}_i} \right)^2 \tag{5.20}$$

where $n_p \geqslant 5$ is the number of properties considered for NSRP calibration, $\hat{f}_i$ are sample estimates of the properties, $f_i(\lambda, \nu, \beta, \eta, \xi)$ are the theoretical values of the properties and w_i are weights that can be eventually assigned to the moments in order to give them more or less importance. Optimization has to be constrained to $\lambda, \beta, \eta, \xi > 0$ and $\nu > 1$.

Estimation of sample properties may be carried out via the following formulas:

- Sample mean $\hat{\mu}_k(h)$:

$$\hat{\mu}_k(h) = \frac{1}{n n_k^{(h)}} \sum_{i=1}^{n} \sum_{j=1}^{n_k^{(h)}} Y_{i,j,k}^{(h)} \tag{5.21}$$

- Sample variance:

$$\hat{\gamma}_k(h) = \frac{1}{n n_k^{(h)} - 1} \sum_{i=1}^{n} \sum_{j=1}^{n_k^{(h)}} \left(Y_{i,j,k}^{(h)} - \hat{\mu}_k(h) \right)^2 \tag{5.22}$$

- Sample lag 1 covariance:

$$\hat{\gamma}_k(h, 1) = \frac{1}{n(n_k^{(h)} - 1) - 1} \sum_{i=1}^{n} \sum_{j=1}^{n_k^{(h)} - 1} (Y_{i,j,k}^{(h)} - \hat{\mu}_k(h))(Y_{i,j+1,k}^{(h)} - \hat{\mu}_k(h)) \tag{5.23}$$

  Covariance for $l > 1$ is estimated analogously.

- Probability of a dry is given by

$$\hat{\phi}_k(h) = \frac{n_k^{(00)}(h) + n_k^{(01)}(h)}{n n_k^{(h)}} \tag{5.24}$$

- Transition probabilities may be estimated after Cancelliere and Salas (2004) :

$$\hat{\phi}_k^{DD}(h) = \frac{n_k^{(00)}(h)}{n_k^{(00)}(h) + n_k^{(01)}(h)} \tag{5.25}$$

and

$$\hat{\phi}_k^{WW}(h) = \frac{n_k^{(11)}(h)}{n_k^{(11)}(h) + n_k^{(10)}(h)} \tag{5.26}$$

where k is a season index (for example, if a NSRP is caibrated separately for each and all of the months of the year, $k = 1, 2, ..., 12$), $Y_{i,j,k}^{(h)}$ is the jth h-hourly rainfall total in year i for season k, $n_k^{(h)}$ is the number of h-hourly totals in season k, n s the number of years of record, while $n_k^{(AB)}(h) = \sum_{i=1}^{n} \sum_{j=1}^{n^(h)_k - 1} I_{i,j,k}^{(AB)}$ where $I_{i,j,k}^{(AB)}$ is an indicator function defined as

$$I_{i,j,k}^{(AB)} = \begin{cases} 1 & \text{if} \quad \text{sign}[Y_{i,j,k}^{(h)}] = A \quad \text{and} \quad \text{sign}[Y_{i,j+1,k}^{(h)}] = B \\ 0 & \text{otherwise} \end{cases}$$

with $A = 0, 1$ and $B = 0, 1$, and sign is the signum function.

Further details on parameter estimation of the NSRP model, and in general of other temporal rainfall models, are given in Obeysekera et al. (1987).

Chapter 6

Landslide triggering physically-based modeling

6.1 The TRIGRS model

6.1.1 Overview

The TRIGRS model (Baum et al., 2008, 2010) is an event-based spatially-distributed model for transient, unsaturated infiltration and slope stability analysis.

TRIGRS program computes transient pore-pressure changes, and attendant changes in the factor of safety, due to rainfall infiltration. The TRIGRS program uses a simple infinite-slope model to compute factor of safety on a cell-by-cell basis. Horizontal heterogeneity is accounted for by allowing material properties, rainfall, and other input values to vary from cell to cell.

TRIGRS is based on analytical solutions for Richards' partial differential equation that represent one-dimensional, vertical flow in vertically-isotropic and homogeneous materials.

As put in evidence by Iverson (2000), vertical infiltration models represent a good approximation of 3-D models, if ratio $\varepsilon = H/\sqrt{A} \ll 1$.

Version 1.0 of the program (Baum et al., 2002), was based on the model of Iverson (2000), and its extension for a finite basal boundary depth by (Savage et al., 2003, 2004). Several applications of this version of the program exist (e.g. Salciarini et al., 2006, 2008; Kim et al., 2010).

Version 2.0, which is used here, is based on hypotheses less restrictive than the previous version. Reference scheme for a simulated hillslope cell is shown in 6.1.

In particular, the Richard's vertical infiltration equation is used with a Soil Water Retention Curve (SWRC) of the exponential type proposed by Gardner (1958). Better approximations of field measurements may be attained by more sophisticated SWRCs, such as the well-known van Genuchten - Mualem model (van Genuchten, 1980). However in that case numerical integration is required to solve

the Richards' equation, while for an exponential SWRC analytical solutions were provided by Srivastava and Yeh (1991). This drastically decreases the simulation time, which may be prohibitively high for a numerical model applied to a wide area. This stands true especially if one want to use high-resolution Digital Elevation Models (DEM) nowadays easily obtained via airborne laser swath mapping (ALSM), that yield to grid spacings on the order of a few meters. Baum et al. (2010) tested model computational performances by comparing it with numerical models HYDRUS1-D (Simunek et al., 2008) and VS2DI (Lappala et al., 1987; Hsieh et al., 2000), and obtained that TRIGRS may be 30-70 times faster than the numerical models, when applied at the catchment scale.

TRIGRS unsaturated layer computations yield, in addition to pore pressures $\psi(Z,t)$ and $FS(Z,t)$, the flux at the base of the unsaturated zone, which is used for computations in the saturated zone. In particular a mass-conservation equation, that includes a leakage term, is used to estimate water table rise. Then the weight as measured by the computed water table rise is applied at the initial top of the saturated zone and pressure heads are computed using formulas adapted from analogous heat-flow problems (Carslaw and Jaeger, 1959).

For a complete description of the TRIGRS model and program the reader is referenced to Baum et al. (2008). The TRIGRS v.2 model can be freely downloaded from website `pubs.usgs.gov/of/2008/1159`. Applications and further details are reported in Baum et al. (2010). Hereafter, equations of the model and main details on the program are given, for the case of finite basal boundary depth d_{LZ}.

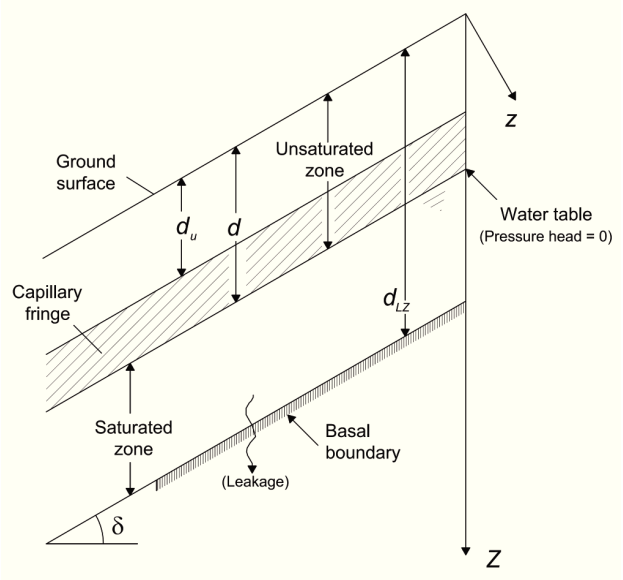

Figure 6.1: Shallow groundwater conditions in hillside soils. Adapted from Baum et al. (2010)

6.1.2 Governing equations

The one-dimensional form of the Richards equation describing infiltration at the ground surface and vertical flow through the unsaturated zone, in the case that the ground surface is tilted (cf., e.g. Freeze and Cherry, 1979) is:

$$\frac{\partial \theta}{\partial t} = \frac{\partial}{\partial Z}\left[K(\psi)\left(\frac{1}{\cos^2\delta}\frac{\partial \psi}{\partial Z} - 1\right)\right] \tag{6.1}$$

where Z is the vertical downward coordinate, t is time $\theta(Z,t)$ is soil water content, $\psi(Z,t)$ is pore pressure, $K(\psi)$ is hydraulic conductivity (this function represents the SWRC) and δ is ground surface slope.

The exponential hydraulic model of Gardner (1958) can be used to linearize equation 6.1 and provide an analytic solution for transient infiltration through the unsaturated zone. Unsaturated conductivity model of (Gardner, 1958), considered appropriate for coarse-grained soils, in represented by the following equations:

$$K(\psi) = K_s \mathrm{e}^{\alpha(\psi-\psi_0)} \tag{6.2}$$

$$\theta = \theta_r + (\theta_s - \theta_r)\mathrm{e}^{\alpha(\psi-\psi_0)} \tag{6.3}$$

where K_S is the saturated hydraulic conductivity, α is a parameter that may be obtained by fitting equation 6.3 to measured data, $-\psi_0 = 1/\alpha$ coincides with the vertical height of the capillary fringe above the water table (cf. figure 6.1), θ_r is the residual water content and θ_s is the water content at saturation.

Substitution of equations 6.2 and 6.3 in into the one-dimensional version of the Richards' equation, leads to a linear partial differential equation in $K(Z,t)$

$$\frac{\alpha_1(\theta_s - \theta_r)}{K_s}\frac{\partial^2 K}{\partial Z^2} = \frac{\partial^2 K}{\partial Z^2} - \alpha_1 \frac{\partial K}{\partial Z} \tag{6.4}$$

where $\alpha_1 = \alpha\cos^2\delta$. Closed-form solution to this equation has been derived by Srivastava and Yeh (1991).

6.1.3 Unsaturated zone

The response to a given rainfall time series $I_Z(t)$ is considered. The series is a sequence of rectangular pulses of intensity I_{nZ}, each starting at instant t_n, $n = 1, 2, ..., N$ and finishing at instant t_{n+1}, and can be expressed as $I_Z(t) = H(t - t_n) - H(t - t_{n+1})$ for $t_n \leqslant t < t_{n+1}$, where $H(t)$ is the Heaviside step-function:

$$H(t) = \begin{cases} 1, & \text{if} \quad t \geqslant 0 \\ 0 & \text{if} \quad t < 0 \end{cases} \tag{6.5}$$

In general, also a long-term (steady-state) I_{ZLT} surface is taken into account. I_{ZLT} can be approximated by the average precipitation in recent weeks or months that is needed to maintain the initial conditions. Due to its minor relevance, in the present work this it is let $I_{ZLT} = 0$.

Pore-pressure response in the unsaturated zone $\psi(Z,t)$, $0 \leqslant Z < d_u$ (cf. figure 6.1) follows from equation 6.2 solved for ψ:

$$\psi(Z,t) = \frac{\cos\delta}{\alpha_1} \ln\left[\frac{K(Z,t)}{K_s}\right] + \psi_0. \tag{6.6}$$

Solving equation 6.4 yields the hydraulic conductivity $K(Z,t)$ needed in the above equation 6.6.

In particular, the initial condition is:

$$K(Z,0) = I_{ZLT} - (I_{ZLT} - K_s \mathrm{e}^{\alpha_1\psi_0})\mathrm{e}^{-\alpha_1(d_u - Z)}; \tag{6.7}$$

while for $t > 0$:

$$K(Z,t) = \sum_{n=1}^{N} H(t-t_n)R_K(Z,t-t_n) - H(t-t_{n+1})R_K(Z,t-t_{n+1}), \tag{6.8}$$

in which R_K is the hydraulic conductivity profile produced by a rectangular hyetograph $I_Z(t) = I_Z$, $t > 0$:

$$\begin{aligned} R_K(Z,t) = I_Z - [I_Z - K_S \exp(\alpha_1\psi_0)\exp(-\alpha_1(d_u - Z)) - 4(I_Z - I_{ZLT}) \\ \exp\left[\frac{\alpha_1 Z}{2}\right]\exp\left[-\frac{D_\psi t}{4}\right]\sum_{m=1}^{\infty}\frac{\sin[\Lambda_m\alpha_1(d_u - Z)]\sin(\Lambda_m\alpha_1 d_u)}{1 + \frac{\alpha_1 d_u}{2} + 2\Lambda_m^2\alpha_1 d_u} \\ \exp(-\Lambda_m^2 D_\psi t), \end{aligned} \tag{6.9}$$

In the previous equation $D_\psi = \frac{\alpha_1 K_S}{\theta_s - \theta_r}$ is a decay constant, while the values of Λ_m are the positive roots of the following pseudo-periodic characteristic equation:

$$\tan(\Lambda\alpha_1 d_u) + 2\Lambda, \tag{6.10}$$

which is numerically solved in TRIGRS.

As rain infiltrates, a flux q at the base of the unsaturated zone ($Z = d_u$) is produced. This flux is given by:

$$q(d_u,t) = \sum_{n=1}^{N} H(t-t_n)R_q(t-t_n) - H(t-t_{n+1})R_q(t-t_{n+1}), \tag{6.11}$$

where R_q is the flux produced by a rectangular hyetograph $I_Z(t) = I_Z$:

$$\begin{aligned} q(d_u,t) = I_Z - 4(I_Z - I_{ZLT})\exp\left[\frac{\alpha_1 d_u}{2}\right]\exp\left[-\frac{D_\psi t}{4}\right] \\ \sum_{m=1}^{\infty}\left\{\frac{\Lambda_m \sin(\Lambda_m\alpha_1 d_u)}{1 + \frac{\alpha_1 d_u}{2} + 2\Lambda_m^2\alpha_1 d_u}\exp\left(-\Lambda_m^2 D_\psi t\right)\right\}. \end{aligned} \tag{6.12}$$

Formulas based on Fourier series of equations 6.9 and 6.12 converge poorly for early times ($D_\psi t > 0.05$). In this case TRIGRS uses more simple formulas (see Baum et al., 2010, Appendix A).

6.1.4 Saturated zone

Flux q given by equation determines water-table rise, if the amount of infiltrating water reaching the water table exceeds the maximum amount that can be drained by gravity at the top of the saturated zone.

TRIGRS computes maximum rate of drainage, q_{Zmax}, as

$$q_{Zmax} = K_s(\beta - 1). \tag{6.13}$$

Excess flux, q_{Zex}, is determined by the following formulas:

$$q_{Zex} = \begin{cases} 0, & \text{if} \quad q(d_u,t) \leqslant c_d(q_{Zmax} - I_{ZLT}) \\ q(d_u,t) - c_d(q_{Zmax} - I_{ZLT}) & \text{if} \quad q(d_u,t) > c_d(q_{Zmax} - I_{ZLT}) \end{cases} \tag{6.14}$$

where the flux exiting from the base of the unsaturated zone $q(d_u,t)$ is given by equation 6.11 and approximately equals the flux reaching the water table. To note that $q_{Zmax} - I_{ZLT}$ is used in equation 6.14 because it is excluded from computation of the transient flux, $q(d_u,t)$.

The model assumes:

$$c_d = \begin{cases} 1, & \text{for the infinite depth case} \\ 0.1 & \text{for the finite depth case} \end{cases} \tag{6.15}$$

To be noted that $c_d = 0$ is consistent with a no-flow boundary (all basal drainage is prevented), but a value of $c_d = 0.1$ is assumed because natural basal boundaries are usually leaky. In cases where the saturated hydraulic conductivities of the colluvium and underlying bedrock are known, their ratio could be substituted for c_d. It is anticipated that, because this information is not available in the model application presented next, it is let $c_d = 0.1$.

To compute the water-table rise in TRIGRS, the excess flux accumulating at the top of the capillary fringe is compared to the available pore space directly above the water table or capillary fringe (see figure 6.2).

The excess flux arriving at the water table given in equation 6.14 is integrated numerically from time 0 to t to compute the volume of water (per plan-view unit area) accumulating at the base of the unsaturated zone, $V_A(t)$.

The volume of available (fillable) pore space is computed as a function of height above the water-table or capillary fringe, $V_f(Z,t)$, by integrating the remaining air space, $\theta_a = (\theta_s - \theta)$, from the initial top of the capillary fringe, d_u, up to various equally spaced heights above the water table, such as Z_k and Z_{k+1} in figure 6.2. By subtracting equation 6.3 from θ_s, using equation 6.2 to eliminate $e^{\alpha(\psi-\psi_0)}$, and integrating, the result is

$$V_f(Z,t) = (\theta_s - \theta_r)[d_u - Z + T(Z,t)], \tag{6.16}$$

with

$$T(Z,t) = \frac{1}{K_s}\int_{d_u}^{Z} K(Z,t)dZ. \tag{6.17}$$

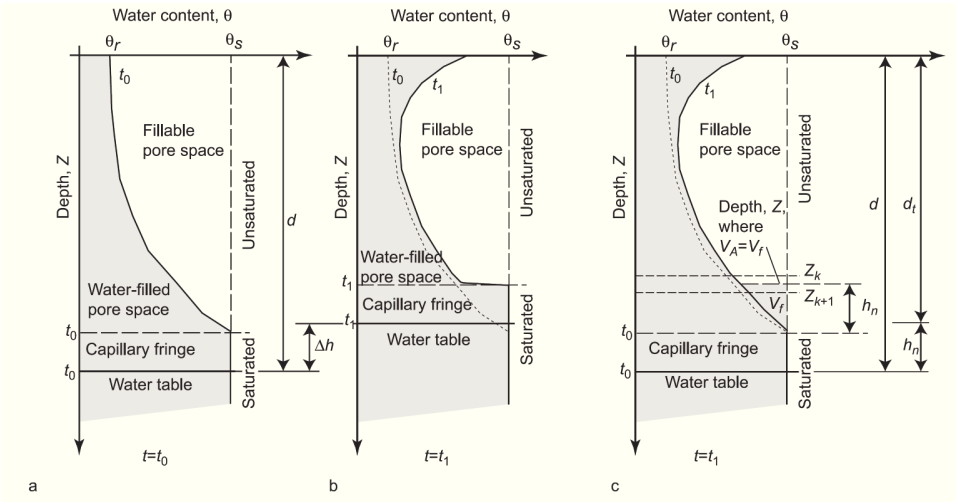

Figure 6.2: Vertical soil-water-content profiles from the ground surface down to an arbitrary depth, Z, showing the water-table-rise as a result of infiltration (after Baum et al., 2010)

In figure 6.2, the roughly triangular areas between the water-content curve labeled t_1, the dashed vertical line labeled θ_s, and the dashed horizontal lines labeled Z_k or Z_{k+1} represent the volume $V_f(Z,t)$ in equation 6.16.

Formulas for $T(Z,0)$ and $T(Z,t)$ are obtained by integrating $K(Z,0)$ from equation 6.7, and $K(Z,t)/K_S$ from equation 6.8 with respect to Z, from d_u to Z (for explicit formulas the reader may refer to (Baum et al., 2010)).

The water-table rise is first bracketed between the two nearest depths, Z_k and Z_{k+1}, at which the available volume has been computed, such that $V_f(Z_k,t) \geqslant V_A(t) \geqslant V_f(Z_{k+1},t)$ and then estimated by linear interpolation between Z_k and Z_{k+1} (figure 6.2). Because of the slope of the water content curve, the method outlined may slightly overestimate the actual rise of the water table, Δh. The error can be reduced by reducing the depth increment, $Z_{k+1} - Z_k$.

Once the water-table rise h_n is computed at a grid cell for time increment n, its weight is applied at the initial top of the saturated zone to compute the pressure head:

$$\psi(Z_w,t) = \sum_{n=1}^{N} \psi_{hn}[H(t-t_n)R_\psi(Z_w,t-t_n) - H(t-t_{n+1})R_\psi(Z_w,t-t_{n+1})], \quad (6.18)$$

in which:

$$R_\psi(Z_w,t) = \psi_{hn}\left\{1 - \frac{4}{\pi}\sum_{m=1}^{\infty}(-1)^{m-1}\frac{1}{2m-1}\exp\left[-\frac{(2m-1)^2\pi^2 D_1 t}{4d_{LZw}^2}\right]\right. \\ \left.\cos\left[\frac{\pi}{2}(2m-1)\left(\frac{Z_w}{d_{LZw}}-1\right)\right]\right\} \tag{6.19}$$

In the last equation ψ_{hn} is the pressure head at depth of initial water table at the nth time step and $d_{LZw} = d_{LZ} - d$.

6.1.5 Infiltration, Runoff, and Flow Routing

Infiltration at each cell, I, is computed as the sum of the precipitation rate P plus any runoff from upslope cells, R_u; with the limitation that infiltration cannot exceed K_S:

$$I = P + R_u, \quad \text{if} \quad P + R_u \leqslant K_S \quad \text{or} \tag{6.20}$$

$$I = K_S, \quad \text{if} \quad P + R_u > K_S \tag{6.21}$$

At each cell where $P + R_u$ exceeds K_s the excess is considered runoff, R_d, and is diverted to adjacent downslope cells. Distribution among downslope grid cells can be accomplished using several weighting factors for runoff distribution (see Baum et al., 2008):

$$R_d = P + R_u - K_S, \quad \text{if} \quad P + R_u - K_S \geqslant 0 \quad \text{or} \tag{6.22}$$

$$R_d = 0, \quad \text{if} \quad P + R_u - K_S < 0 \tag{6.23}$$

In TRIGRS overland flow between adjacent cells is assumed to occur instantaneously and overland flow rate is not modeled. Hence, individual storm periods should be long enough to flow to adjacent cells.

6.1.6 Slope stability

Factor of safety is finally computed with the following formula (cf. section 2.3):

$$FS(Z,t) = \frac{\tan\phi'}{\tan\delta} + \frac{c' - \psi(Z,t)\gamma_w \tan\phi'}{\gamma_S Z \sin\delta\cos\delta}, \tag{6.24}$$

where symbols are as in section 2.3.

In the case of finite basal boundary depth (the one considered in this study), the minimum factor of safety (i.e. maximum pore-pressure) is at $Z = d_{LZ}$. Consequently, the outputs of interest for most of the studies may be $\psi(d_{LZ},t)$ and $FS(d_{LZ},t)$.

6.2 Integration of TRIGRS with a water table recession model

The initial water table depth is required as an initial condition to simulate infiltration and slope stability with the TRIGRS model.

In order to estimate such initial condition, the TRIGRS model is integrated with a Water Table Recession (WTR) model, that it is applied in the dry periods in between storms, as described in chapter 4.

The adopted WTR model is based on the one by Rosso et al. (2006), described in 2.3. For dry periods, i.e. when the precipitation rate $p = 0$, the mass- conservation equation 2.9 simplifies as follows:

$$BhK_S \sin\delta = -A\theta_s \frac{dh}{dt}. \tag{6.25}$$

where here $t = 0$ at the *end* of the storm.

This equation has the following solution:

$$h(t) = h(0) \exp\left(-\frac{BK_S \sin\delta}{A\theta_s} t\right). \tag{6.26}$$

The initial condition for the WTR model $h(0)$ may is taken from TRIGRS. If $\psi(d_{LZ}, t_f)$ is the pore pressure at basal boundary at the end of the storm event simulated with TRIGRS, the water table height is computed as $h(0) = \psi(d_{LZ}, t_f)/\beta$, where $\beta = \cos^2\delta$, if slope parallel flow is assumed ($I_{ZLT} = 0$), (cf. Iverson, 2000). The initial condition for TRIGRS for the successive storm is then given by equation 6.26, by letting $t = \Delta t_i$, where Δt is the interarrival time between rainfall event i and the next one. Moreover, operating on a cell-basis, B equals the grid cell size and the upslope contributing area results $A = B^2 N_d$, where N_d is the number of cells draining in the one local one (Tarboton, 1997). Flow accumulation map, that may be easily derived from GIS software applied to a DEM, provides N_d for each cell of a drainage basin.

With these assumptions, equation 6.26 becomes:

$$h(t) = \frac{\psi(d_{LZ}, t_f)}{\cos^2\delta} \exp\left(-\frac{K_S \sin\delta}{BN_d\theta_s} t\right). \tag{6.27}$$

Equation is plotted in figure 6.3, assuming a slope $\delta = 40^\circ$ and hydraulic properties for the Loco catchment in table 7.IV, for different values of upslope draining cells N_d and $B = 2$m.

6.3 Model performance assessment

Model simulation for one or more rainfall events that triggered landslides, allows, by confrontation of predicted unstable cells and map of observed landslides, to assess model's performance (cf., e.g. Rosso et al., 2006; Baum et al., 2010).

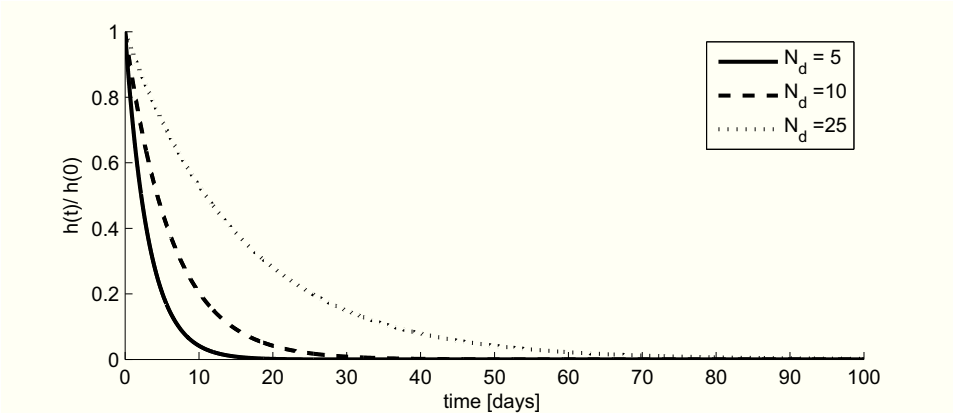

Figure 6.3: Plot of equation 6.2 assuming a slope $\delta = 40°$ and hydraulic properties for the Loco catchment in table 7.IV, for different values of upslope draining cells N_d

.

Signal detection theory concepts (cf., e.g. Macmillan and Creelman, 2004) provide perhaps the most correct way to do such a confrontation. Cells may belong to one of the four classes of table 6.I.

Table 6.I: Confusion matrix for spatial output of an hydrologic model

		Actual	
		Landslide (P)	No landslide (N)
Model	Unstable (P')	True Positive, TP (rightly simulated unstable cells)	False positive, FP (wrongly simulated unstable cells)
	Stable (N')	False Negative, FN (wrongly simulated stable cells)	True Negative, TN (rightly simulated unstable cells)

Most used performance indexes calculated on the basis of table 6.I are:

- True Positive Rate

$$TPR = \frac{TP}{P} = \frac{TP}{TP + FN}; \tag{6.28}$$

- False Positive Rate

$$FPR = \frac{FP}{N} = \frac{FP}{FP + TN}; \tag{6.29}$$

- Accuracy

$$ACC = \frac{TP + TN}{P + N}; \tag{6.30}$$

- Precision

$$PRE = \frac{TP}{TP + FP}. \tag{6.31}$$

Furthermore, the Receiver Operating Characteristic (ROC) plot, may allow to compare several models, or to analyze how model performance varies with a parameter that is not completely known. ROC plot consists in the abscissa the FPR and in ordinate the TPR. An ideal model has $FPR = 0$ and $TPR = 1$, i.e. model is represented by a point in the upper left corner of the ROC space. On the contrary, a completely random guess is characherized by $FPR = TPR$, i.e. a model point that lays on the diagonal line from the left bottom to the top right corners of the ROC space.

Chapter 7

Application to Loco catchment in the Peloritani Mountains, Italy

7.1 Preliminary remarks

In this chapter application of the Monte Carlo methodology, illustrated in chapter 4 is carried out with reference to the Loco catchment in the Peloritani Mountains, Italy.

Firstly, the application of the stochastic rainfall model is illustrated. Calibration and validation of the NSRP model is carried out for the Fiumedinisi SIAS rain gauge, utilizing 10-minutes precipitation series.

Successively the TRIGRS-WTR model is applied to simulate the 1 October 2009 landslide event triggering, for which maps of occurred slides are available.

Model performance is assessed by comparing the predicted unstable areas with the map of observed landslides. This analysis is carried out by model simulation for the rainfall sequence that starts at the first rainfall event of the hydrological year to the one on 1 October 2009, in order to compute, through the combined use of TRIGRS and the WTR model, the initial conditions required to simulate correctly the mainly triggering rainfall event of 1 October 2009. In fact, two significative rainfall events occurred before that date, that determined an increase on the probability of landslide occurrence.

Finally, the Monte Carlo approach is applied. Return period of cell slope failure is estimated, and the direct link between rainfall and landslide occurrence is analyzed in terms of rainfall intensity and duration.

7.2 Calibration and validation of the NSRP rainfall model

7.2.1 Analysis of Fiumedinisi rainfall data

Data from the Fiumedinisi rain gauge are available, at a temporal resolution of 10-minutes, for the almost 9 years-long period 21 February 2002 – 9 February 2011. Within this period several landslides have been experienced in the Peloritani area (see section 3.2).

Statistics that useful for calibration and validation of the NSRP model are shown in table 7.I, relatively to the hourly series. Seasonality of the series has been mainly investigated on the basis of the seasonality of these statistics, represented in the plot of figure 7.1. Similarly to other researchers (cf., e.g., Cowpertwait et al., 1996; Obeysekera et al., 1987), this investigation was carried out on a month-per-month basis.

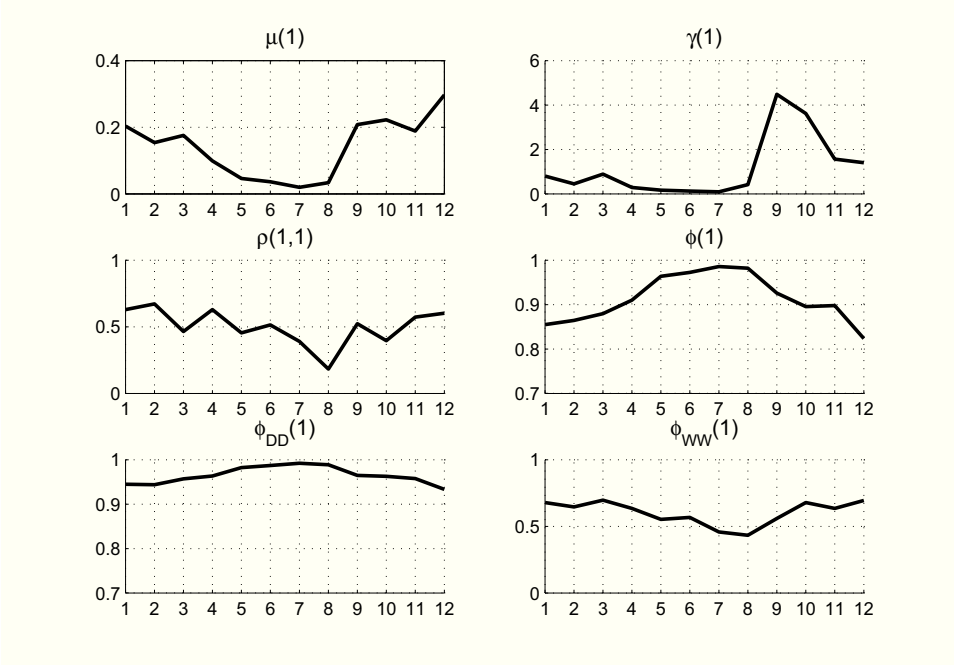

Figure 7.1: Moments for each month for Fiumedinisi SIAS rainfall data

Based on the plot of figure 7.1 one can state that:

- The series exhibits seasonality; in particular 6 seasons seem to exist:
  1. September and October;

Table 7.I: Statistics of the sample of Fiumedinisi SIAS hourly rainfall data

	Jan	Feb	Mar	Apr	May	Jun	Jul	Aug	Sept	Oct	Nov	Dec
N[yr]	9.0	8.6	8.0	8.0	8.9	9.0	9.0	9.0	9.0	9.0	9.0	8.8
μ[mm]	0.203	0.154	0.175	0.099	0.046	0.036	0.019	0.034	0.208	0.222	0.189	0.297
σ[mm^2]	0.798	0.447	0.892	0.289	0.168	0.125	0.092	0.417	4.482	3.620	1.567	1.400
$\rho(1)$	0.629	0.672	0.465	0.629	0.455	0.514	0.390	0.183	0.523	0.396	0.573	0.601
ϕ	0.855	0.864	0.880	0.910	0.964	0.973	0.986	0.982	0.926	0.896	0.898	0.823
ϕ_{DD}	0.945	0.944	0.957	0.964	0.982	0.987	0.992	0.989	0.965	0.963	0.958	0.933
ϕ_{WW}	0.678	0.645	0.697	0.635	0.552	0.567	0.458	0.433	0.560	0.678	0.635	0.694

2. November;
3. December;
4. January, February and March;
5. April;
6. May-August;

- The last two seasons listed above have low precipitation, i.e. the probability of a landslide triggering event is reasonably very low.

Based on these considerations, separate sets of parameters of the NSRP model are determined for each one of the seasons listed above (in total 20 parameter values). The last two seasons have been considered of negligible rainfall, with reference to potential for landslide triggering; this means that in the Monte Carlo simulations null precipitation has been assumed for the months from April to August.

7.2.2 Model Calibration

A preliminary analysis relative to calibration of the NSRP model consisted in trying different sets of moments at various time scales ranging in the interval of 10min-24 h in order to best calibrate the NSRP model. The plot of the six moments $\mu(h), \gamma(h), \rho(h,1), \phi(h), \phi_{DD}(h)$ and $\phi_{WW}(h)$ versus scale of aggregation h has been considered as a reference for assessment of the goodness of fit, besides the value of the objective function (weights were assumed all equal to one).

With reference to the situation in which only two different times scales are considered accross the moments used, according to results obtained by Calenda and Napolitano (1999), the choice of two distant time scales rather than two close ones, seemed to lead to better results. Moreover, that choice seemed to lead to a quite good reproduction of moments for the times scales in between the ones used for calibration.

Among the tentatives done, the following set of moments resulted most suitable: $\gamma(1), \phi(1), \phi_{DD}(1), \phi_{WW}(1), \mu(24), \gamma(24), \phi(24)$.

To be noticed that accounting for $\phi(1), \phi_{DD}(1), \phi_{WW}(1)$ is redundant, being them related by equation 5.18. As observed by (Cowpertwait et al., 1996) this is the same to give some extra weight to match the dry spell sequences.

Results of the calibration are shown in tables 7.II and 7.III. The Weibull distribution was chosen to model rainfall intensities, with a fixed value of $b = 0.6$, which seemed to be the most appropriate, after an exponential distribution (which corresponds to $b = 1$) resulted unable to model peaks exhibited by the observed series.

Relatively high values were obtained for the ν parameter. From a physical standpoint, the number of rain cells per storm may be bounded to a lower value of the one obtained (cf., e.g., Cowpertwait et al., 1996, utilized the bound $\nu \leqslant 20$). However, other researchers have obtained from calibration even higher values for this parameter (cf., e.g. Obeysekera et al., 1987).

Calibration performances, as measured by the objective function, are worse for the one-month season of December and best for the months of September and October; this may be somehow related to the fact that the same value of the b parameter was adopted for all seasons in conjunction with the fact that December is more rainy but with less accentuated peaks.The lower performances for the three-months season January-March, may be quite expected for the obvious reason that more months, that may include more heterogeneity of data characteristics, are modeled with just one set of parameters.

From the table it can also be noticed how the parameters relative to the season September-October are significantly different form the other three seasons among which significant differences exist but are not so accentuated. In fact, rainfall in September and October seems to have distinct extreme characteristics, being these months the only ones for which landslides were observed in the last years (except for one date: 1 March 2011).

Figures 7.2 to 7.5 the moments vs. aggregation time scale plot used for best calibration, as mentioned before. Also a verification of the correct simulation of the model by the developed software is demonstrated by those figures, by the superimposition of the same plots relative to theoretical moments computed by formulas 5.10 - 5.19 and relative to a 200-years long synthetic rainfall series.

Good reproduction, at all time scales, of the three most important statistics, μ, γ and ϕ can be noticed from those plots. Also the lag-1 autocorrelation is quite well reproduced, even though it has not been accounted for. This may be due to the presence of zeros that mainly controls the autocorrelation, and thus that good modeling of ϕ implies good modeling for $\rho(h,1)$. Yet, $\rho(h,1)$ together with transition probabilities ϕ_{WW} have a trend that departs upward from the plots relative to the observed series (this occurs in less measure for the September-October season). This kind of trend in autocorrelation has however been observed in real time series (cf., e.g. Calenda and Napolitano, 1999, fig.13, where $\rho(h,1)$ increases when going from a 10 to a 20 hours aggregation scale), and thus does not represent a physically unrealistic behavior. This is also true relatively to ϕ_{WW}, for which the increasing trend is present sometimes also in the Fiumedinisi rain series (cf. 7.5)

Table 7.II: Results of NSRP calibration

Parameter	Jan,Feb,Mar	Sept,Oct	Nov	Dec
$\lambda[\mathrm{h}^{-1}]$	0.002295	0.021195	0.001485	0.003185
ν	44.28	1.57	42.41	42.61
$\beta[\mathrm{h}^{-1}]$	0.010161	2.1179	0.0059551	0.0098760
$\eta[\mathrm{h}^{-1}]$	0.72113	0.83999	0.94053	0.67735
$\xi[\mathrm{h}^b/mm^b]$	1.13441	0.46260	0.69261	1.03521
S	0.0137	0.0018	0.0037	0.0166

Table 7.III: Comparison between sample and theoretical moments (sample, theoretical and relative error in percentage)

Model	$\gamma(1)$[mm^2]	$\phi(1)$	$\phi_{DD}(1)$	$\phi_{WW}(1)$	$\mu(24)$[mm]	$\gamma(24)$[mm^2]	$\phi(24)$
Jan,Feb,Mar	0.72	0.87	0.95	0.67	4.23	91.39	0.49
	0.75	0.83	0.94	0.73	4.12	88.44	0.49
	(-4.14)	(4.56)	(0.44)	(-9.07)	(2.45)	(3.23)	(-0.15)
Sept,Oct	4.04	0.91	0.96	0.63	5.18	289.82	0.58
	4.05	0.95	0.98	0.63	5.17	289.72	0.58
	(-0.09)	(-3.85)	(-1.60)	(-0.51)	(0.11)	(0.04)	(0.56)
Nov	1.57	0.90	0.96	0.63	4.57	143.15	0.54
	1.65	0.89	0.95	0.63	4.46	140.90	0.54
	(-5.14)	(0.71)	(0.32)	(1.29)	(2.42)	(1.57)	(0.67)
Dec	1.40	0.82	0.93	0.69	7.15	180.96	0.37
	1.46	0.77	0.92	0.75	6.83	176.73	0.37
	(-4.25)	(6.93)	(0.91)	(-8.60)	(4.44)	(2.34)	(-0.19)

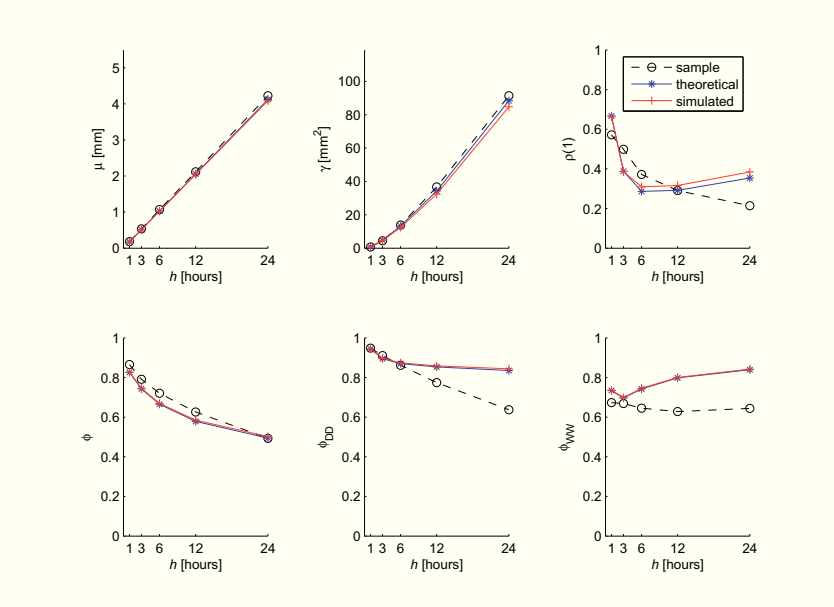

Figure 7.2: Moments varying aggregation time scale: January-February-March season model

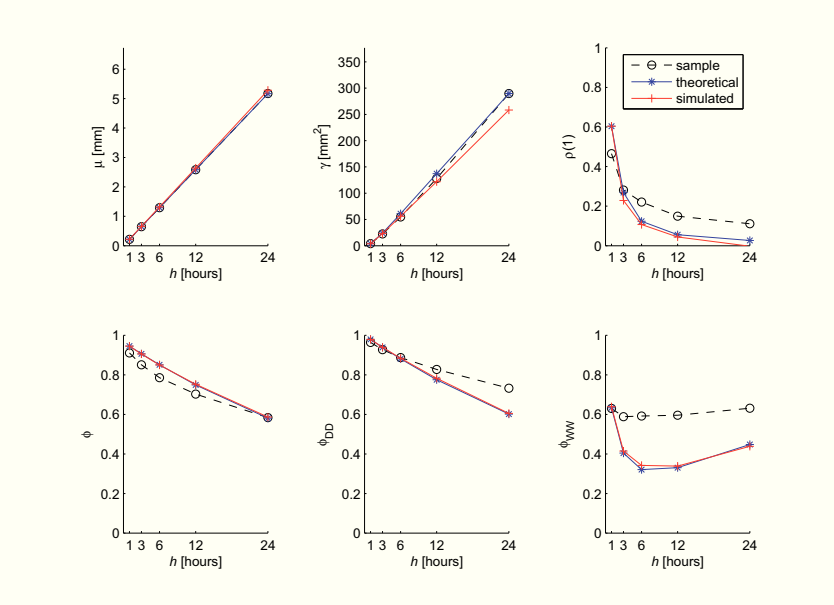

Figure 7.3: Moments varying aggregation time scale: September-October model

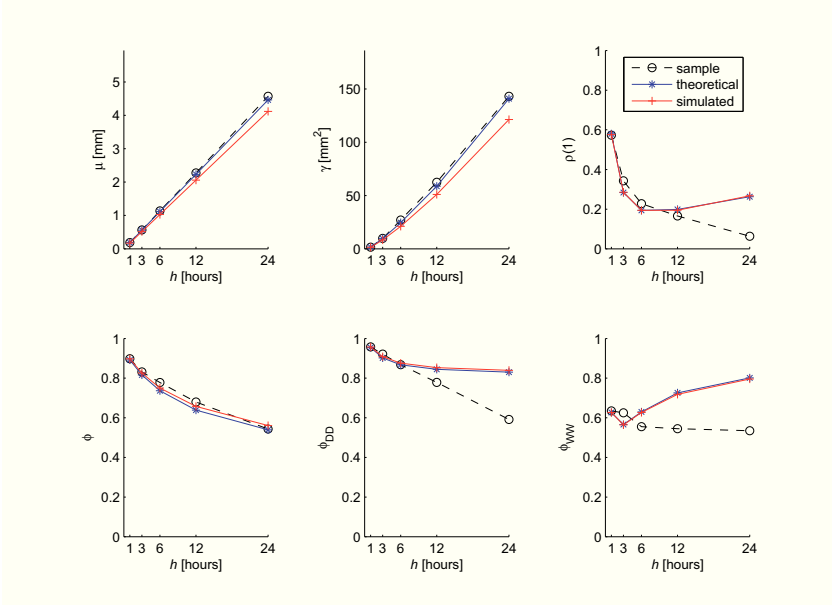

Figure 7.4: Moments varying aggregation time scale: November model

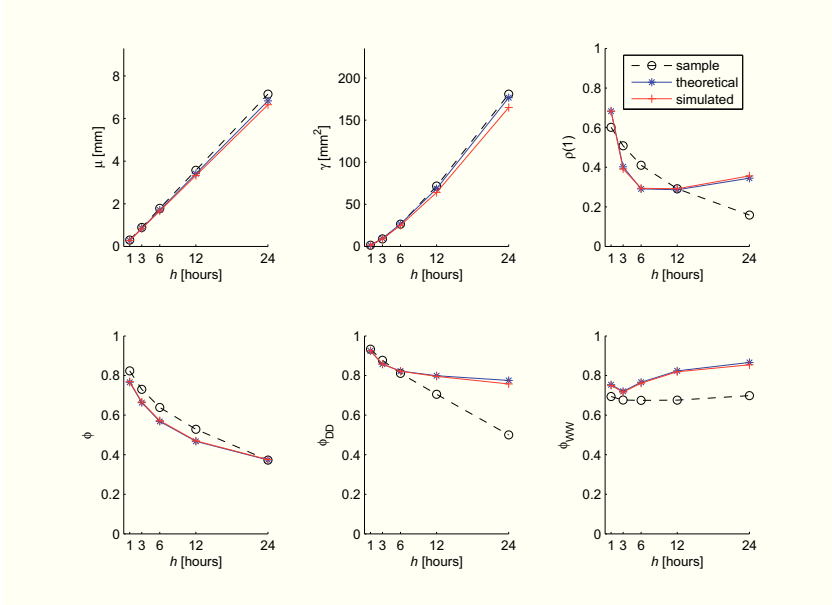

Figure 7.5: Moments varying aggregation time scale: December model

7.2.3 Model validation

In addition to the plots of figures 7.2 - 7.5, which also represent a validation test for the model, model performance was tested against the capability to reproduce characteristics that are important with respect to the potential of rainfall events to trigger landslides.

In particular, reproduction of total event cumulative rainfall W_{tot} and total event duration D_{tot} was investigated (see definitions of these variables in figure). It may be worthwhile to notice that those cumulative rainfall and duration are, obviously, different from the ones relative to the instant of incipient failure, i.e. the ones plotted, for instance, to develop and empirical $I - D$ model.

For the analysis the following parameters of rainfall event separation (see section for definitions) values have been assumed: $\Delta h_{min} = 0.2$ mm, $\Delta t_{min} = 24$ h, $W_{min} = 35$ mm, $\Delta t_a = 6$ h. These event separation was applied to both the simulated and the observed series. Moreover for the observed series, the almost-dry seasons (months from April to August) have been assumed of zero precipitation. Hourly rainfall has been considered for these analyses.

The 1000-years long synthetic series, used in the Monte Carlo simulation, has been used to test these kind of performances, by comparing the behavior of 9-years long series excerpted from the 1000-years synthetic series (total of 111 series) with the observed Fiumedinisi data, of almost 9-years length too. In particular, the following analyses have been conducted on W_{tot} and D_{tot}:

- Comparison of the empirical cumulative frequency marginal distributions (figures 7.6 and 7.7);
- Comparison of linear correlation between the logarithms of $I_{tot} = W_{tot}/D_{tot}$ and D_{tot} and of the intercept and slope of linear regression between these two variables 7.8.

In figures 7.6 and 7.7 the colored and continuous lines represent cumulative frequencies of the 111 simulated 9-year series. Good results were obtained for the cumulative event rainfall I_{tot}: the plot for the sample (black dotted line) is entirely within the region spanned by the curves relative to the synthetic series. Worse results were obtained for the duration: the sample has a lower dispersion of all the synthetically-generated curves, short durations are more probable and long durations are less probable. However, the result seems to be acceptable.

In figure 7.8, the box plots for the results of the 111 series are compared with the observed series (represented by the blue circle in each plot). Moreover, in the figure each green point is representative of one 9-year long simulation.

Trend of correlation is well reproduced as demonstrated by the regression intercept and slope plots, though the linear - correlation is significantly higher in magnitude (negative values) for the modeled series in comparison to the observed series, about -0.75 against about -0.90. This may be expected in a certain sense, due to the fact the reality (observed series) is more complicated than model-process.

In conclusion, the model, although improvable, seems suitable for rainfall simulation within the context of the illustrated Monte Carlo approach for the analysis

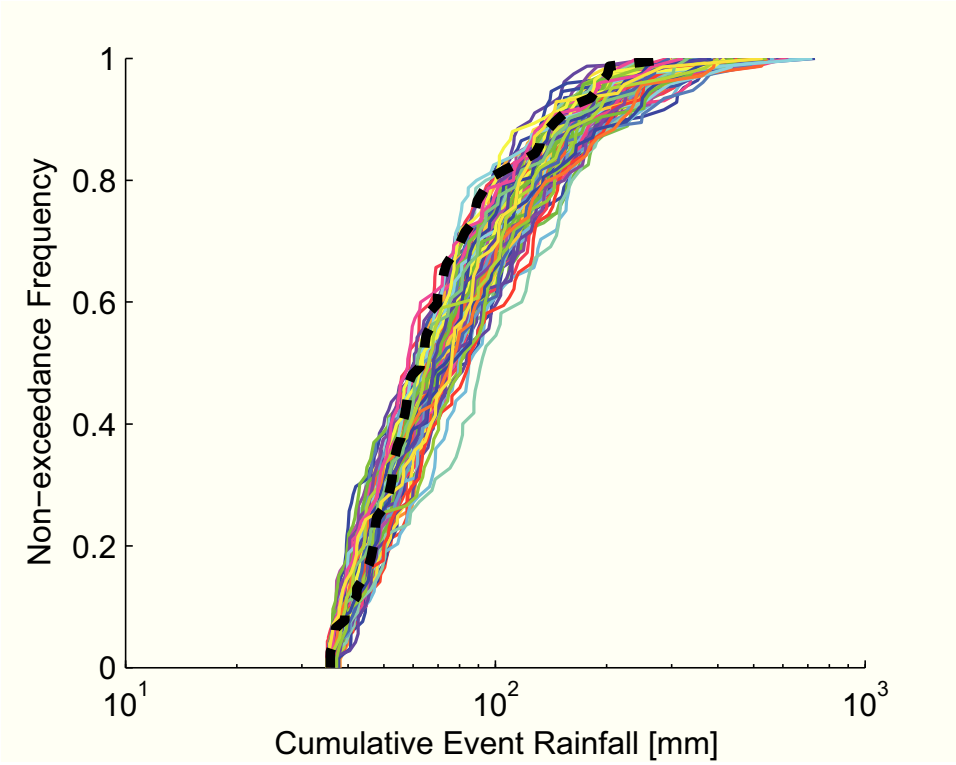

Figure 7.6: Comparison of Empirical Cumulative Frequency for Cumulative Event Rainfall for observed series (black dotted line) and simulated series (1000 years)

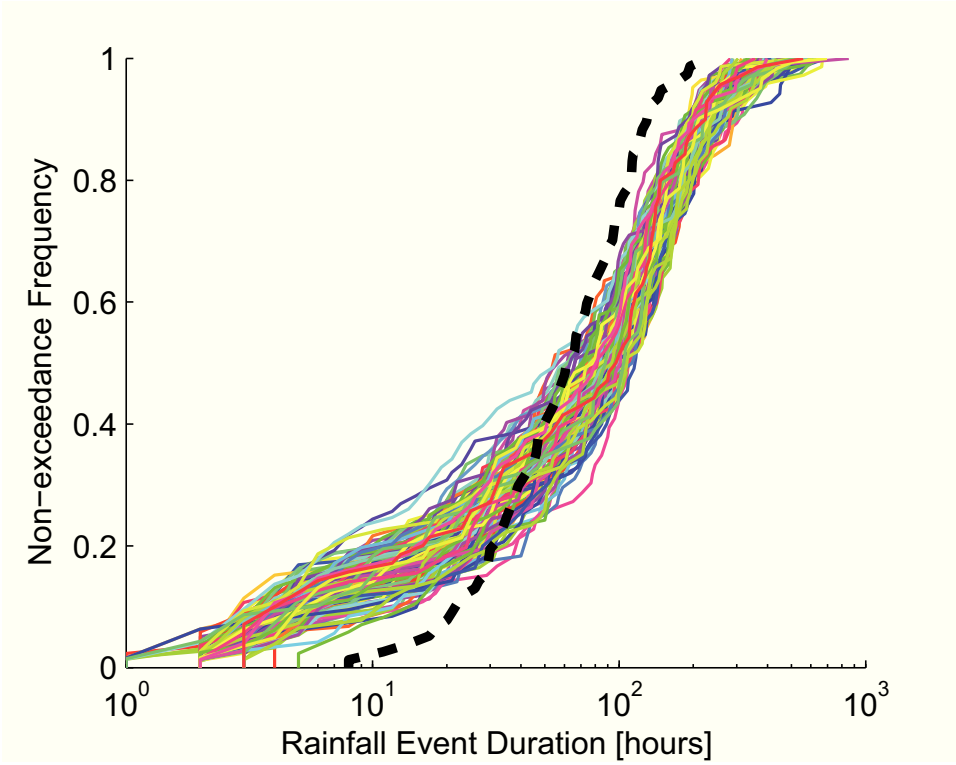

Figure 7.7: Comparison of Empirical Cumulative Frequency for Cumulative Event Rainfall for observed series (black dotted line) and simulated series (1000 years)

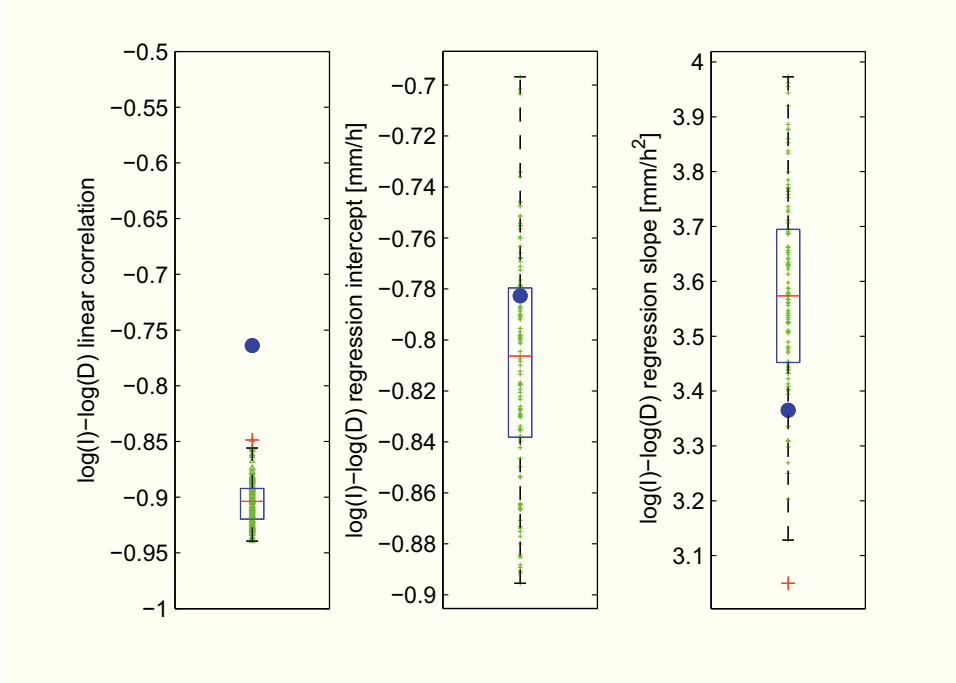

Figure 7.8: Comparison of $\log(I_{tot}) - \log(D_{tot})$ correlation for observed (blue circle) and simulated data

of the hydrologic control on shallow landslides.

7.3 Application of the physically-based model

7.3.1 Data and preliminary analyses

Rainfall data

Rainfall of the Santo Stefano di Briga rain gauge (see figure 3.3), distant about 2 km from Loco catchment, is utilized for simulating the 1 October 2009 debris-flow event. This rain gauge is nearer to the Loco catchment than Fiumedinisi, but its length is of about four years instead of nine (this is the reason why for calibration of the NSRP model use of Fiumedinisi station was preffered at S.Stefano di Briga).

The input considered for simulating the 1 October 2009 event is shown in figure 7.9, and consists of the following sequence:

- 1stSeptember: total duration and rainfall of the event are of 11 h and 49.7 mm respectively. This was also the first significant rainfall event of the hydrological year, following the almost completely dry summer season.
- 23rd-24thSeptember event, in which 44.9 mm fell in 10 h. This event occurred 182 h after the end of the previous one.
- 1stOctober. This event of 226.4 mm in 15 h provoked debris-flow-evolving-landslides. It occurred 168 h after the end of the 24thSeptember event.

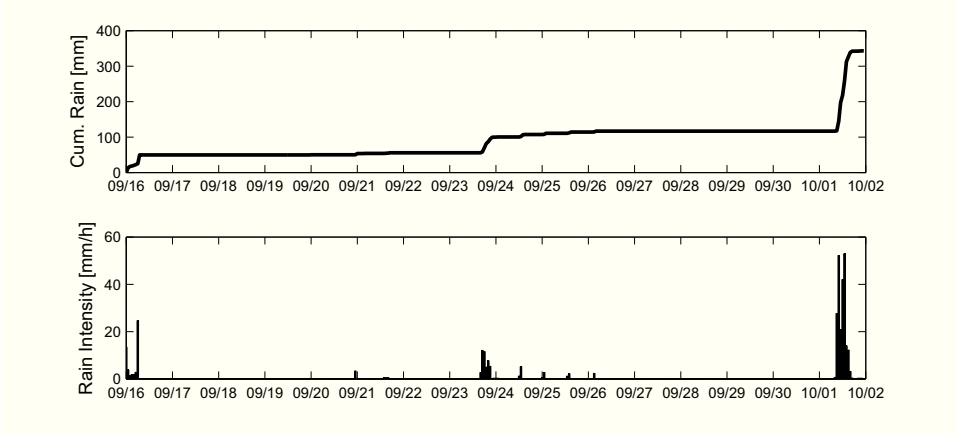

Figure 7.9: Sequence of rainfall events considered for simulation of the 1stOctober 2009 debris-flow event

Few millimeters of rainfall fell in between of the events of the sequence, but they were neglected in the successively illustrated simulation, because of they very modest entity. This is also consistent with the event separation parameters adopted,

and in particular with the $W_{min} = 35$ mm threshold and 24 h minimum interarrival time (see sections 7.2.3 and 7.2.3).

Topographic data

The Loco catchment, is represented in figure 7.10. Figure reports also location of the catchment and of the slides triggered on 1st October 2009, and the representation of the DEM used in the applications. This DEM has been derived few months before 1st October 2009 event, from airborne laser swath mapping (ALSM) at an high resolution (2×2 m).

GRID maps of interest for model application are shown in figure 7.11, and in particular: slope δ , depth to basal boundary d_{LZ}, flow accumulation map (number of upslope draining cells N_d) and $\varepsilon = d_{LZ} \cos^2 \delta / \sqrt{A}$.*Slope*$\delta$ was derived from the DEM.

Depth d_{LZ} of the erodible strata, mainly composed of loamy sands with an high proportion of gravel, has been measured to be ranging from 4 m to 2 m, on points of slope varying from 30° to 40°. Following other researchers (DeRose, 1996; Salciarini et al., 2006, 2008; Baum et al., 2010) a negative exponential relationship between depth d_{LZ} and slope has been assumed. In particular, the relationship $d_{LZ} = 32 \exp(-0.07\delta)$ has been adopted, which gives $d_{LZ}(30) = 4$ m and $d_{LZ}(40) = 2$ m. Bedrock outcropping has been considered in areas with slope $\delta > 50$, while an upper bound of $d_{LZ} = 5$ m has been imposed. Map of depth d_{LZ} obtained is shown in 7.11.

Flow accumulation map, that expresses the of draining cells N_d, and hence upslope contributing area A has been computed using D-∞ method (Tarboton, 1997).

The map of the ratio $\varepsilon = H/\sqrt{A}$ was calculated to check the suitability of vertical infiltration models, such as the one used, which requires that the ratio $\varepsilon \ll 1$ (Iverson, 2000). From the map it can be noticed that for most of the potentially unstable areas ε is in the range $0.1 - 0.5$, which is acceptably less than one. Ratio is less than 0.1 in the drainage network. A small proportion of the catchments has a ratio in the range $0.5 - 1$, and few cells have a ratio greater than 0.5 (maximum value is 2.5). Globally it can be stated that the condition $\varepsilon \ll 1$ is acceptable satisfied.

Hydrological and geotechnical parameters

The hydrological parameters required by the model are: the saturated hydraulic conductivity K_S, saturated hydraulic diffusivity D_0, residual water content θ_r, saturated hydraulic content or porosity θ_s and the α parameter of the Gardner SWR model (equation 6.2). Geotechnical parameters required are soil and water unit weights γ_s and $\gamma_w = 9800\text{N/m}^3$, soil friction angle for effective stress ϕ' and c'.

For some of these parameters direct measurements were available.

In particular, measurements of soil strength parameters by direct shear test were available for some points in the catchment. Averaged values $\phi' = 39\circ$ and $c' = 4$

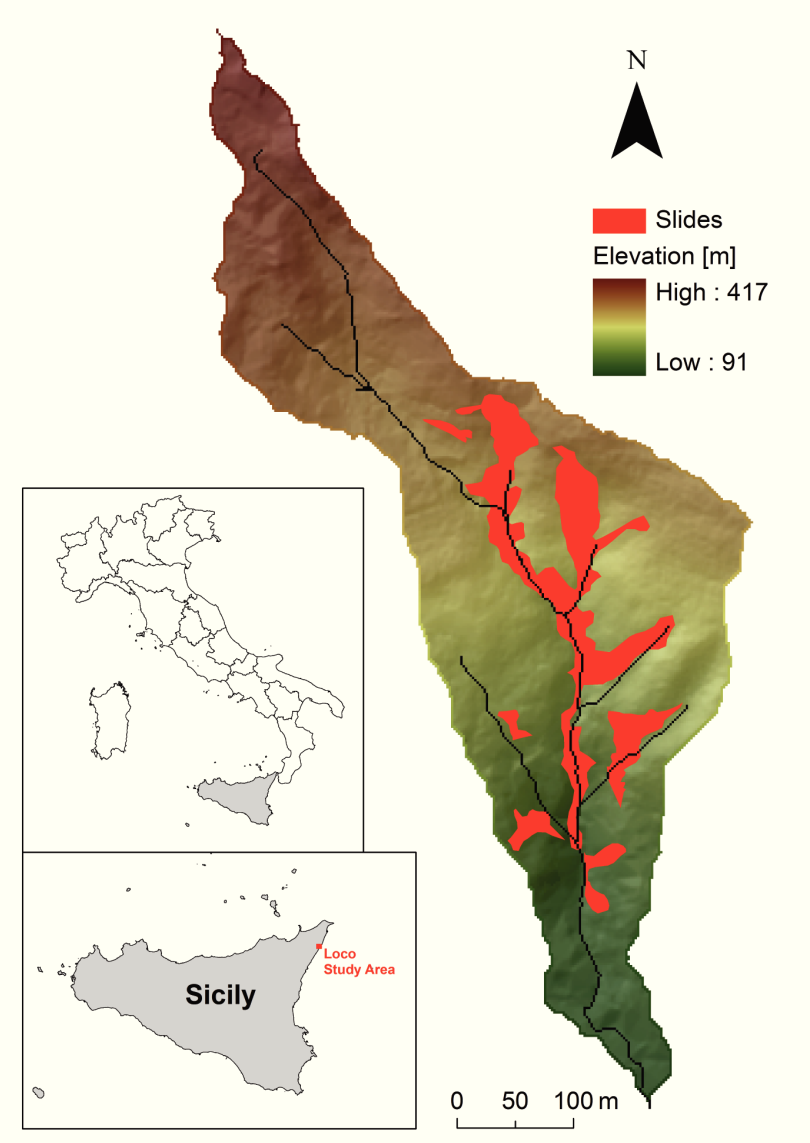

Figure 7.10: Map showing the location and 2-meters-resolution digital terrain model of the study area, Loco catchment, Sicily (Italy)

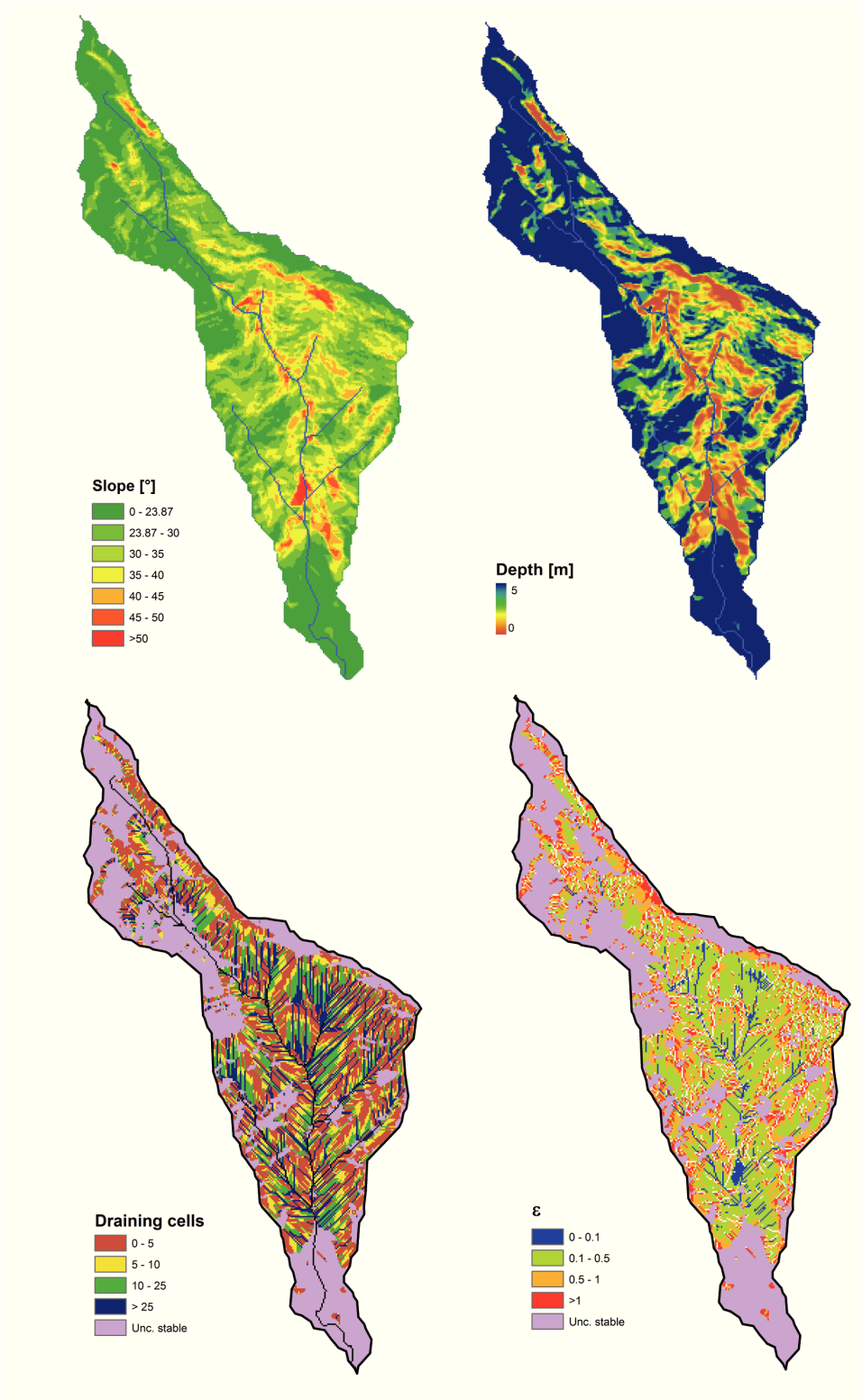

Figure 7.11: GRID maps of interest for model application

kPa have been assumed. Unit weight of soil has been measured to be $\gamma_s = 19000$ kN/m^3. An averaged value of measurements for hydraulic content at saturation (porosity), $\theta_s = 0.35$ has been used.

No direct measurements of the remaining hydraulic parameters $K_S, D_0, \theta_r, \alpha$ were available.

Indirect methods allow estimation of parameters of the SWR models soil properties from other more available, easily, routinely, or cheaply measured properties (cf. Leij et al., 1978). The program ROSETTA (Schaap et al., 2001), was used to compute those missing parameters starting from soil grain size distribution measured in the area.

The ROSETTA program allows estimation of the parameters of the van Genuchten-Mualem SWRC. Soil hydraulic conductivity resulted of $K_S = 2 \times 10^{-5}$ m/s. A best fit between the van Genuchten-Mualem SWR and the Gardner model, yielded a value of $\alpha = 3.5$ m^{-1}. Soil hydraulic diffusivity, has been assumed $D_0 = 5 \times 10^{-5}$ m^2/s, considering that typical values for the specific storage $S_S = K_S/D_0 = 0.005 - 0.5$ m $^{-1}$ for surficial strata in similar landslide-prone areas (Baum et al., 2010).

Table 7.IV summarizes data utilized in the application.

Table 7.IV: Material strength and hydraulic properties for surficial strata of Loco catchment

ϕ' [$\circ$]	c' [kPa]	γ_s [N/m^3]	θ_s [-]	K_S [m/s]	θ_r [-]	α [m^{-1}]	D_0 [m^2/s]
39	4	19000	0.35	2×10^{-5}	0.045	3.5	5×10^{-5}

Data determine distribution of factors of safety for dry (wetness $\omega = (d_{LZ} - d)/d_{LZ} = 0$) and fully saturated ($\omega = 1$) conditions. These can expressed as a function of slope, because of the univocal relationship with depth to basal boundary, as shown in figure 7.12.Cells result unconditionally stable for slope less than $\delta_{us} = 23^\circ.87$. Data also the critical wetness is determined for all cells of the catchment, as shown in figure 7.13. Critical wetness decreases from 1 to a minimum value of about 0.3 going from δ_{us} to about 46°. Values of critical wetness can be converted into critical pore pressure, by multiplying them for $d_{LZ} \cos^2 \delta$. The values $\psi_{cr} = 2.14, 0.99, 0.42, 0.19$ and 0.14 m result, for slopes $\delta = 30^\circ, 35^\circ, 40^\circ, 45^\circ$ and 50° respectively.

7.3.2 Results

Starting with a initial water table height of zero everywhere in the catchment for the 16 September rain event, simulation of slope stability for the two rainfall events preceding the 1 October rain event was conducted alternating the TRIGRS model (applied within the storm + 6 hours after) and the WTR model (applied within the interarrival of the TRIGRS simulations), according to the rainfall sequence

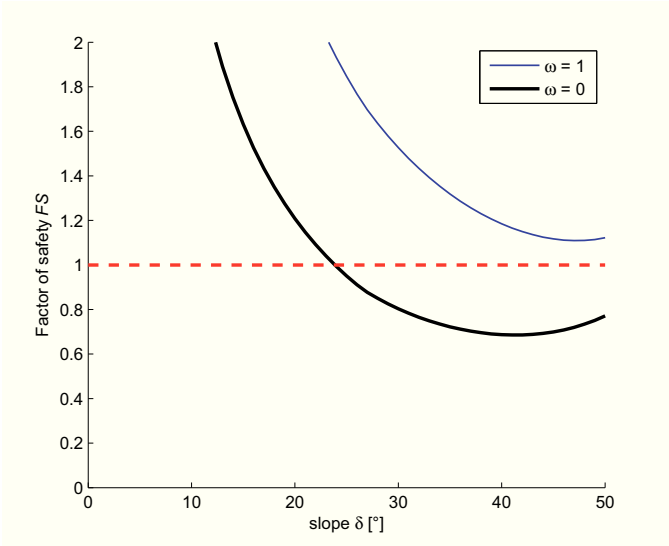

Figure 7.12: Factor of safety corresponding to $\omega = 0$ and $\omega = 1$ for cells of the Loco Catchment

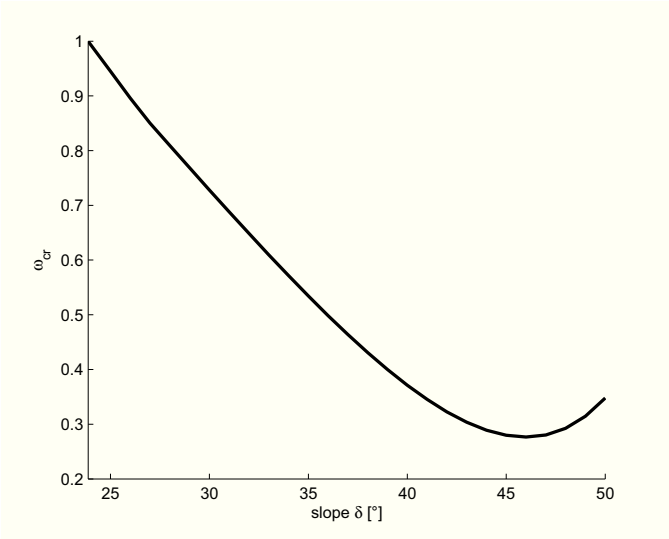

Figure 7.13: Critical wetness for cells of the Loco catchment

described in section 7.3.1.

Simulating for the antecedent rainfall sequence yielded to the distribution of water table depths shown in figure7.14 in terms of wetness ω for better representation. A significant increase in water table levels resulted.

Sparse cells, summing to 83 (0.24% of basin area), result unstable after the two-event sequence (cf. figure fig:timeseriesloco). These cells are however parts of the drainage network (high memory $N_d > 25$), where unstabilization and sediment transport occur at a very short time scale.

Results of the simulation for the last and main event of the rainfall sequence and the derived water table initial condition of figure 7.14, are shown in figures 7.16 to 7.17.

Figure 7.15 shows the temporal evolution of synthetic quantities, in terms of spatial mean pore pressure at the base of the pervious layer (at $Z = d_{LZ}$) and number of unstable cells. Triggering of cells starts after 2 h from the start of the event and about 80 mm of rainfall. From that instant, the number of unstable cells increases almost linearly at a rate of about 500 cells per hour, through 6 hours after. Then this rate decreases and a maximum is reached at after 8 hours. Pore pressures have a similar behavior, yet, after 16 hours in some parts of the catchment pore pressures still continue increasing until 20 hours from event start, but no increase occurs in the number of unstable cells, because this increase in pore pressure is relative to cells of low slope, that have an high ψ_{cr}.

Model performance may be assessed by comparison of cells that result unstable according to model simulation and cells that have been actually observed as unstable, using methods described in 6.3.

Map of figure 7.16 shows this comparison. Even though differences do exist between the model output and actual slides, reproduction of the location of slides is satisfactory.

In figure 7.17, various results are compared in the Receiver Operating Characteristic (ROC) space and table 7.V shows results in terms of the ROC indices, accuracy $ACC = \frac{TP+TN}{P+N}$ and precision $PRE = \frac{TP}{TP+FP}$ Results obtained indicate, firstly, that performance obtained herein are comparable with the ones obtained by (Baum et al., 2010) for the Mulikteo study case, near Seattle, WA, United States, with the TRIGRS model.

Results obtained with other models, relatively to another case study (Metmann Ridge catchment), retrieved from Rosso et al. (2006), confirm that mass-conservation based models may be more conservative than vertical infiltration models such as TRIGRS (cf. Baum et al., 2010). In fact, the increase of the False-positive rate seems not balanced by increase of the True-positive rate observed for these models, as results from the precision indicator, shown in table 7.V, which is significantly lower than the ones obtained with both TRIGRS v. 2 applications.

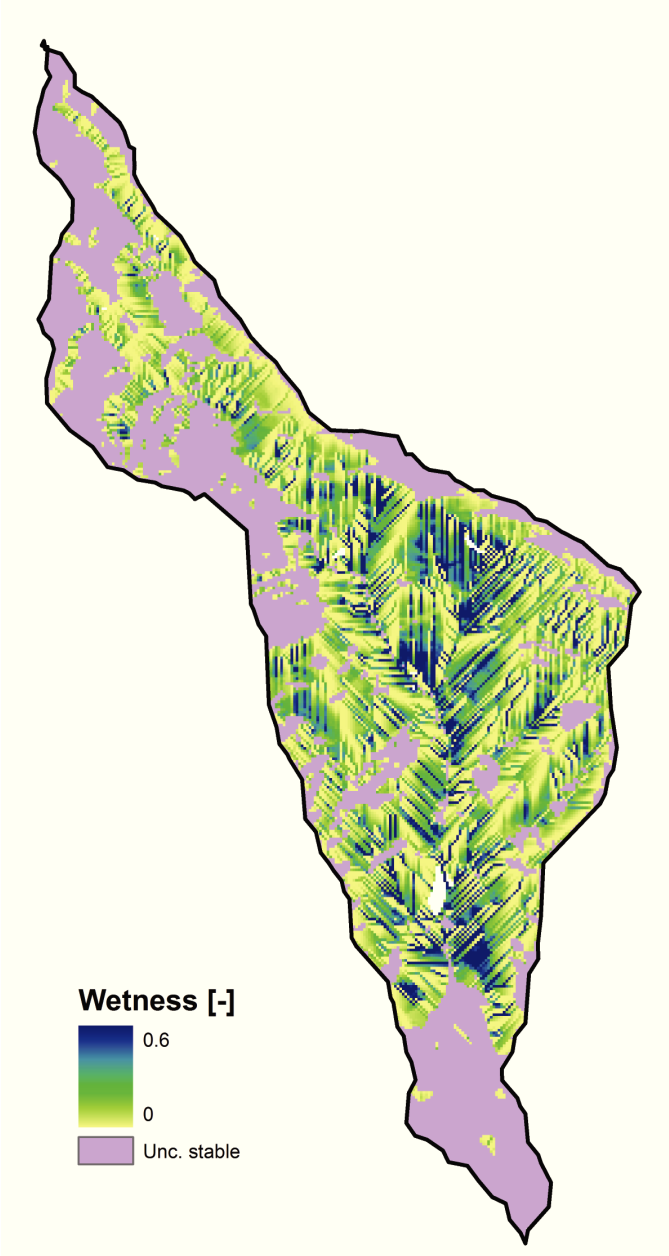

Figure 7.14: Initial wetness grid for the 1st October 2009 event simulation

Table 7.V: Comparison of model performance with results of literature

Model	ACC	PRE
TRIGRS + WTR, Loco	0.84	0.34
TRIGRS, Mulikteo (Baum et al., 2010)	0.83	0.33
Rosso et al. (2006), Mettman Ridge	0.78	0.04
Montgomery and Dietrich (1994), Mettman Ridge	0.83	0.05

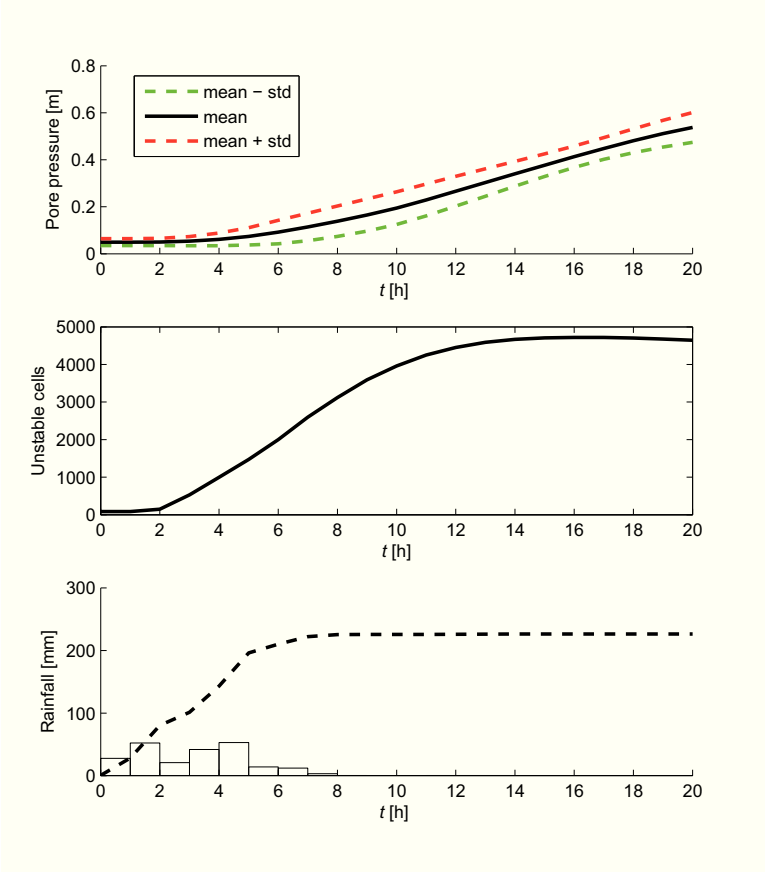

Figure 7.15: Time series of pore pressures and number of unstable cells for 1st October 2009 event

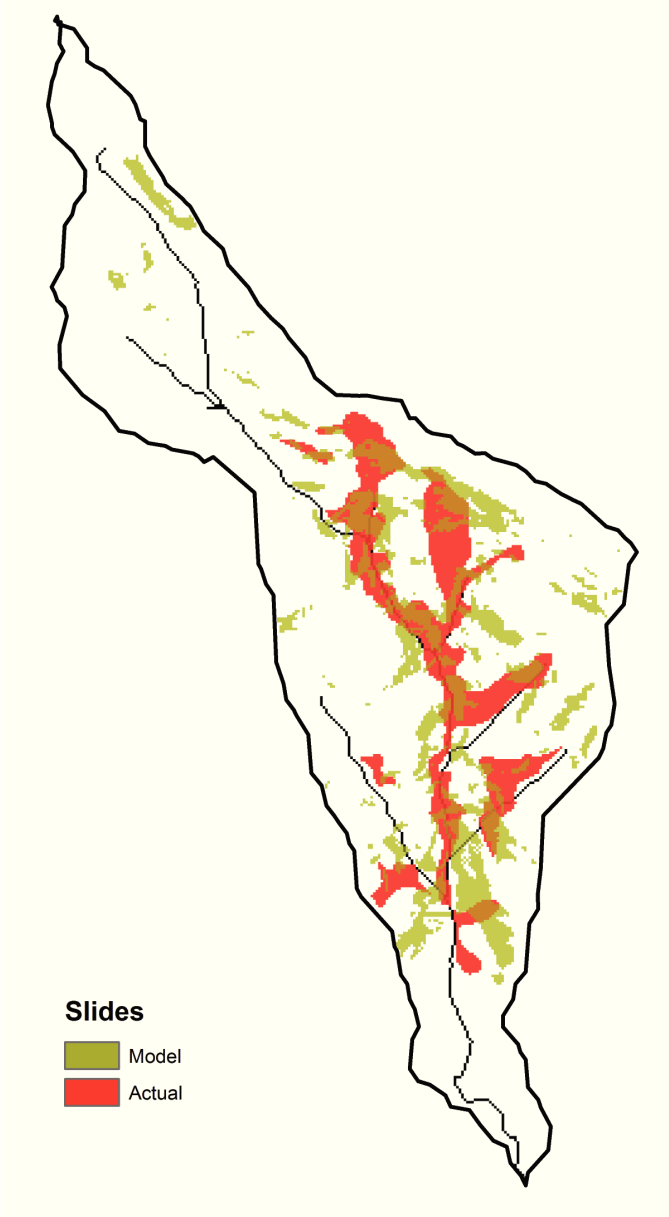

Figure 7.16: Comparison of actual slides on 1stOctober 2009 event and model output

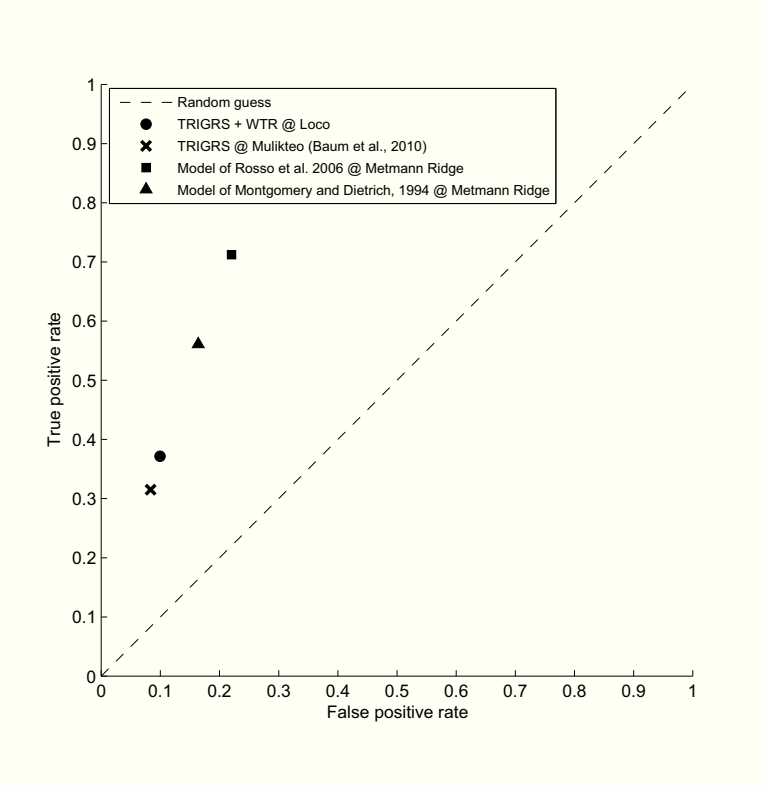

Figure 7.17: Model performance in terms of ROC and comparison with some results of literature (see descriptions in text)

7.4 Applications of the Monte Carlo physically-based approach

One-thousand years of simulation were performed, for a discretization of slopes δ (to which correspond unique values of depth d_{LZ}) and number of drained cells N_d (or equivalently upslope contributing areas $A = 4N_d$ m^2). In particular, the slope was discretized with a interval of 5, $\delta = 30°, 35°, 40°, 45°$ and 50, while the values $N_d = 5, 10, 25$ (which correspond to $A = 20, 40$ and 100 m^2) were considered. To cover the range of values present in the catchment results were then interpolated and extrapolated as later described.

7.4.1 Return period estimation

The Monte Carlo methodology allows to determine return period of maximum pore pressure and of minimum factor of safety.

Because of the memory present in the system, which is accounted for by the WTR model, pore pressures and factors of safety have statistical dependence. The presence of a long summer dry season however allows to consider this statistical dependence limited to the values within an hydrological year, as it is sufficient to bring water table heights to zero, event for relatively high values of N_d, for which the memory is very high. Hence, return periods have been determined considering annual maxima of the pore pressure ψ or annual minima of FS at depth d_{LZ} (see section 4.4.1.

Results of such an analysis are shown in figure 7.18, for the all values of δ and N_d of the discretization.

Because pore pressures are bounded by the saturation value $\psi_{sat} = d_{LZ} \cos^2 \delta$, there is a finite probability associated with the value of ψ_{sat} and return period is upper bounded, as one may notice from the plots of 7.18 (this is more evident for high slope values and more when also N_d is high). In fact, return period may approach infinity for ψ_{sat}, in the case of low N_d and high depth d_{LZ}. Also, from the plots of return period of max pore pressure, it can be noticed how slope affects little return period of a given pore pressure within the range $\psi = 0 - 0.5$.

In order to map return period on a cell basis, the results just illustrated have been interpolated and extrapolated to derive a function $T_R(FS = 1) = T_R(\delta, N_d)$.

Extrapolation may respect the condition $T_R \to \infty$ for $\delta \to \delta_{us}$. At the same time the function should pass for the points derived directly from simulation.

An homographic function of the type $\frac{\beta_1 \delta + \beta_2}{\delta - \delta_{us}}$ which has a vertical asymptote for $\delta \to \delta_{us}$, does not provide a good approximation of the simulation results (it is also unable to pass through more than two points).

The following procedure satisfies the expressed desiderata for interpolation - extrapolation, has been followed:

The quantile functions of pore pressure $Q_\psi(\delta, N_d) : [0 \quad 1] \to [0 \quad \psi_{sat}]$ have been interpolated linearly within the domain $\delta \times N_d = [30° \quad 50°] \times [5 \quad 25]$:

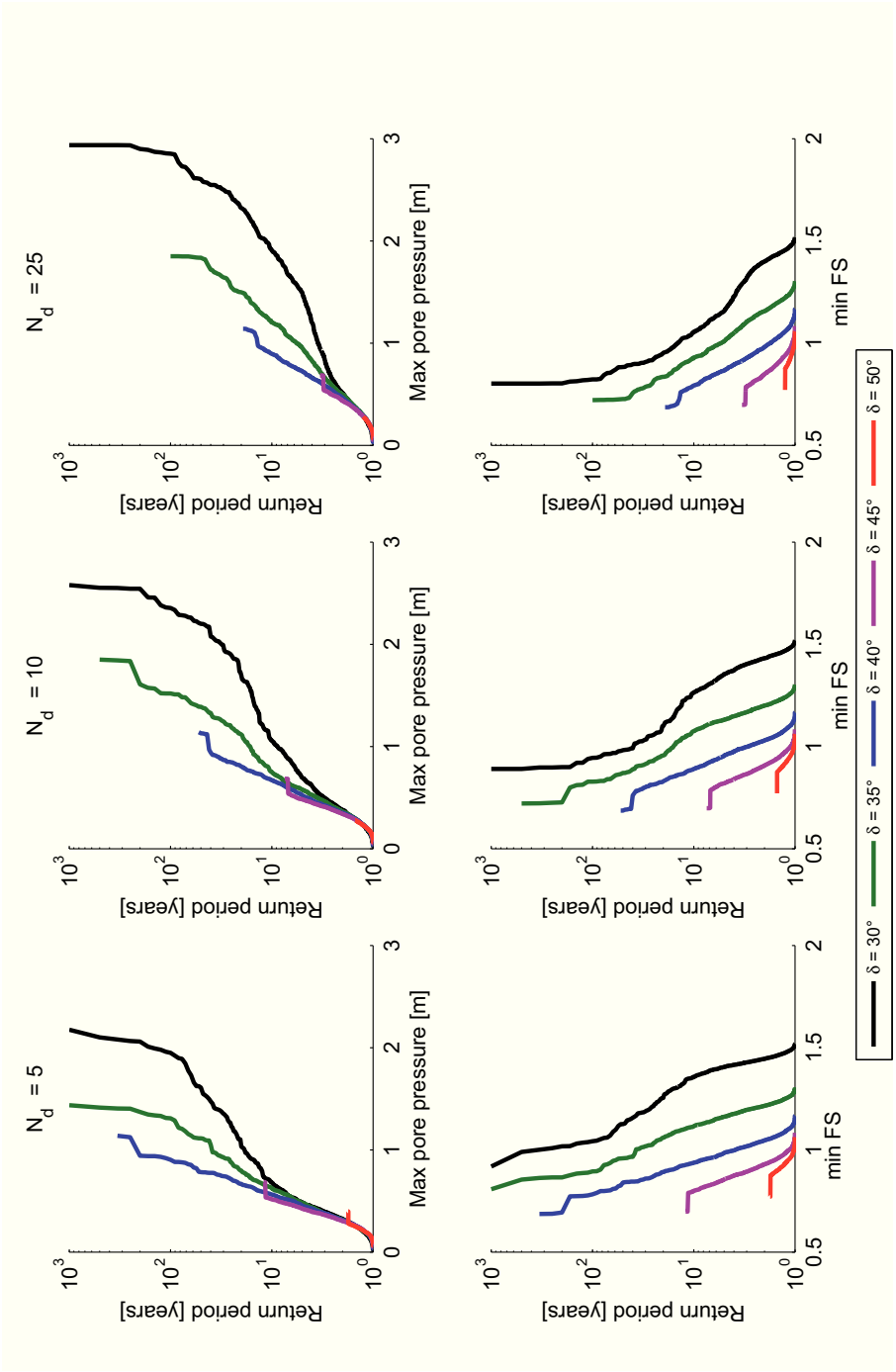

Figure 7.18: Return period of maximum (i.e. at depth d_{LZ}) pore pressure and minimum factor of safety, varying slope and number of drained cells

$$\begin{aligned} Q_\psi(\delta, N_d) &= w_{N_{d,1}}(N_d)[w_{\delta_1}(\delta)Q_\psi(\delta_1, N_{d,1}) + w_{\delta_2}(\delta)Q_\psi(\delta_2, N_{d,1})] \\ &+ w_{N_{d,2}}(N)[w_{\delta_1}(\delta)Q_\psi(\delta_1, N_{d,2}) + w_{\delta_2}(\delta)Q_\psi(\delta_2, N_{d,2})] \end{aligned} \quad (7.1)$$

where $\delta_1 \leqslant \delta < \delta_2$, $N_{d,1} \leqslant N_d < N_{d,2}$, $w_{N_{d,1}} = \frac{N_d - N_{d,1}}{N_{d,2} - N_{d,1}}$, $w_{N_{d,2}} = \frac{N_d - N_{d,2}}{N_{d,2} - N_{d,1}}$, $w_{\delta_1} = \frac{\delta - \delta_1}{\delta_2 - \delta_1}$ and $w_{\delta_2} = \frac{\delta - \delta_2}{\delta_2 - \delta_1}$.

Quantile functions Q_{FS} for factor of safety FS can be derived from Q_ψ by transforming the function value with equation 6.24. Extrapolation for slopes in the δ interval $[\delta_{us} \quad 30^\circ]$ was conducted considering $\delta_1 = \delta_2 = 30^\circ$ in equation 7.2. Extrapolation in the N_d interval $[0 \quad 5]$ was carried out considering $N_{d,1} = N_{d,2} = 5$, while for $N_d > 25$, $Q_\psi(N_{d,2}) = d_{LZ}(\delta)1_A(1)$, where $1_A = 1 \quad$ if $\quad p = 1, \text{and} \quad 1_A = 0 \quad$ otherwise, from which corresponds to $N_{d,2} \to +\infty$ (memory is so high that soil is always fully saturated).

This procedure leads to the curves of figure 7.19. From the curves it can be noticed that number of N_d of cells significantly affects return period, that drastically decreases going from $N_d = 5$ to $N_d = 25$.

The map of return period of cell failure, resulting from application of the Monte Carlo method, is shown in figure 7.20.

Combining information from the map and depth d_{LZ} map, total volumes associated with cell failure as a function of return period were derived, in order to synthetically represent results of the map of figure 7.20. Besides, a curve like this may be useful for design of mitigative structures, such as debris-flow basins and retaining walls. Triggered volumes are also expressed as rate of total potentially unstable volume (that is total basin area minus area of unconditionally stable and bedrock outcropping total areas). This rate is equal to $0.1, 0.18, 0.42, 0.52$ and 0.62 for $T_R = 5, 10, 50, 100$ and 1000 years, respectively.

Based on these results, return period of events of the magnitude of the one occurred on 1$^{\text{st}}$October 2009 at Loco catchment may be of the order of 20 - 50 years, which is significantly less than return periods associated to the rainfall event via IDF curves, that results of the order of hundreds of years (cf. Foti et al., 2012).

7.4.2 Intensity-Duration model evaluation

The Monte Carlo simulation allows to evaluate, from a stochastic and physically-based perspective, empirical models. Here the widely-used $I - D$ model is tested.

In an ideal situation, the pore pressure (equivalently, the factor of safety) may be constant for curves that are represented by the empirical model's equation. For instance, for the $I - D$ empirical model, iso$-\psi$ curves should be linear in the $\log(I) - \log(D)$ plane.

Because of the stochastic nature of rainfall, events with different time history, that have the same duration and mean intensity (defined as in figure 4.3), may lead to different pore pressures, or viceversa, the same pore pressure may be determined by events of different duration and mean intensity.

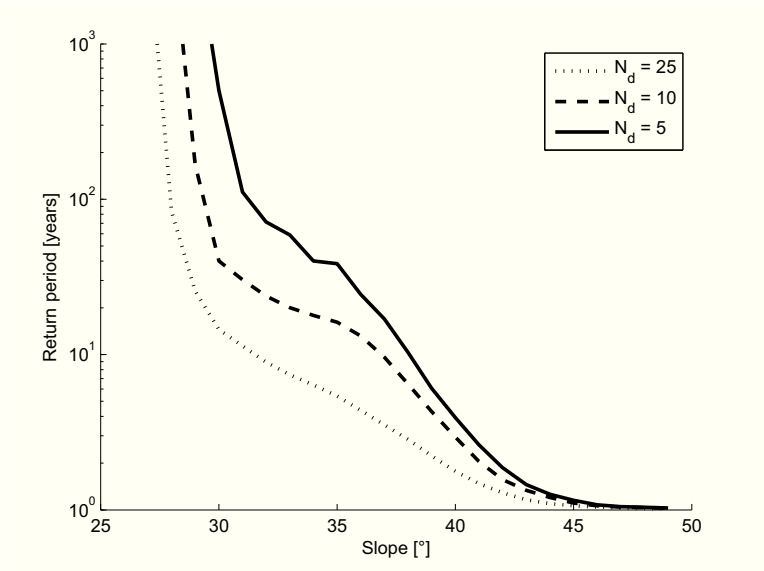

Figure 7.19: Return period as a function of slope and number of number of draining cells for the Loco catchment

This introduces variability in the model output, but may change significantly the relationship between pore pressure and rainfall characteristics, that may be finally respect in average by the empirical model.

A comparison with constant intensity hyetographs has also been performed, in order to investigate the influence of a real-like randomly-variable-intensity hyetographs on potential to landsliding. For the biunivocal relationship between Intensity-Duration and rectangular hyetographs (to a given Intensity and Duration a single rainfall corresponds, and viceversa), iso-pore pressure curves are represented in the $I - D$ plane by a well-defined curves.

Results relative to ψ_{cr} are shown in figures 7.22 $-$ 7.25 varying slope δ and number of drained cells N_d, in the $\log(I) - \log(D)$ space.

Constant hyetograph simulations lead to iso$-\psi$ curves that differ significantly from the linear relation in the bi-logarithmic $I-D$ plane . Similar results have been obtained for physically-based models in general (e.g. Rosso et al., 2006; Salciarini et al., 2008).

One may distinguish four regions in the $I - D$ plane, relatively to the constant hyetograph results. The first region is the one delimited by the vertical asymptote, $D = D^*$, presented by the plotted curves. No matter what the intensity is, the pore pressure does not reach the fixed value if duration is less than D^*. This corresponds to the minimum duration that it is needed to the pore pressures to build up at the basal boundary and reach the fixed value, and depends on hydraulic characteristics and depth d_{LZ}. The second region may be located by the horizontal asymptote of the plots, $I = I^*$. Intensities below I^* are insufficient to build up

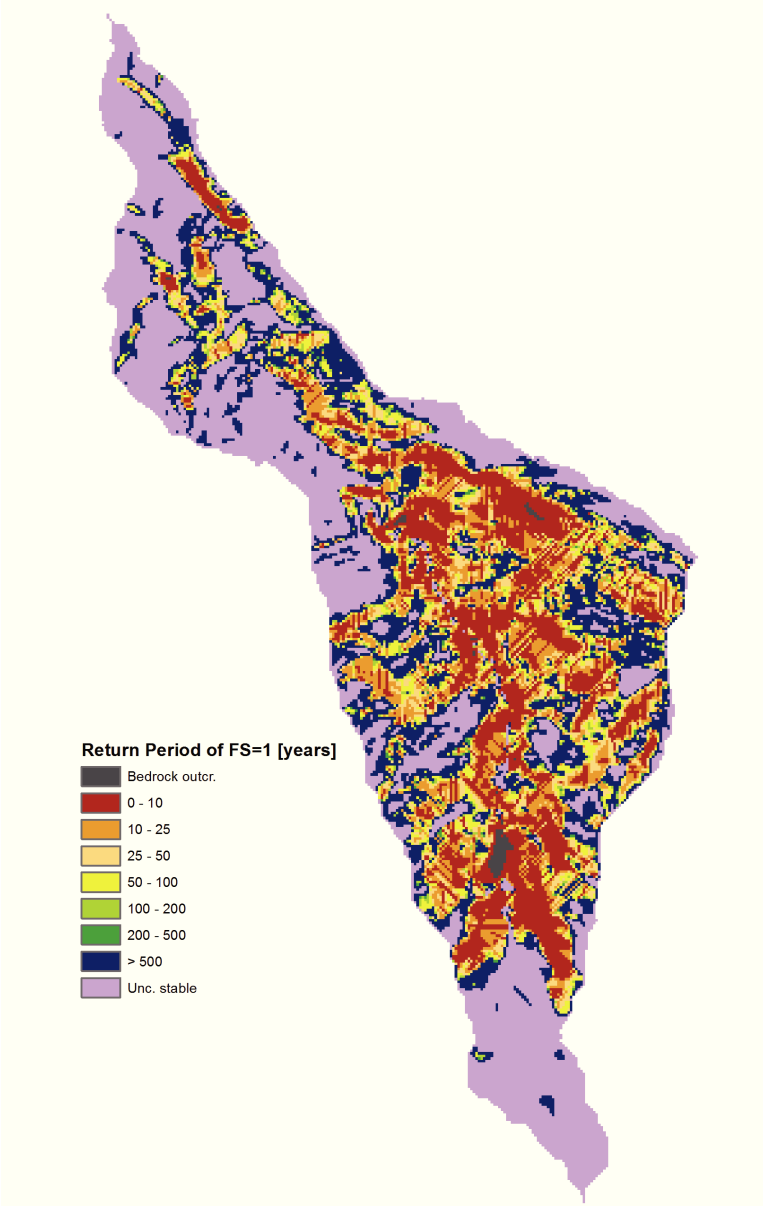

Figure 7.20: Return period of cell failure for Loco catchment

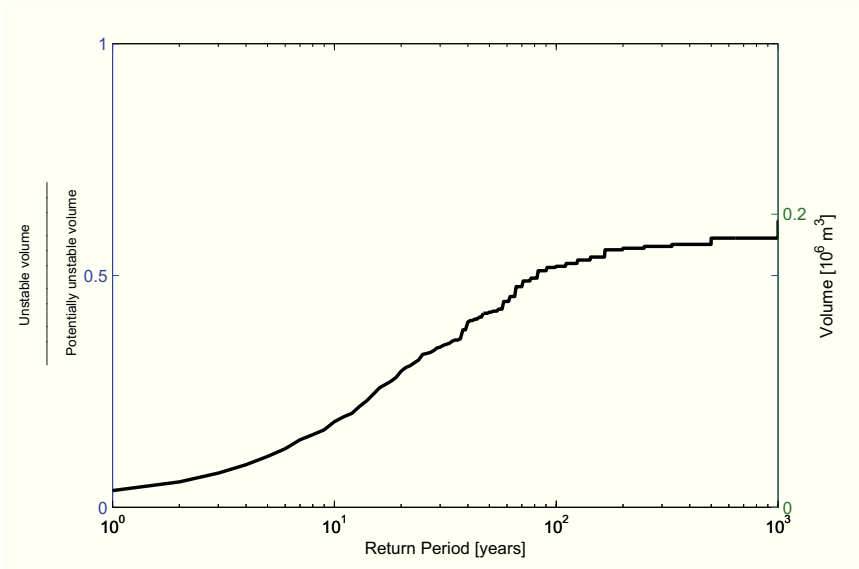

Figure 7.21: Return period of unstable volume

pore pressures, no matter how prolonged precipitation is. This is related to the accounting of leakage in the model. The remaining two regions have one boundary that coincides with the curve relative to $\psi = \psi_{sat}$. $I - D$ points above that curve, determine $\psi = \psi_{sat}$. Pore pressures vary within the range $\psi = 0 - \psi_{sat}$ in the remaining region.

Results of the Monte Carlo simulations have to be distinguished into two categories, when these are compared with the constant-hyetograph simulations. Because the latter have been determined considering an initial wetness $\omega = 0$, comparison of their trend with the former may be valid only for cases where this occurs for simulated events. Hence in the figures 7.22-7.25 simulation points, representing rainfall events that produced the fixed (critical) pore pressure, are plotted separately the two cases $\omega(t = 0) = 0$ (plots on the left) and $\omega(t = 0) > 0$ (plots on the right).

Looking at the points of the relative to the case $\omega = 0$ one finds that, although with a non negligible degree of scattering, iso$-psi$ points tend to be sensibly linear-like.

Things change drastically when one considers the case $\omega > 0$. In this case the scattering is very high and it is very difficult to interpret with a line, nether as an average curve or a lower envelope curve. This occurs even for the case of $N_d = 5$ - which is, in fact, the most representative in small steep catchments, cf. figure 7.11 - where pore-pressure memory is less than for the other cases.

This results obtained allow to conclude the following:

- In the case that pore-pressure memory is low, which may be the case of

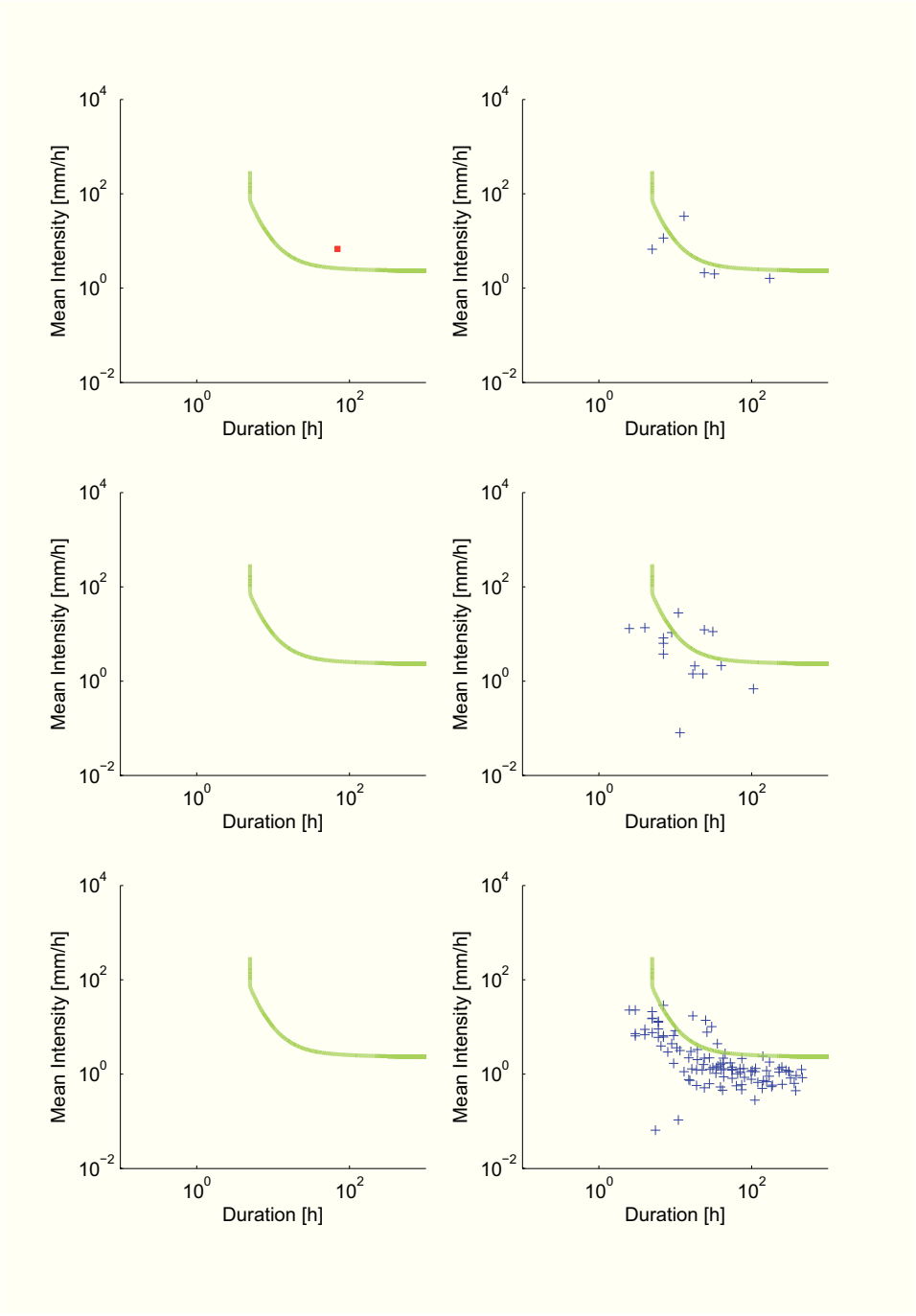

Figure 7.22: Intensity-Duration plot for slope $\delta = 35°$

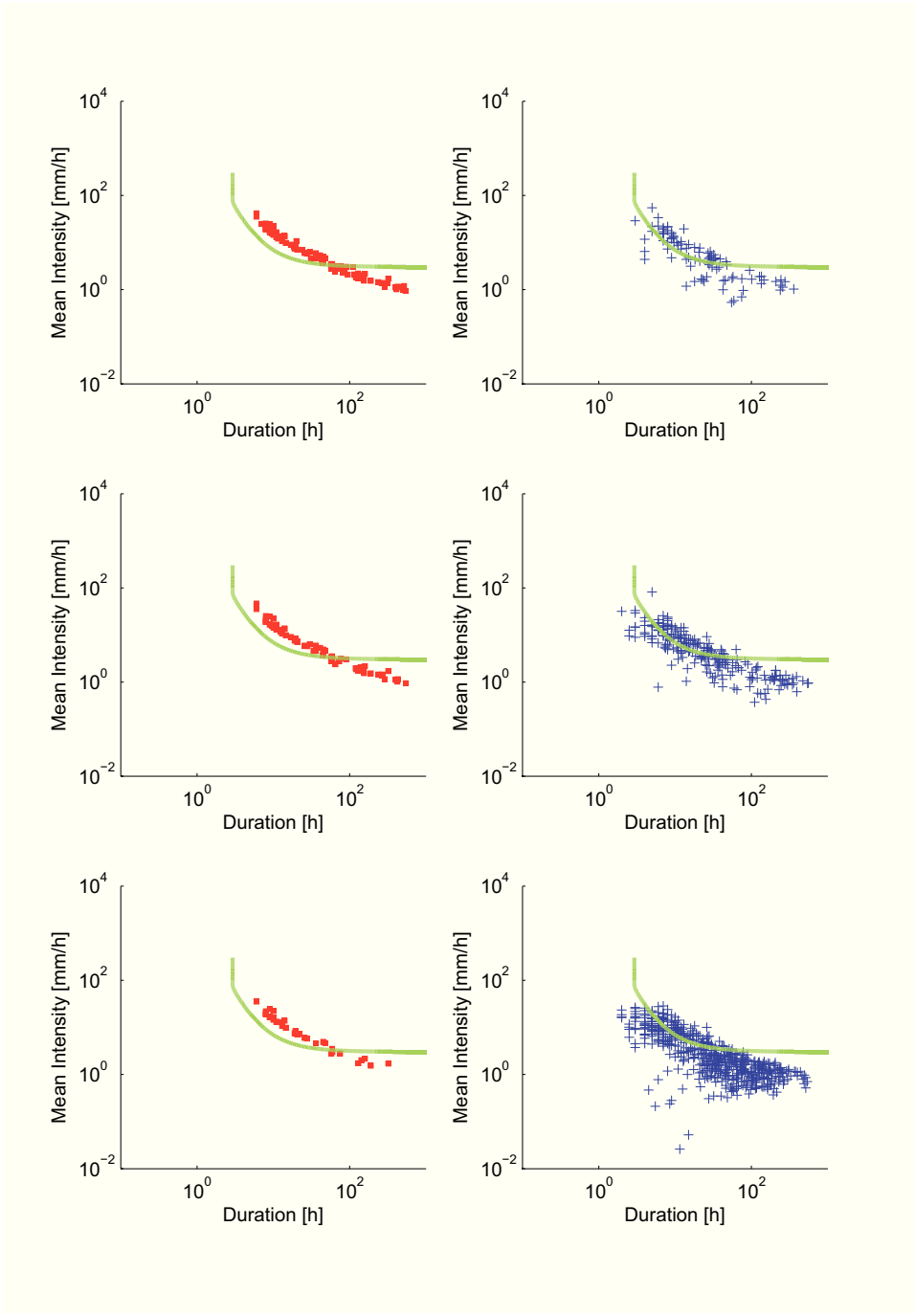

Figure 7.23: Intensity-Duration plot for slope $\delta = 40°$

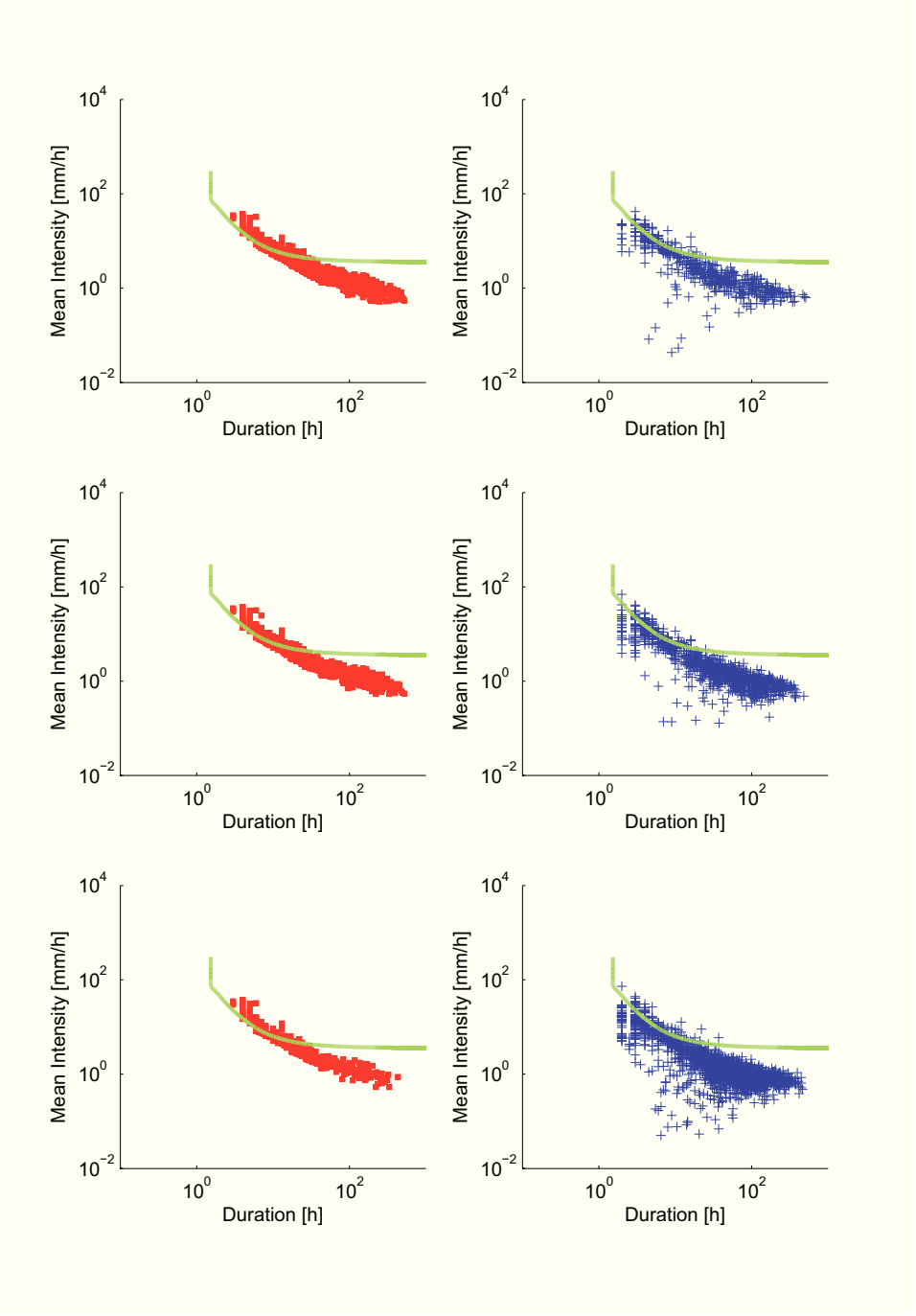

Figure 7.24: Intensity-Duration plot for slope $\delta = 45°$

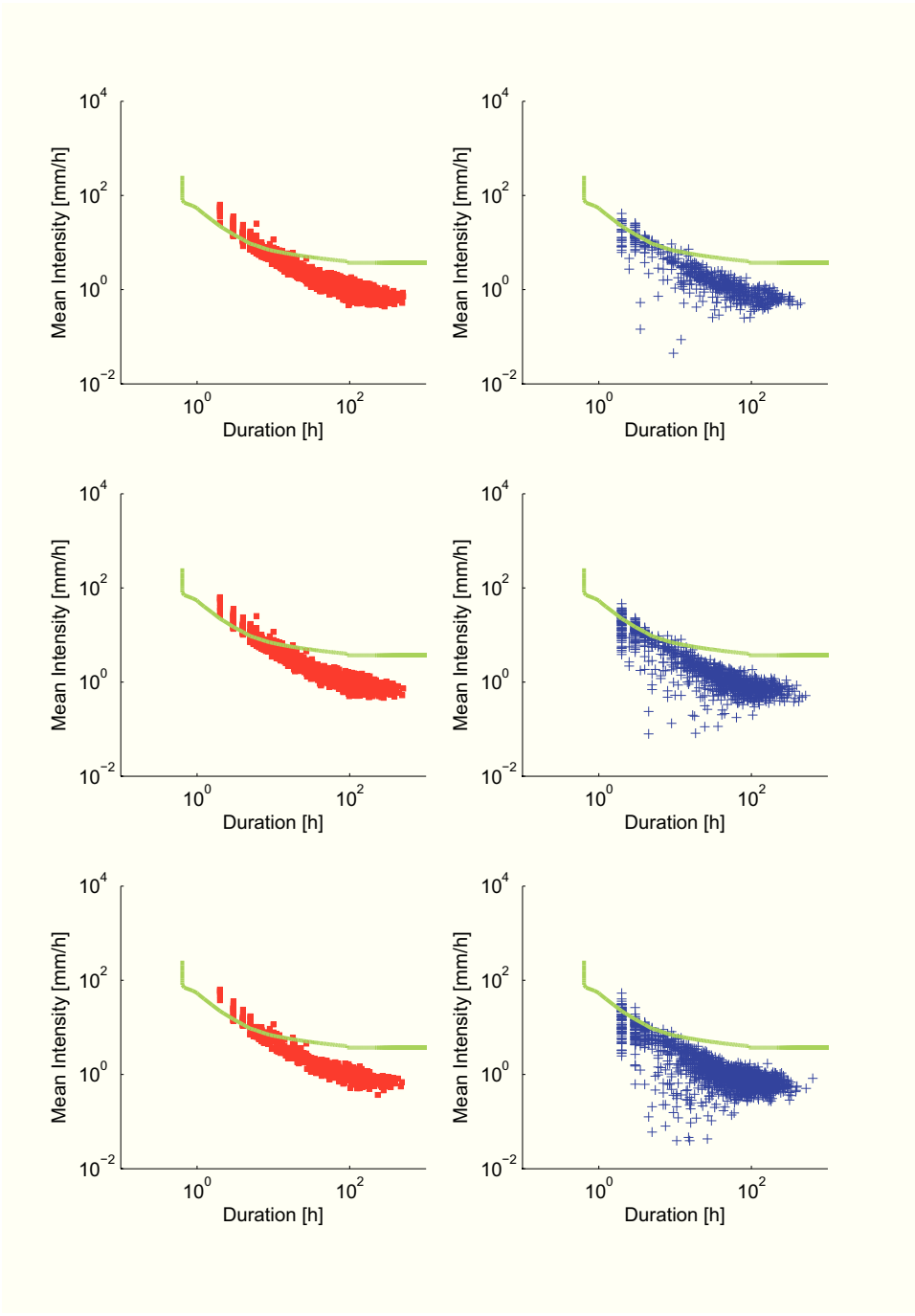

Figure 7.25: Intensity-Duration plot for slope $\delta = 50°$

hillslopes in small catchments (relatively upslope contributing area A) and relatively high hydraulic permeability (indicatively $K_S > 10^{-4}$), and rainfall events occur sufficiently distant one from each other, so that initial water table depth is neglegible at the beginning of events, the structure of rainfall induce a regolarization of iso-pore-pressure curves (rainfall thresholds for landslide triggering) with respect to deterministic thresholds based on rectangular hyetographs, that may be interpreted with a good degree of accuracy by a straight line in the $log(I) - log(D)$ plane. Hence, the $I - D$ model may have a stochastic-physically-based justification, in the cases that pore-pressure memory is low, i.e. listed above conjectures hold to be true with good approximation.

- Such a regularization is so that for relatively regular rainfall durations, say $D < 12$ h, a real hyetograph is more likely to produce a lower pore pressure than a rectangular hyetograph of the same duration and mean intensity to landsliding of the real one. For this duration range, rectangular hyetographs may be a little conservatory for estimating of return periods of landslide triggering, For higher durations, the opposite occurs. This means, that even neglecting pore-pressure memory, a rectangular hyetograph leads to an overestimation of the return period of landslide triggering in the case of high durations.

- In the general case, memory has to be accounted for. The presence of memory may drastistically decrease the return period of landsliding.

- If ψ_{cr} is high (cf., e.g., 7.22), which may occur for relatively high basal depths d_{LZ}, critical pore pressures can be reached only in response of a sequence of relatively intense and near events.

- Deterministic thresholds, based on the hypothesis of rectangular hyetographs, suffer the limitations related to the above issues, and in particular that they are not conservative for rainfall events of long duration. Moreover, estimation of return period in this case may suffer of arbitrariness of initial conditions (initial water table depth), when performed via IDF curves. In fact, in this case analyses are needed to assess the probability of a given hyetograph conditioned to a given initial water table depth. An initial water table depth of zero, as any other value, is an event that has a given non-exceedance probability, that has to be accounted for in estimating return periods, and is equal to one only if pore-pressure memory can be neglected.

Chapter 8

Conclusions

Understanding the hydrological control on shallow landslide triggering, is a fundamental step towards an efficient landslide risk mitigation. Indeed, landslide early warning systems require information on the link between rainfall and landslide occurrence. Furthermore knowledge of the hydrologic conditions that trigger landslides in a spatially-distributed fashion enables to map return period of landslide triggering within a landslide-prone region, which combined with appropriate propagation models allow for the development of hazard and risk maps that may be effectively used as an aid for urban and landslide mitigation planning.

In this study the hydrological control on shallow landslide triggering has been analyzed making use of a Monte Carlo methodology, that combines stochastic and deterministic modeling approaches. The developed methodology comprises the following components: (i) a seasonal Neyman-Scott Rectangular Pulses (NRSP) model to generate synthetic point hourly rainfall data; (ii) a module for rainfall event identification and separation from dry intervals; (iii) the Transient Rainfall Infiltration and Grid-Based Regional Slope-Stability (TRIGRS) model, version 2 (Baum et al., 2008, 2010) to simulate landslide triggering by rainfall infiltration, combined with a water table recession (WTR) model that computes the initial water table height to consider in simulating rainfall events with TRIGRS.

The modeling approach has been applied to the Loco catchment in the Peloritani Mountains in northeastern Sicily of Italy, an area with high landslide risk, as recently demonstrated by the regional debris-flow event that occurred on 1 October 2009, which caused 37 casualties and millions of euros of damage.

A 9-years-long 10-minutes rainfall time series measured at Fiumedinisi SIAS rain gauge station, has been used to calibrate and validate the stochastic rainfall model. A Weibull distribution, of shape parameter $b = 0.6$, has been used to model the intensity of rectangular pulses and seasonality in the series was reproduced by calibrating separately the model for the four homogeneous rainy seasons that were identified on the observed series (total number of parameters equals to twenty).

The NRSP model proved to be capable of preserving several stochastic features of the observed rainfall time series. Model validation has been carried out by testing

the reproduction of rainfall event characteristics important with respect to landslide triggering. In particular, reproduction of total cumulative event rainfall H_{tot} and duration D_{tot}, and of the correlation between the mean intensity $I = H_{tot}/D_{tot}$ and the duration, were considered for the validation. The results of this test are globally satisfactory, even though model seems to have a tendency to overestimate the $\log I_{tot}$-$\log D_{tot}$ linear correlation.

Suitability for modeling the triggering of landslides in the investigated area of the TRIGRS - WTR model has been tested by applying it to the three-event rainfall sequence that triggered landslides on 1 October 2009. Model performance has been assessed by comparing mapped slides for the 1 October 2009 event with model output, also in terms of ROC-based (Receiver Operating Characteristic) indices. Model performs at least as well as other known applications of the TRIGRS v. 2 model to other study cases areas (ROC-Accuracy $>$ 0.80 and ROC-Precision $>$ 0.30). Model performance seems better than more simple models, such as the ones by Montgomery and Dietrich (1994) and Rosso et al. (2006), which have a comparable ROC-Accuracy but very low ROC-Precision, being more conservative than TRIGRS.

The Monte Carlo modeling scheme has been applied to single cells for the range of slope, basal boundary depth and upslope contributing areas (or, equivalently, number of drained cells) observed in the case-study catchment. One-thousand-years-long simulations have been performed for all combination of values. Following previous studies an univocal relationship between basal boundary depth, which is in this case also the depth of the potential sliding surface, has been adopted for analyzing a range of slopes (TRIGRS) and upslope contributing areas (WTR model).

The Monte Carlo approach has been applied for estimation of return periods of shallow landslide triggering and for the evaluation of the most commonly-used types of empirical rainfall threshold.

Simulations of the type described above have been utilized to map return period of cell geomechanical failure in a spatially-distributed fashion. Results of the single cell simulations have been appropriately interpolated for that purpose. Simulating for single cells and then applying the results to the catchment drastically increases computational efficiency of the procedure, that may be prohibitively time-consuming if directly applied to the entire catchment.

In exploiting the simulations for return period estimation, in general there is statistical dependence among the response variables (and in particular of pore pressure), because the water table depth at the beginning of a given storm is determined, in general, by the entire past time history of rainfall. However, for the arid climate that characterizes the analyzed study case, this statistical dependence is limited to the hydrological year, because the summer season, which is practically completely dry, is long enough to allow neglecting initial water table depth (of the surficial strata interested by landslide phenomena) at the beginning of the hydrological year (September). This still does not open the possibility to compute return period of stability failure (i.e. of a factor of safety $FS < 1$) as the mean interarrival time between $FS < 1$ occurrences, yet it allows to estimate the return

period by analyzing the cumulative frequency distribution derived from annual minimum series of FS (or, equivalently pore pressure annual maxima series).

On this issue it should be mentioned that return period estimation based on rainfall IDF curves, common to many studies of other researchers, is in principle flawed, because of the arbitrariness of the initial condition that is assumed. In fact, in this case analyses are needed to assess the probability of a given hyetograph conditioned to a given initial water table depth. An initial water table depth of zero, as any other value, is an event that has a given non-exceedance probability, that has to be accounted for in estimating return periods, and it is always equal to 1 only if response memory can be neglected, which is seldom the case.

Relatively to the second issue analyzed in the dissertation (rainfall characteristics - landslide occurrence relationship), specific analyses have been conducted on the Intensity-Duration (I-D) model, widely used to interpret observed rainfall-landslide data: as it is well-known, rainfall thresholds for the initiation of landslide have been expressed by many different researches as $I = \alpha D^{\beta}$, which is obviously a straight line in a $\log(I)$-$\log(D)$ plane. Then, points of equal factor of safety, or iso-pore-pressure curves, in the $\log(I)$-$\log(D)$ plane have to lay on a straight line.

The obtained results allow to state that, actually, stochastic structure of real rainfall events combined with the infiltration response reveal in a certain sense a theoretical justification to the I-D relationship. Iso-pore-pressure points, in the bi-logarithmic rainfall (mean) Intensity - Duration plane, lay, with relatively low scattering, around a straight line, in the cases that initial water table height is negligible.

This means that the I-D model represents a valid model to interpret data in the case that memory of pore pressures is negligible. This holds true basically when the hydraulic conductivity of the soil is relatively high (an indicative minimum value may be $10^{-4} - 10^{-3}$ m/s), depending on rainfall characteristics (relatively isolated rainfall events) and hillslope position in the catchment (low values of upslope contributing area).

In other, most likely, cases, the I-D model should be coupled with an antecedent rainfall model.

The iso-pore-pressure scatter plots derived from the Monte Carlo simulations have been also compared with iso-pore-pressure curves that result in response to a rectangular hyetograph of same (mean) intensity and duration (assuming in this case an initial water table depth of zero), in order to study the influence of rainfall intensity stochastic variability on landslide triggering . This analysis has been conducted considering separately the simulation points relative to a negligible initial water table height from the ones relative to a not negligible initial water table height.

Comparison in the former case reveal that for relatively short rainfall event durations, say $D < 12$ h, a variable-intensity hyetograph may produce a pore-pressure response less than the one induced by a rectangular hyetograph of the same (mean) intensity and duration, while the opposite occurs for high durations. From the comparison relative to the case of significant water table depth, it can be stated that in dependence of the initial water table depth (i.e. rainfall time history

preceding the event) even rainfall events of relatively low intensity and duration may trigger landslides.

The overall conclusion of the dissertation is that coupling a stochastic rainfall generator with physically-based hydrological models within a Monte Carlo approach can provide useful insight on the hydrologic control on shallow landslides, since it enables to take into account the variable intensity of precipitation within an event, as well as the inter-arrival times and the resulting water table recession between storms. Indeed, both factors can affect significantly potential landslide triggering and therefore should be properly taken into account both for planning mitigation measures, as well as for early warning of landslide phenomena.

List of Figures

2.1 Landslide types (after Highland and Bobrowsky, 2008) 13
2.2 Scheme for infinite slope equilibrium analysis (adapted from Rosso et al., 2006). On the left, the coordinate system used by Iverson (2000) 17
2.3 Scheme of contour-based models (adapted from Rosso et al., 2006) . 19

3.1 Map of landslides triggered on 1 October 2009 in the Peloritani area 26
3.2 Some photographs showing destruction caused by debris flows occurred on 1 October 2009 in the Peloritani Mountains area, southern-eastern Sicily, Italy 27
3.3 Map showing location of the Peloritani area and location of rain gauges of interest 29
3.4 Cumulative rainfall path that yielded debris flows in the Peloritani Mountains on 1 October 2009, in rain gauges located nearby the area 30
3.5 Sketch relative to calibration of FLaIR model (cf. Sirangelo and Versace, 1996) 30
3.6 Admissibility region for the parameters of the gamma impulse response function and difference between upper limit and lower limit functions. Best pair of parameters is $a = 17.615$, $b = 0.115$ 33
3.7 Filter function for the FLaIR model, resulting from calibration . . . 33
3.8 Plot of the mobility ratio and comparison with warning levels and rainfall hourly series 34
3.9 Time plot of number of landslides from the AVI database and simultaneous rainfall data availability 37
3.10 Plot showing empirical thresholds and data from which they are derived 38

4.1 Scheme of the Monte Carlo Simulation used to investigate hydrologic control on landslide triggering 43
4.2 Definition of total duration, volume and interarrival time of rainfall events 44
4.3 Definition of rainfall duration D and (mean) intensity I to landsliding 46

5.1 Sketch of the Neyman-Scott Rectangular Pulses process (adapted from Cowpertwait et al. (1996) and Salas (1993)) 52

6.1 Shallow groundwater conditions in hillside soils. Adapted from Baum et al. (2010) . . . 58
6.2 Vertical soil-water-content profiles from the ground surface down to an arbitrary depth, Z, showing the water-table-rise as a result of infiltration (after Baum et al., 2010) . . . 62
6.3 Plot of equation 6.2 assuming a slope $\delta = 40^\circ$ and hydraulic properties for the Loco catchment in table 7.IV, for different values of upslope draining cells N_d . . . 65

7.1 Moments for each month for Fiumedinisi SIAS rainfall data . . . 68
7.2 Moments varying aggregation time scale: January-February-March season model . . . 73
7.3 Moments varying aggregation time scale: September-October model 73
7.4 Moments varying aggregation time scale: November model . . . 74
7.5 Moments varying aggregation time scale: December model . . . 74
7.6 Comparison of Empirical Cumulative Frequency for Cumulative Event Rainfall for observed series (black dotted line) and simulated series (1000 years) . . . 76
7.7 Comparison of Empirical Cumulative Frequency for Cumulative Event Rainfall for observed series (black dotted line) and simulated series (1000 years) . . . 77
7.8 Comparison of $\log(I_{tot}) - \log(D_{tot})$ correlation for observed (blue circle) and simulated data . . . 78
7.9 Sequence of rainfall events considered for simulation of the 1^{st} October 2009 debris-flow event . . . 79
7.10 Map showing the location and 2-meters-resolution digital terrain model of the study area, Loco catchment, Sicily (Italy) . . . 81
7.11 GRID maps of interest for model application . . . 82
7.12 Factor of safety corresponding to $\omega = 0$ and $\omega = 1$ for cells of the Loco Catchment . . . 84
7.13 Critical wetness for cells of the Loco catchment . . . 84
7.14 Initial wetness grid for the 1^{st} October 2009 event simulation . . . 86
7.15 Time series of pore pressures and number of unstable cells for 1^{st} October 2009 event . . . 87
7.16 Comparison of actual slides on 1^{st} October 2009 event and model output . . . 88
7.17 Model performance in terms of ROC and comparison with some results of literature (see descriptions in text) . . . 89
7.18 Return period of maximum (i.e. at depth d_{LZ}) pore pressure and minimum factor of safety, varying slope and number of drained cells 91
7.19 Return period as a function of slope and number of number of draining cells for the Loco catchment . . . 93
7.20 Return period of cell failure for Loco catchment . . . 94
7.21 Return period of unstable volume . . . 95
7.22 Intensity-Duration plot for slope $\delta = 35^\circ$ . . . 96

7.23 Intensity-Duration plot for slope $\delta = 40°$ 97
7.24 Intensity-Duration plot for slope $\delta = 45°$ 98
7.25 Intensity-Duration plot for slope $\delta = 50°$ 99

List of Tables

3.I Confusion matrix 36
3.II Thesholds maximizing the objective function, at various cumulative rain durations a w values. Results of validation of the thresholds . . 39

6.I Confusion matrix for spatial output of an hydrologic model 65

7.I Statistics of the sample of Fiumedinisi SIAS hourly rainfall data . . 69
7.II Results of NSRP calibration 71
7.III Comparison between sample and theoretical moments (sample, theoretical and relative error in percentage) 72
7.IV Material strength and hydraulic properties for surficial strata of Loco catchment 83
7.V Comparison of model performance with results of literature 87

References

Aleotti, P. (2004). A warning system for rainfall-induced shallow failures. *Engineering Geology*, 73(3-4):247–265. Rainfall-triggered landslides and debris flows.

Armanini, A., Fraccarollo, L., and Rosatti, G. (2009). Two-dimensional simulation of debris flows in erodible channels. *Computers & Geosciences*, 35(5):993 – 1006.

Baum, R. L. and Godt, J. W. (2010). Early warning of rainfall-induced shallow landslides and debris flows in the usa. *Landslides*, 7:259–272.

Baum, R. L., Godt, J. W., and Coe, J. A. (2011). Assessing Susceptibility and Timing of shallow landslide and Debris Flow initiation in the Oregon Coast Range, USA. *Italian Journal of Engineering Geology and Environment*, pages 825–834.

Baum, R. L., Godt, J. W., Coe, J. A., and Reid, M. E. (2012). Assessment of shallow landslide potential using 1-D and 3-D slope stability analysis. In Eberhardt, E., Froese, C., Turner, A. K., and Leroueil, S., editors, *Landslides and Engineered Slopes: Protecting Society through Improved Understanding*.

Baum, R. L., Godt, J. W., and Savage, W. Z. (2010). Estimating the timing and location of shallow rainfall-induced landslides using a model for transient, unsaturated infiltration. *J. Geophys. Res.*, 115:F03013.

Baum, R. L., Savage, W. Z., and Godt, J. W. (2002). TRIGRS-A FORTRAN Program for Transient Rainfall Infiltration and Grid-Based Regional Slope-Stability Analysis.

Baum, R. L., Savage, W. Z., and Godt, J. W. (2008). TRIGRS-A FORTRAN program for transient rainfall infiltration and grid-based regional slope-stability analysis, version 2.0.

Bras, R. L. (1990). *Hydrology: An introduction to hydrologic science*. Addison-Wesley, Reading, Mass.

Burlando, P. and Rosso, R. (1996). Scaling and muitiscaling models of depth-duration-frequency curves for storm precipitation. *Journal of Hydrology*, 187(1âĂŞ2):45 – 64. <ce:title>Fractals, scaling and nonlinear variability in hydrology</ce:title>.

Caine, N. (1980). The rainfall intensity: Duration control of shallow landslides and debris flows. *Geografiska Annaler. Series A, Physical Geography*, 62(1/2):pp. 23–27.

Calenda, G. and Napolitano, F. (1999). Parameter estimation of neyman-scott processes for temporal point rainfall simulation. *Journal of Hydrology*, 225(1-2):45 – 66.

Calvo, B. and Savi, F. (2009). A real-world application of monte carlo procedure for debris flow risk assessment. *Computers & Geosciences*, 35(5):967 – 977. Modelling and Simulation of Dangerous Phenomena for Hazard Mapping.

Campbell, R. H. (1975). *Soil Slips, Debris Flows, and Rainstorms in the Santa Monica Mountains and Vicinity, Southern California*. Washington, D.C.

Cancelliere, A. and Salas, J., D. (2004). Drought length properties for periodic-stochastic hydrologic data. *Water Resour. Res.*, 40(2):W02503.

Cannon, S. (1988). *Landslides, Floods, and Marine Effects of the Etorm of January 3-5, 1982, in the San Francisco Bay Region, California*, chapter Regional rainfall-threshold conditions for abundant debris-flow activity, pages 35–42. Number 1434 in US Geological Survey Professional Paper. US Geological Survey, Washington, D.C.

Capparelli, G. and Tiranti, D. (2010). Application of the moniflair early warning system for rainfall-induced landslides in piedmont region (italy). *Landslides*, 7:401–410.

Capparelli, G. and Versace, P. (2011). FLaIR and SUSHI: two mathematical models for early warning of landslides induced by rainfall. *Landslides*, 8:67–79. 10.1007/s10346-010-0228-6.

Carslaw, H. S. and Jaeger, J. C. (1959). *Conduction of Heat in Solids*. Oxford Univ. Press, New York.

Cowpertwait, P. (1991). Further developments of the Neyman-Scott clustered point process for modeling rainfall. *Water Resour. Res.*, 27(7):1431 – 1438.

Cowpertwait, P. S. P. (1994). A generalized point process model for rainfall. *Proceedings of the Royal Society of London. Series A: Mathematical and Physical Sciences*, 447(1929):23–37.

Cowpertwait, P. S. P. (2004). Mixed rectangular pulses models of rainfall. *Hydrology and Earth System Sciences*, 8(5):993–1000.

Cowpertwait, P. S. P. and O'Connell, P. E. (1997). A regionalised neyman-scott model of rainfall with convective and stratiform cells. *Hydrology and Earth System Sciences*, 1(1):71–80.

Cowpertwait, P. S. P., O'Connell, P. E., Metcalfe, A. V., and Mawdsley, J. (1996). Stochastic point process modelling of rainfall. I. Single-site fitting and validation. *Journal of Hydrology*, 175(1-4):17 – 46.

Cruden, D. M. and Varnes, D. J. (1996). *Landslides-Investigation and mitigation: Transportation Research Board, Special report no. 247*, chapter Landslide types and processes, pages 36–75. National Research Council, National Academy Press, Washington, D.C.

DeRose, R., C. (1996). Relationships between slope morphology, regolith depth, and the incidence of shallow landslides in eastern Taranaki hill country. *Z. Geomorphol.*, 105:49–60.

D'Odorico, P., Fagherazzi, S., and Rigon, R. (1995). Potential for landsliding: Dependence on hyetograph characteristics. *J. Geophys. Res.*, 31. 10.1029/95WR01136.

Evin, G. and Favre, A.-C. (2008). A new rainfall model based on the Neyman-Scott process using cubic copulas. *Water Resour. Res.*, 44(3):W03433.

Fathani, T. F., Karnawati, D., Sassa, K., Fukuoka, H., and Honda, K. (2009). Development of landslide monitoring and early warning system in Indonesia. In *Proceedings of The First World Landslide Forum*, pages 195–198, Tokyo.

Favre, A.-C., Musy, A., and Morgenthaler, S. (2004). Unbiased parameter estimation of the neyman-scott model for rainfall simulation with related confidence interval. *Journal of Hydrology*, 286(1):168–178.

Foti, E., Faraci, C., Scandura, P., Cancelliere, A., La Rocca, C., Musumeci, R. E., Nicolosi, V. M., Peres, D. J., and Stancanelli, L. M. (2012). Da giampilieri a saponara: Analisi delle cause scatenanti e delle cause predisponenti. In *Atti dell'incontro-dibattito: Cosa non funziona nella difesa dal rischio idro-geologico nel nostro Paese? Analisi e Rimedi (in press)*, Roma. Accademia Nazionale dei Lincei.

Frattini, P., Crosta, G., and Sosio, R. (2009). Approaches for defining thresholds and return periods for rainfall-triggered shallow landslides. *Hydrological Processes*, 23(10):1444–1460.

Freeze, R. A. and Cherry, J. A. (1979). *Groundwater*. Prentice Hall, Englewood Cliffs, NJ.

Gardner, W. R. (1958). Some steady-state solutions of the unsaturated moisture flow equation with evaporation from a water table. *Soil Science*, 85:228–232.

Glade, T., Crozier, M., and Smith, P. (2000). Applying Probability Determination to Refine Landslide-triggering Rainfall Thresholds Using an Empirical "Antecedent Daily Rainfall Model". *Pure and Applied Geophysics*, 157:1059–1079. 10.1007/s000240050017.

Guzzetti, F., Cardinali, M., and Reichenbach, P. (1994). The avi project: A bibliographical and archive inventory of landslides and floods in italy. *Environmental Management*, 18:623–633. 10.1007/BF02400865.

Guzzetti, F., Peruccacci, S., Rossi, M., and Stark, C. P. (2007). Rainfall thresholds for the initiation of landslides in central and southern europe. *Meteorology and Atmospheric Physics*, 98:239–267.

Guzzetti, F., Stark, C. P., and Salvati, P. (2005). Evaluation of Flood and Landslide Risk to the Population of Italy. *Environmental Management*, 1:15–36.

Guzzetti, F. and Tonelli, G. (2004). Information system on hydrological and geomorphological catastrophes in Italy (SICI): a tool for managing landslide and flood hazards. *Natural Hazards and Earth System Sciences*, 4:213–232.

Haefeli, R. (1948). The stability of slopes acted upon by parallel seepage. In *Proc. Int. Conf. Soil Mech. Found. Eng.*

Highland, L. M. and Bobrowsky, P. (2008). The landslide handbook - a guide to understanding landslides. Technical Report 1325, 129 p., U.S. Geological Survey, Reston, Virginia.

Hsieh, P. A., Wingle, W., and Healy, R. W. (2000). *VS2DI-A graphical software package for simulating fluid flow and solute or energy transport in variably saturated porous media.* U. S. Geol. Surv. Water-Resources Investigations Rep. 99-4130.

Istanbulluoglu, E., Tarboton, D. G., Pack, R. T., and Luce, C. H. (2004). Modeling of the interactions between forest vegetation, disturbances, and sediment yields. *Journal of Geophysical Research*, 109:F01009.

Iverson, R. M. (1997). The physics of debris flows. *Rev. Geophys.*, 35:245–296.

Iverson, R. M. (2000). Landslide triggering by rain infiltration. *Water Resour. Res.*, 36:1897–1910. 10.1029/2000WR900090.

Kahn, M. E. (2005). The Death Toll from Natural Disasters: The Role of Income, Geography, and Institutions. *Review of Economics and Statistics*, pages 271–284.

Keefer, D. K., Wilson, R. C., Mark, R. K., Brabb, E. E., Brown, W. M., Ellen, S. D., Harp, E. L., Wieczorek, G. F., Alger, C. S., and Zatkin, R. S. (1987). Real-time landslide warning during heavy rainfall. *Science*, 238(4829):921–925.

Kim, D., Im, S., Lee, S., Hong, Y., and Cha, K.-S. (2010). Predicting the rainfall-triggered landslides in a forested mountain region using trigrs model. *Journal of Mountain Science*, 7:83–91. 10.1007/s11629-010-1072-9.

Lappala, E. G., Healy, R. W., and Weeks, E. P. (1987). *Documentation of the computer program VS2D to solve the equations of fluid flow in variably saturated porous media*. U. S. Geol. Surv. Water-Resources Investigations Rep. 83-4099.

Leij, P., Schaap, M., and Arya, L. (1978). *Methods of Soil Analysis - Part 4 Physical Methods*, chapter Indirect Methods, pages 1009–1045. Soil Science Society of America, Madison, WI.

Luna, B. Q., Cepeda, J., Stumpf, A., van Westen, C. J., Malet, J. P., and van Asch, T. W. J. (2012). Application of a Monte Carlo method for modeling debris flow run-out. In Abbasi, A. and Giesen, N., editors, *EGU General Assembly Conference Abstracts*, volume 14 of *EGU General Assembly Conference Abstracts*, page 13718.

Macmillan, N. A. and Creelman, C. D. (2004). *Detection Theory: A User's Guide*. Lawrence Erlbaum.

Metropolis, N. and Ulam, S. (1949). The Monte Carlo Method. *Journal of the American Statistical Association*, 44(247):pp. 335–341.

Montgomery, D. R. and Dietrich, W. E. (1994). A physically based model for the topographic control on shallow landsliding. *Water Resour. Res.*, 30:1153–1171.

Mood, A., Graybill, F., and Boes, D. (2001). *Introduction to the theory of statistics*, page 580. McGraw-Hill, Boston.

Nelder, J. A. and Mead, R. (1965). A simplex method for function minimization. *The Computer Journal*, 7(4):308–313.

Obeysekera, J. T. B., Tabios, G. Q., I., and Salas, J. D. (1987). On parameter estimation of temporal rainfall models. *Water Resour. Res.*, 23(10):1837–1850.

O′Brien, J., Julien, P., and Fullerton, W. (1993). Two-Dimensional Water Flood and Mudflow Simulation. *Journal of Hydraulic Engineering*, 119:244–261.

Parise, M. and Cannon, S. (2012). Wildfire impacts on the processes that generate debris flows in burned watersheds. *Natural Hazards*, 61(1):217–227. cited By (since 1996) 1.

Peres, D. and Cancelliere, A. (2011). Defining rainfall thresholds for early warning of rainfall-triggered landslides: the case of North-East Sicily. In *Proceedings of the Second World Landslide Forum*, Rome.

Peres, D. and Cancelliere, A. (2012). Utilizzo dei dati di precipitazione di massima intensitÃă per la determinazione di soglie pluviometriche per il preannuncio di frana - Applicazioni in Sicilia. In *Atti del XXXIII Convegno Nazionale di Idraulica e Costruzioni Idrauliche*, pages 627–630, Brescia. EdiBios.

Richards, L. (1931). Capillary conduction of liquids through porous mediums. *Physics*, 1:219–233.

Rodriguez-Iturbe, I., Cox, D. R., and Isham, V. (1987a). Some models for rainfall based on stochastic point processes. *Proceedings of the Royal Society of London. Series A, Mathematical and Physical Sciences*, 410(1839):pp. 269–288.

Rodriguez-Iturbe, I., De Power, B. F., and Valdes, J. B. (1987b). Rectangular pulses point process models for rainfall: Analysis of empirical data. *J. Geophys. Res.*, 92(D8):9645–9656.

Rosso, R., Rulli, M. C., and Vannucchi, G. (2006). A physically based model for the hydrologic control on shallow landsliding. *Water Resources Research*, 42(6):1–16.

Rulli, M., Moreni, S., Vigano', M., and Rosso, R. (2006). Modeling of Forest Roads Impact on Shallow Landslides Triggering. *AGU Fall Meeting Abstracts*, page B480.

Rulli, M. and Rosso, R. (2002). An integrated simulation method for flash-flood risk assessment: 1. Frequency predictions in the Bisagno River by combining stochastic and deterministic methods. *Hydrology and Earth System Sciences*, 6(2):267–283.

Rulli, M. C. and Rosso, R. (2005). Modeling catchment erosion after wildfires in the San Gabriel Mountains of southern California. *Geophys. Res. Lett.*, 32:L19401.

Salas, J. D. (1993). *Analysis and Modeling of Hydrologic Time Series*, chapter 19, Handbook of Hydrology. McGraw-Hill.

Salciarini, D., Godt, J. W., Savage, W. Z., Baum, R. L., and Conversini, P. (2008). Modeling landslide recurrence in Seattle, Washington, USA. *Engineering Geology*, 102(3-4):227 – 237.

Salciarini, D., Godt, J. W., Savage, W. Z., Conversini, P., Baum, R. L., and Michael, J. A. (2006). Modeling regional initiation of rainfall-induced shallow landslides in the eastern umbria region of central italy. *Landslides*, 3:181–194.

Savage, W. Z., Godt, J. W., and Baum, R. L. (2003). *A model for spatially and temporally distributed shallow landslide initiation by rainfall infiltration*, pages 179–187. Number 1325, 129 p. Millpress, Rotterdam.

Savage, W. Z., Godt, J. W., and Baum, R. L. (2004). *Landslides:Evaluation and Stabilization, Proceedings of the 9th International Symposium on Landslides*, chapter Modeling timedependent aerial slope stability, pages 23–36. Number 1325, 129 p. Millpress, Balkema,London.

Schaap, M. G., Leij, F. J., and van Genuchten, M. T. (2001). ROSETTA: a computer program for estimating soil hydraulic parameters with hierarchical pedotransfer functions. *Journal of Hydrology*, 251(3-4):163 – 176.

Simoni, S., F. Zanotti, F., Bertoldi, G., and Rigon, R. (2008). Modelling the probability of occurrence of shallow landslides and channelized debris flows using GEOtop-FS. *Hydrol. Processes*, 22:532–545.

Simunek, J., Sejna, M., Saito, H., Sakai, M., and van Genuchten, M. T. (2008). *The Hydrus-1D Software Package for Simulating the Movement of Water, Heat, and Multiple Solutes in Variably Saturated Media, Version 4.0, HYDRUS Software Series 3*. Dept. of Env. Sci. , Univ. of Calif. Riverside, Riverside, CA.

Sirangelo, B. and Braca, G. (2004). Identification of hazard conditions for mudflow occurrence by hydrological model: Application of FLaIR model to Sarno warning system. *Engineering Geology*, 73(3-4):267 – 276. Rainfall-triggered landslides and debris flows.

Sirangelo, B., Iiritano, G., and Versace, P. (1996). Il preannuncio dei movimenti franosi innescati dalle piogge. Valutazione della probabilita di mobilizzazione in presenza di indeterminatezza nell'identificazione dei parametri nel modello FLaIR. In *Atti del XXV Convegno di Idraulica e Costruzioni Idrauliche*, Torino.

Sirangelo, B. and Versace, P. (1992). Modelli stocastici di precipitazione e soglie pluviometriche di innesco dei movimenti franosi. In *Atti del XXIII Convegno di Idraulica e Costruzioni Idrauliche*, Firenze.

Sirangelo, B. and Versace, P. (1996). A real time forecasting model for landslides triggered by rainfall. *Meccanica*, 31:73–85. 10.1007/BF00444156.

Sirangelo, B., Versace, P., and De Luca, D. L. (2007). Rainfall nowcasting by at site stochastic model P.R.A.I.S.E. *Hydrol. Earth Syst. Sci.*, 11:1341–1351.

Srivastava, R. and Yeh, T. C. J. (1991). Analytical solutions for one dimensional, transient infiltration toward the water table in homogeneous and layered soils. *Water Resour. Res.*, 27:753–762.

Stedinger, J., Vogel, R. M., and Foufoula-Georgiou, E. (1993). *Frequency Analysis of Extreme Events*, chapter 18, Handbook of Hydrology. McGraw-Hill.

Takara, K. and Apip Bagiawan, A. (2009). Study on early warning system for debris flow and landslide in the Citarum River Basin, Indonesia. In *Proceedings of The First World Landslide Forum*, pages 573–576, Tokyo.

Tarboton, D. G. (1997). A new method for the determination of flow directions and upslope areas in grid digital elevation models. *Water Resources Research*, 33(2):309–319.

Taylor, D. (1948). *Fundamentals of Soil Mechanics*. John Wiley, New York.

van Genuchten, M. T. (1980). A closed-form equation for predicting the hydraulic conductivity of unsaturated soils. *Soil Sci. Soc. Am. J.*, 44:892–898.

Vanapalli, S. K. and Fredlund, D. G. (2000). Comparison of different procedures to predict unsaturated soil shear strength. In *Advances in Unsaturated Geotechnics, Proceedings of Sessions of Geo-Denver 2000 (Aug), Geotechnical Special Publication*, number 99, pages 195–209, Reston, Virginia. ASCE.

Varnes, D. (1978). *Landslides-Analysis and control: Transportation Research Board Special Report no. 176*, chapter Slope movement types and processes, pages 11–23. Number 1325, 129 p. National Research Council, Washington, D.C.

Versace, P., Arcuri, S., Biondi, D., Capparelli, G., Cruscomagno, F., De Luca, D. L., Leone, S., Maletta, D., and Niccoli, R. (2012). Sistemi di allertamento e difesa del suolo in Calabria. In *Atti del XXXIII Convegno Nazionale di Idraulica e Costruzioni Idrauliche*, Brescia. EdiBios.

Versace, P. and Capparelli, G. (2008). Empirical Hydrological Models for Early Warning of Landslides Induced by Rainfall. In *Proc. of The First World Landslide Forum*, pages 627–630, Tokyo.

Versace, P., Sirangelo, B., and De Luca, D. L. (2009). A space-time generator for rainfall nowcasting: the PRAISEST model. *Hydrol. Earth Syst. Sci.*, 13:441–452.

Wu, W. and Sidle, R. C. (1995). A distributed slope stability model for steep forested basins. *Water Resour. Res.*, 31:2097–2110. 10.1029/95WR01136.

Yano, K. and Senoo, K. (1985). How to set standard rainfalls or debris flow warning and evacuation. In *Sabo Symposium, SEDD Japan*, pages 451–455.

Zhou, G., Esaki, T., Mitani, Y., Xie, M., and Mori, J. (2003). Spatial probabilistic modeling of slope failure using an integrated gis monte carlo simulation approach. *Engineering Geology*, 68(3 - 4):373 – 386.